Grasping Deformable Planar Objects: Squeeze, Stick/Slip Analysis, and Energy-Based Optimalities

Yan-Bin Jia Feng Guo Huan Lin
Department of Computer Science
Iowa State University
Ames, IA 50011, USA
jia,fguo,linhuan@iastate.edu

Abstract

Robotic grasping of deformable objects is difficult and under-researched not simply due to the high computational cost of modeling. More fundamentally, several issues arise with the deformation of an object being grasped: a changing wrench space, (generally) growing finger contact areas, and pointwise varying contact modes inside these areas. Consequently, constraints needed for deformable modeling by the finite element method (FEM) are hardly established at the beginning of the action. This paper presents a grasping strategy that squeezes the object with two fingers under specified displacements rather than forces. Assuming linear elasticity, an FEM-based analysis ensures equilibrium and the uniqueness of deformation during the action. An event-driven algorithm tracks the contact regions as well as the modes of contact in their interiors, which in turn serve as the needed constraints for deformation update. The classes of "stable" and "pure" squeezes are introduced. Grasp quality is characterized by the amount of work done by the grasping fingers to resist a known disturbance by some adversary finger. An optimization algorithm is progressively developed for segment contacts under Coulomb friction. Simulation and multiple experiments have been conducted to validate the results over solid and ring-like 2D objects.

1 Introduction

Grasping deformable objects is inherently different from grasping rigid ones for which two types of analysis have been developed. Form closure (Reuleaux,1875) on a rigid object eliminates all of its degrees of freedom, while force closure (Nguyen 1988) keeps the object in equilibrium with the ability to resist any external wrench. On a deformable object, however, form closure is impossible to achieve because of its infinite degrees of freedom. Meanwhile, a force-closure analysis is inapplicable to grasping of the object because the applied torques would change as the object deforms, even if the contact forces stay the same.

Robot grasping of deformable objects is an under-researched area for reasons that come from both mechanics and computation. Besides its changing geometry, under deformation an object being grasped has its contacts with the fingers growing from points into areas. Inside such a contact area, a point that sticks to the finger may later slide while a point that slides on the finger may later stick.

Specifying grasping forces like over a rigid body is not a viable approach, for two reasons. First, the specified forces cannot guarantee equilibrium on a deformed shape. In our recent work (Jia et al. 2011) that considered force specifications for a grasp, extra geometric constraints had to be imposed on the finger contacts in order to model the deformation. However, enforcement of such constraints required torques that could not be generated by the grasp itself in a real situation. Second, the classical elasticity theory (Saada,

1993; Fung and Tong, 2001) only treats deformation of a fully constrained object under some applied load, which is balanced by the constraint forces. Angular momentum (thus torque equilibrium) is conserved under force equilibrium (Bower, 2009, pp. 49–52). At the start of a grasp, however, the object is under no such constraints.

Determining a small deformation based on linear elasticity comes down to solving a system of fourth order differential equations (Crandall et al., 1978, p. 288), which generally has no closed-form solution. In practice, computation is conducted using the finite element method (FEM) (Gallagher, 1975) under positional constraints. Forces and torques obtained under FEM will guarantee equilibrium as a consequence of the fact that the object's stiffness matrix has a null space made up of all of its rigid body movements.[1]

In practice it is also much easier to command a finger to move to a designated position than to control it to exert a prescribed force. Also, force magnitudes are not much of our concern as long as an object can be grasped.

For the above reasons, we choose to specify desired displacements of the grasping fingers (rather than the forces they exert). Knowing the finger locations, we hope to infer the locations of the FEM nodes in contact with the deformed object, and obtain the needed positional constraints for an FEM-based deformation update. This is not a trivial task. Since no part of the object is fixed during a grasp operation, contacts are maintained by friction only to some extent. They evolve with deformation. To complicate the issue further, a contact point sliding on a finger imposes a force constraint (that the force must be along an edge of the contact friction cone) rather than a position constraint. Not only do we need to track which nodes are in contact, but also in which contact mode (stick or slip), in order to exert the correct constraints during an update of the deformed shape.

There is also a paradox that comes with the classical elasticity theory. Despite being a gradual physical process, deformation is assumed to happen instantaneously. This makes it almost impossible to predict the final configuration of a grasp with area contacts that did not even exist at the beginning. To cope with this issue, deformable modeling needs to be conducted step by step. We track the varying set of finger contacts and their modes, and apply them as displacement constraints in predicting additional deformation. The shape change will eventually trigger a change in the contact configuration, starting a new round of deformation update. This will require a contact mode analysis with event detection that is quite different from the one performed on a rigid body.

The computational issue we have to face is the high cost of FEM-based deformable modeling. The subcubic time complexity in the number of discretization nodes is typically high for accurate modeling. A large deformation, meanwhile, can only be modeled by nonlinear elasticity (and computed using the even more expensive nonlinear FEM). To make the matter worse, repeated deformation computations are needed in searching for a successful grasp or choosing one with the best quality.

The standard FEM procedure exerts every fixed node constraint by eliminating the corresponding row and column from the object's stiffness matrix. This is inapplicable in a grasping situation, since the (reduced) stiffness matrix varies whenever the fingers are relocated. An improvement is made possible in this paper by having all computation performed directly on the original stiffness matrix, which has its spectral decomposition computed in the preprocessing.

The last issue that will be tackled in this paper is how to measure the quality of a grasp of a deformable object. On a rigid body, the grasping forces do not cause any deformation, thereby conducting no work. Existing metrics for rigid body grasps are mostly force-centered, either to minimize the possibility of violating some hard constraints, to maximize the worst-case adversary force resistible by a "unit" total grasping force, or to minimize the maximum contact force by some finger to resist a known adversary force. On a

[1] This will be revealed more clearly by the force-displacement relationship (12) in Section 2.2.

deformable object, the grasping fingers perform work, most of which is converted into the object's strain energy via deformation. It is therefore natural for a grasp metric to be energy-based. Particularly, we may measure a grasp in terms of stability from the energy point of view, or by the amount of work it will perform to resist an external disturbing force under a known movement.

1.1 Paper Outline

This paper investigates two-finger grasping of a deformable object by squeezing it via finger translations. We refer to the grasp thus formed a *squeeze grasp*. The following assumptions are made:

(a) The object is deformable, isotropic, and either planar or thin 2-$\frac{1}{2}$D.

(b) The two grasping fingers are rigid.

(c) The fingers are coplanar with the object, making frictional point or area contact with it.

(d) Gravity is ignored.

(e) The grasp yields small deformations within the applicability range of the linear elasticity theory.

In the classical elasticity theory, deformation happens instantaneously. In this paper, we will often picture deformation as a continuous process happening in an infinitesimal amount of time. This will allow us to characterize the growing contact areas between the object and the fingers.

The initial finger placement needs to prevent all Euclidean motions, leaving deformation the only possible displacement. In the presence of friction, the placement would be force closure if the object were rigid. From a result by Nguyen (1988), the segment connecting the two initial contact points must lie inside their friction cones. Under a squeeze, each contact point will grow into a segment in which the points may switch their contact modes between stick and slip. The contact segment is not regarded as sliding as long as one point on the segment sticks.

Section 2 will briefly review some basics of linear elasticity and FEM. Section 3 will describe how to compute the deformation of an object from specified displacements of some nodes in the object's mesh representation (and from zero external forces at all other nodes). Section 4 will investigate deformation caused by translating two nodes — an action referred to as "squeezing". We will look at stable squeezes, which maximize the object's strain energy among all squeezes of the "same amounts", and pure squeezes, which prevent any rigid body motion. Section 5 will present an event-driven grasping algorithm that tracks deformation and contact configuration during a squeeze under contact friction. A contact mode analysis will be performed. In Section 6, we will construct grasps that perform minimum work to resist an adversary finger, progressing from the cases of fixed point and segment contacts to that of frictional segment contacts. Section 7 will be on grasping ring-like objects that make frictional point contacts with the grasping fingers. Several experiments will be described in Sections 5.5, 6.4, and 7.3 to validate the described grasping and optimization algorithms. Discussion on future research will follow in Section 8.

1.2 Related Work

Rigid body grasping is an extensively studied topic rich with theoretical analyses, algorithmic syntheses, and implementations with robotic hands (Bicchi and Kumar 2000). Salisbury and Roth (1983) deemed a hand design acceptable if the hand could not only immobilize a grasped object but also impart a desired force and displacement to the object that it interacted with.

First-order form closure (Rimon and Burdick, 1996) is widely regarded as equivalent to force closure with frictionless contacts. Mishra et al. (1987) gave upper bounds on the numbers of contact points sufficient and/or necessary for form closure. Tighter bounds were later derived for 2D and 3D objects with piecewise smooth boundaries (Markenscoff et al., 1990). Algorithms were developed to compute all form closure grasps of polygonal parts (Brost and Goldberg 1994; van der Stappen et al., 2000). There was also work (Rimon and Blake, 1999; Rodriguez et al., 2012) on "caging" an object with imposed frictionless contacts such that it could move but not escape.

Two-finger force-closure grasps of 2D objects are efficiently computable for polygons (Nguyen, 1988) and piecewise smooth curved shapes (Ponce et al., 1993). Ponce et al. (1997) also gave algorithms for grasping 3-D objects. Trinkle (1992) formulated the test for force closure as a linear program with an objective function to measure the distance from losing the closure.

The notion of task ellipsoid (Li and Sastry 1988) formulated an idea that the choice of a grasp ought to be based on its capacity to generate wrenches that were relevant to the task. Grasp quality measures for multifingered hands considered selection of internal grasp forces that were furthest from violating any closure, friction, and mechanical constraints (Kerr and Roth, 1986), or were directly derived from the grasp matrix which characterized the wrench space of a grasp (Li and Sastry 1988). Grasp metrics for polygons and polyhedra often sought to maximize the worst-case external force that could be resisted by a unit grasping force (Markenscoff and Papadimitriou 1989; Mirtich and Canny 1994; Jia 1995). Mishra (1995) gave a summary on various grasp metrics, addressing the trade-offs among grasp goodness, object geometry, the number of fingers, and the computational complexity for grasp synthesis. Some recent work (Buss et al., 1998; Boyd and Wegbreit 2007) focused on minimizing the maximum magnitude of the applied force at any frictional contact of a grasp in order to maintain equilibrium against a known adversary wrench, via the use of semidefinite programming techniques.

Much less work exists on grasping deformable objects, a problem that needs to deal with changes in the local contact geometry as well as the global object geometry caused by the physical action. The concept of bounded force-closure (Wakamatsu et al., 1996) was proposed for deformable object grasping. Hirai et al. (2001) showed visual and tactile information to be effective on controlling the motion of a grasped deformable object. The deformation-space approach (Gopalakrishnan and Goldberg 2005) characterized the optimal grasp of a deformable part as the one where the potential energy needed to release the part equals the amount needed to squeeze it to its elastic limit.

In contrast, manipulation of flexible linear objects such as wires or ropes has been a very active area, with work on static modeling (Wakamatsu and Hirai, 2004), knotting and unknotting (Saha and Isto, 2006; Matsuno and Fukuda, 2006; Ladd and Kavraki 2004; Wakamatsu et al., 2006), pickup (Remde et al. 1999), and path planning (Moll and Kavraki 2006). These operations, however, can be carried out without a serous need for FEM-based deformable modeling.

Sinha and Abel (1992) proposed a model for deformation of the contact regions under a grasp that predicted normal and tangential contact forces with no concern of global deformation or grasp computation. Luo and Xiao (2006) demonstrated that simulation accuracy and efficiency could be improved based on derived geometric properties at deformable contact. The recent work involving the first author (Tian and Jia 2010) investigated deformable modeling of shell-like objects that were already grasped under point contacts.

More thorough investigations on the elastic contact problem were conducted by the mechanics community on determining the contact areas on two deformable bodies under a known applied load. The gradual nature of the physical process suggests iterative updates of the growing contact regions. In the work by Francavilla and Zienkiewicz (1975), an FEM-based solution was given for 2D elastic contact problems with no friction. It was extended to solve contact problems under Coulomb friction by Okamoto and Nakazawa

(1979) and Sachdeva and Ramakrishnan (1981) via iterative updating of the contact zone and the modes of individual contact nodes: stick, slip, contact break, or contact establishment. In each iteration, FEM computed the deformed shape based on position and friction constraints derived from the contact modes under Coulomb friction. This event-based approach was extended by Chandrasekaran et al. (1987) to handle geometric and physical nonlinearities as well as node-edge contacts, solving for the exact loading condition from prescribed displacements.

1.3 Notation

In the paper, sets of integers (or indices) are represented by English letters in the blackboard bold font (e.g., $\mathbb{I}$). Points and vectors are always denoted by bold face letters, English or Greek (e.g., $\boldsymbol{v}$). A vector with a caret (e.g., $\hat{\boldsymbol{v}}$) is a unit vector. A subvector consisting of some entries from a vector $\boldsymbol{v}$ is denoted as $\bar{\boldsymbol{v}}$. A cross product of two 2-vectors is treated as a scalar whenever no ambiguity arises.

By convention, an $n \times n$ identity matrix, integer $n > 0$, is denoted by I_n. The null space, column space, and rank of a matrix M are denoted by $\mathrm{null}(M)$, $\mathrm{col}(M)$, and $\mathrm{rank}(M)$, respectively.

Whether an object deforms or not, a node in its FEM representation with n nodes is referred to as $\boldsymbol{p}_i$, for $1 \leq i \leq n$, . When appearing in an expression, $\boldsymbol{p}_i$ also refers to the node's original location (before deformation). A displacement of the node $\boldsymbol{p}_i$ is referred to as $\boldsymbol{\delta}_i$, and the displaced location as $\tilde{\boldsymbol{p}}_i = \boldsymbol{p}_i + \boldsymbol{\delta}_i$.

Metric system units are used throughout the paper. In particular, we use meter for length, Newton for force, Pascal for pressure, and Joule for work and energy. These units will be omitted from now on.

2 Finite Element Method

This section begins with a review of plane linear elasticity. It then characterizes the null space of the stiffness matrix for an unconstrained object in FEM. The result will be used later in our design of a squeeze-based grasping strategy and strategies for grasp resistance to an adversary finger.

2.1 Linear Plane Elasticity

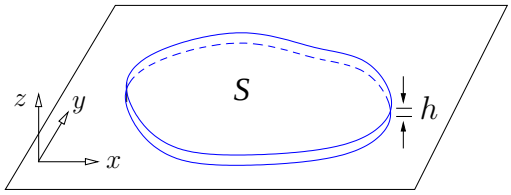

Figure 1: Thin flat object.

Consider a thin flat object shown in Figure 1 with its thickness h significantly less than its two other dimensions. Essentially, the object is bounded by a generalized cylinder that results from translating a closed simple curve in the xy-plane along the z-direction. In this paper, we consider *plane stress* (Fung and Tong, 2001, pp. 280–281) parallel to the xy-plane. It assumes zero normal stress σ_z along the z-axis and zero shear stresses τ_{xz} and τ_{yz} in the x-z and y-z planes.

Under a displacement field $(u(x,y), v(x,y))^T$, every point $(x,y)^T$ inside the object moves to $(x+u, y+v)^T$. The normal strains ϵ_x and ϵ_y, and the shearing strain γ_{xy} within a cross section S are given below:

$$\begin{aligned} \epsilon_x &= \frac{\partial u}{\partial x}, \\ \epsilon_y &= \frac{\partial v}{\partial y}, \\ \gamma_{xy} &= \frac{\partial u}{\partial y} + \frac{\partial v}{\partial x}. \end{aligned} \tag{1}$$

We denote by σ_x and σ_y the normal stress components at the same point in the x- and y-directions, respectively, and by γ_{xy} the sheer stress. Under Hooke's law (Crandall et al., 1978, p. 284), the following stress-strain relationships hold:

$$\begin{aligned} \epsilon_x &= \frac{1}{E}(\sigma_x - \nu\sigma_y), \\ \epsilon_y &= \frac{1}{E}(\sigma_y - \nu\sigma_x), \\ \gamma_{xy} &= \frac{2(1+\nu)}{E}\tau_{xy}. \end{aligned} \tag{2}$$

The strain energy is (Crandall et al., 1978, p. 302)

$$U = \frac{h}{2}\iint_S \left(\frac{E}{1-\nu^2}\left(\epsilon_x^2 + 2\nu\epsilon_x\epsilon_y + \epsilon_y^2\right) + \frac{E}{2(1+\nu)}\gamma_{xy}^2 \right) dxdy, \tag{3}$$

where E and ν are Young's modulus and Poisson's ratio of the material, respectively, with $E > 0$ and $-1 \le \nu \le \frac{1}{2}$.

The proportional limit (Crandall et al., 1978, p. 270) is the greatest stress for which the stress is still proportional to the strain, that is, Hooke's law of stress-strain relationship still holds. This limit is $E\epsilon^*$ for some strain $\epsilon^* > 0$. We transplant the maximum principal strain theory (aka, the St. Venant theory) (Negi, 2008, p. 196) to assume that linear elasticity holds as long as

$$|\epsilon_x| \le \epsilon^* \qquad \text{and} \qquad |\epsilon_y| \le \epsilon^*. \tag{4}$$

Theorem 1 *Under linear elasticity, any displacement field $(u(x,y), v(x,y))^T$ that yields zero strain energy is linearly spanned by three fields: $(1,0)^T$, $(0,1)^T$, and $(-y,x)^T$.*

Below is our simple proof of this known result.

Proof Suppose $U = 0$ under a displacement field $(u,v)^T$. Since the integrand in (3) is non-negative, we infer that the strains ϵ_x, ϵ_y, γ_{xy} must vanish everywhere inside the body. Using (1), we integrate $\epsilon_x = 0$ and $\epsilon_y = 0$ to obtain $u = u(y)$ and $v = v(x)$. Since $\gamma_{xy} = 0$, $du/dy + dv/dx = 0$ holds inside the body. Because u and v do not share variables, the only possibility is that $dv/dx = -du/dy = c$, for some constant c. Integration of the two derivatives gives

$$\begin{pmatrix} u \\ v \end{pmatrix} = c\begin{pmatrix} -y \\ x \end{pmatrix} + d\begin{pmatrix} 1 \\ 0 \end{pmatrix} + e\begin{pmatrix} 0 \\ 1 \end{pmatrix},$$

for some constants d and e. □

A displacement field $(u,v)^T$ that generates no deformation is a rigid body transformation. The fields $(1,0)^T$ and $(0,1)^T$ respectively describe unit translations along the x and y axes, and the field $(-y,x)^T$ represents (or essentially, approximates) a rotation about the origin under linear elasticity.

2.2 Stiffness Matrix

Generally, the strain energy integral (3) has no closed form. It is computed using the FEM as follows. The object's cross section is discretized into a finite number of elements with n vertices (or nodes) $\boldsymbol{p}_k = (x_k, y_k)^T$, for $1 \le k \le n$. In this paper, triangular elements are used. Figure 2 shows an example.

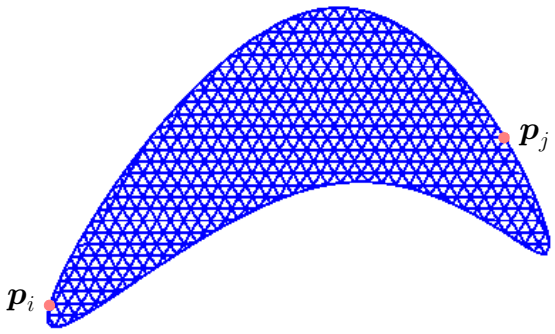

Figure 2: Meshed object with 517 nodes, including 112 on the boundary.

We place the origin at the centroid of these vertices so

$$\sum_{k=1}^{n} \boldsymbol{p}_k = \mathbf{0}. \tag{5}$$

Under deformation, every node $\boldsymbol{p}_k$ is displaced by $\boldsymbol{\delta}_k = (\delta_{kx}, \delta_{ky})^T$ to the location $\tilde{\boldsymbol{p}}_k = \boldsymbol{p}_k + \boldsymbol{\delta}_k$. The displacement of any interior point of an element is linearly interpolated over those of its three vertices. The deformed shape of the object is thus completely described by $\boldsymbol{\delta} = (\boldsymbol{\delta}_1^T, \ldots, \boldsymbol{\delta}_n^T)^T$. We obtain the strain energies of individual elements via respectively integrations of (3) over these elements, and then assemble the results into the total strain energy:

$$U = \frac{1}{2}\boldsymbol{\delta}^T K \boldsymbol{\delta}, \tag{6}$$

where the matrix K is $2n \times 2n$ and referred to as the *stiffness matrix*. The symmetry of K follows from Betti's law (Saada, 1993, pp. 447–448).[2] The non-negativeness of strain energy ensures that K is positive semidefinite.

The strain energy U is zero if and only if $K\boldsymbol{\delta} = 0$, that is, $\boldsymbol{\delta} \in \mathrm{null}(K)$. Such a vector $\boldsymbol{\delta}$ represents a rigid body motion (Gallagher, 1975, p. 48). Meanwhile, from (3) U is zero if and only if it is zero over every triangular element. By Theorem 1 and from linear interpolation within an element, we infer that $\mathrm{null}(K)$ is spanned by the following three $2n$-vectors:

$$\begin{aligned} \boldsymbol{w}_x &= (1, 0, \ldots, 1, 0)^T, \\ \boldsymbol{w}_y &= (0, 1, \ldots, 0, 1)^T, \\ \boldsymbol{w}_r &= (-y_1, x_1, \ldots, -y_n, x_n)^T. \end{aligned} \tag{7}$$

The two vectors $\boldsymbol{w}_x$ and $\boldsymbol{w}_y$ are orthogonal to each other. Since $\sum_{k=1}^n x_k = \sum_{k=1}^n y_k = 0$ from (5), $\boldsymbol{w}_r$ is orthogonal to both $\boldsymbol{w}_x$ and $\boldsymbol{w}_y$.

Thus, the matrix K has $2n-3$ positive eigenvalues $\lambda_1, \lambda_2, \ldots, \lambda_{2n-3}$. Let $\boldsymbol{v}_1, \boldsymbol{v}_2, \ldots, \boldsymbol{v}_{2n-3}$ be the corresponding unit eigenvectors that are orthogonal to each other. Since $\boldsymbol{w}_x, \boldsymbol{w}_y, \boldsymbol{w}_r$ are orthogonal to each other, we normalize them to obtain three more eigenvectors:

$$\boldsymbol{v}_{2n-2} = \frac{\boldsymbol{w}_x}{\sqrt{n}}, \quad \boldsymbol{v}_{2n-1} = \frac{\boldsymbol{w}_y}{\sqrt{n}}, \quad \text{and} \quad \boldsymbol{v}_{2n} = \frac{\boldsymbol{w}_r}{\sqrt{\sum_{i=1}^n \|\boldsymbol{p}_i\|^2}}. \tag{8}$$

[2]Betti's law states that the deflection at one point in a given direction caused by a load at another point in a second direction equals the deflection at the second point in the second direction due to a unit load at the first point in the first direction.

It follows from the Spectral Theorem (Strang, 1993, p. 273) that

$$K = V\Lambda V^T, \tag{9}$$

where $V = (v_{ij}) = (\boldsymbol{v}_1, \boldsymbol{v}_2, \ldots, \boldsymbol{v}_{2n})$ and $\Lambda = \mathrm{diag}(\lambda_1, \ldots, \lambda_{2n-3}, 0, 0, 0)$. Because K is singular, constraints will have to be imposed to prevent any rigid body movement of the object.

In this paper, the nodal displacements $\boldsymbol{\delta}_1, \ldots, \boldsymbol{\delta}_n$ are due to the forces exerted by grasping fingers at some boundary nodes. Zero external forces are applied at all interior nodes and the remaining boundary nodes not in contact with a finger. Aggregate the external forces applied at all n nodes into a force vector $\boldsymbol{f}$. The potential of these external forces is

$$W = -\boldsymbol{\delta}^T \boldsymbol{f}. \tag{10}$$

Its sum with the strain energy constitutes the total potential energy of the system:

$$\Pi = U + W. \tag{11}$$

Minimization of Π yields the following familiar force-displacement relationship:

$$K\boldsymbol{\delta} = \boldsymbol{f}. \tag{12}$$

Equations (6) and (10)–(12) together imply that, at equilibrium,

$$\Pi = -U. \tag{13}$$

3 Deformation from Displacements of Multiple Contact Nodes

Denote by $\boldsymbol{p}_{i_1}, \ldots, \boldsymbol{p}_{i_m}$, $i_1 < i_2 < \cdots < i_m$, the boundary nodes that are in contact with some fingers.[3] In Figure 2, for instance, we may assume $m = 2$ with $i_1 = i$ and $i_2 = j$. Suppose the displacement $\boldsymbol{\delta}_{i_k}$ of every node $\boldsymbol{p}_{i_k}$, $1 \le k \le m$, is known[4]. We also know that no external force is applied at a node $\boldsymbol{p}_k$ not in contact, i.e.,

$$\boldsymbol{f}_k = \boldsymbol{0}, \qquad 1 \le k \le n \text{ and } k \ne i_1, \ldots, i_m. \tag{14}$$

We would like to determine the contact forces $\boldsymbol{f}_{i_k}$ exerted by the fingers at the nodes $\boldsymbol{p}_{i_k}$, $1 \le k \le m$, and the displacements of all n nodes (which together determine the deformed shape). Note that $m > 1$ nodes must be in contact. Otherwise, specifying the displacement of only one node would be equivalent to pushing the object by the specified amount and then rotating it about the node. This would be a rigid body movement.

3.1 Displacement Field

We substitute the decomposition (9) into (12), and left multiply both sides of the resulting equation with V^T. Because V is an orthogonal matrix, this yields

$$\Lambda V^T \boldsymbol{\delta} = V^T \boldsymbol{f}.$$

[3] One finger may be in contact with multiple nodes.

[4] from sensor measurements, for instance

Write $V = (\boldsymbol{v}_1, \boldsymbol{v}_2, \ldots, \boldsymbol{v}_n)$ and expand the above into $2n$ equations:

$$\begin{aligned} \boldsymbol{v}_k^T \boldsymbol{\delta} &= \frac{1}{\lambda_k} \boldsymbol{v}_k^T \boldsymbol{f}, \qquad k = 1, \ldots, 2n-3; \\ 0 &= \boldsymbol{v}_k^T \boldsymbol{f}, \qquad k = 2n-2, 2n-1, 2n. \end{aligned}$$

With them we represent $\boldsymbol{\delta}$ in terms of $\boldsymbol{v}_1, \boldsymbol{v}_2, \ldots, \boldsymbol{v}_{2n}$:

$$\boldsymbol{\delta} = \sum_{k=1}^{2n-3} \frac{1}{\lambda_k} (\boldsymbol{v}_k^T \boldsymbol{f}) \boldsymbol{v}_k + \sum_{k=2n-2}^{2n} g_k \boldsymbol{v}_k, \tag{15}$$

where $g_k = \boldsymbol{v}_k^T \boldsymbol{\delta}$, $k = 2n-2, 2n-1, 2n$.

From now on, we denote by $\bar{\boldsymbol{a}}$ the vector that selects those entries from a $2n$-vector $\boldsymbol{a}$ with indices $2i_1 - 1, 2i_1, \ldots, 2i_m - 1, 2i_m$. For instance,

$$\bar{\boldsymbol{v}}_k = (v_{2i_1-1,k}, v_{2i_1,k}, \ldots, v_{2i_m,k})^T, \tag{16}$$

for $1 \le k \le n$, and $\bar{\boldsymbol{f}} = (\boldsymbol{f}_{i_1}^T, \ldots, \boldsymbol{f}_{i_m}^T)^T$. Since $\boldsymbol{f}_k = \boldsymbol{0}$, for $k \notin \{i_1, \ldots, i_m\}$, $\bar{\boldsymbol{v}}_k^T \bar{\boldsymbol{f}} = \boldsymbol{v}_k^T \boldsymbol{f}$. From (15) we have,

$$\boldsymbol{\delta} = \sum_{k=1}^{2n-3} \frac{1}{\lambda_k} (\bar{\boldsymbol{v}}_k^T \bar{\boldsymbol{f}}) \boldsymbol{v}_k + \sum_{k=2n-2}^{2n} g_k \boldsymbol{v}_k. \tag{17}$$

Assemble the equations for $\boldsymbol{\delta}_{i_1}, \ldots, \boldsymbol{\delta}_{i_m}$ within (17) into the following form:

$$\bar{\boldsymbol{\delta}} = \begin{pmatrix} \boldsymbol{\delta}_{i_1} \\ \vdots \\ \boldsymbol{\delta}_{i_m} \end{pmatrix} = A \bar{\boldsymbol{f}} + B \boldsymbol{g}, \tag{18}$$

where $\boldsymbol{g} = (g_{2n-2}, g_{2n-1}, g_{2n})^T$, and

$$A = \sum_{k=1}^{2n-3} \frac{1}{\lambda_k} \bar{\boldsymbol{v}}_k \bar{\boldsymbol{v}}_k^T, \tag{19}$$

$$B = (\bar{\boldsymbol{v}}_{2n-2}, \bar{\boldsymbol{v}}_{2n-1}, \bar{\boldsymbol{v}}_{2n}). \tag{20}$$

It follows from (8) that

$$\mathrm{span}\{\bar{\boldsymbol{v}}_{2n-2}, \bar{\boldsymbol{v}}_{2n-1}, \bar{\boldsymbol{v}}_{2n}\} = \mathrm{span}\{\bar{\boldsymbol{w}}_x, \bar{\boldsymbol{w}}_y, \bar{\boldsymbol{w}}_r\}.$$

This implies

$$\mathrm{col}(B) = \mathrm{span}\{\bar{\boldsymbol{w}}_x, \bar{\boldsymbol{w}}_y, \bar{\boldsymbol{w}}_r\}.$$

Meanwhile, left multiplications of $\boldsymbol{v}_{2n-2}^T$, $\boldsymbol{v}_{2n-1}^T$, $\boldsymbol{v}_{2n}^T$ respectively with both sides of $K\boldsymbol{\delta} = \boldsymbol{f}$ yield

$$\begin{aligned} 0 &= (\boldsymbol{v}_{2n-2}, \boldsymbol{v}_{2n-1}, \boldsymbol{v}_{2n})^T \boldsymbol{f} \\ &= B^T \bar{\boldsymbol{f}}. \qquad \text{by (14)} \end{aligned} \tag{21}$$

In other words, $\bar{\boldsymbol{w}}_x^T \bar{\boldsymbol{f}} = \bar{\boldsymbol{w}}_y^T \bar{\boldsymbol{f}} = \bar{\boldsymbol{w}}_r^T \bar{\boldsymbol{f}} = 0$. Vanishing of the first two products implies force equilibrium $\sum_{j=1}^m \boldsymbol{f}_{i_j} = 0$, and that of the last product implies torque equilibrium $\sum_{j=1}^m \boldsymbol{p}_{i_j} \times \boldsymbol{f}_{i_j} = 0$. Combine (18) and (21):

$$M \begin{pmatrix} \bar{\boldsymbol{f}} \\ \boldsymbol{g} \end{pmatrix} = \begin{pmatrix} \bar{\boldsymbol{\delta}} \\ 0 \\ 0 \\ 0 \end{pmatrix}, \tag{22}$$

where

$$M = \begin{pmatrix} A & B \\ B^T & \mathbf{0} \end{pmatrix}. \tag{23}$$

By definition (19), A is symmetric, and so is M.

3.2 Uniqueness of Deformation

If we can solve $\bar{\boldsymbol{f}}$ and $\boldsymbol{g}$ from (22), we will be able to determine the displacement field $\boldsymbol{\delta}$ and thus the deformed shape using (17). Let us first give a negative result.

Lemma 2 *The matrix M is singular if $m = 1$, that is, if the displacement of only one node is specified.*

Proof Suppose $m = 1$. The tuple $\bar{\boldsymbol{\delta}} = \boldsymbol{\delta}_i$, for some i, is part of at least two rigid body movements $\boldsymbol{\delta}$: a translation by $\boldsymbol{\delta}_i$ and such a translation followed by some rotation about $\tilde{\boldsymbol{p}}_i = \boldsymbol{p}_i + \boldsymbol{\delta}_i$. These two values of $\boldsymbol{\delta}$ are linearly independent and both spanned by $\boldsymbol{v}_{2n-2}, \boldsymbol{v}_{2n-1}, \boldsymbol{v}_{2n}$. Thus, the corresponding two values of $\boldsymbol{g} = (\boldsymbol{v}_{2n-2}, \boldsymbol{v}_{2n-1}, \boldsymbol{v}_{2n})^T \boldsymbol{\delta}$ must be linearly independent. Meanwhile, (22) is derived from $K\boldsymbol{\delta} = \boldsymbol{f}$. Since $\boldsymbol{\delta} \in \mathrm{null}(K)$, $\boldsymbol{f} = \mathbf{0}$, which implies $\bar{\boldsymbol{f}} = \mathbf{0}$. Now we have two linearly independent solutions $\binom{\mathbf{0}}{\boldsymbol{g}}$ to (22). Hence M is singular. □

The good news is that M becomes nonsingular for $m \geq 2$. To establish this, we need the following lemma.

Lemma 3 *The product $\boldsymbol{x}^T A \boldsymbol{x} > 0$ whenever $B^T \boldsymbol{x} = \mathbf{0}$, for any $2m$-vector $\boldsymbol{x} \neq 0$ with $m \geq 2$.*

Proof Consider the matrix $\bar{V} = (\bar{\boldsymbol{v}}_1, \ldots, \bar{\boldsymbol{v}}_{2n})$. The rows of $\bar{V}$ are also of V and therefore are orthogonal to each other. So, $\mathrm{rank}(\bar{V}) = 2m$, which is also the matrix's column rank. Therefore, every $2m$-vector $\boldsymbol{x} \neq 0$ must be spanned by the columns of $\bar{V}$.

Suppose $B^T \boldsymbol{x} = \mathbf{0}$. Namely, the vector $\boldsymbol{x}$ is orthogonal to $\bar{\boldsymbol{v}}_{2n-2}, \bar{\boldsymbol{v}}_{2n-1}, \bar{\boldsymbol{v}}_{2n}$. It must then be a linear combination of $\bar{\boldsymbol{v}}_1, \bar{\boldsymbol{v}}_2, \ldots, \bar{\boldsymbol{v}}_{2n-3}$. There exists some $\bar{\boldsymbol{v}}_j$, $1 \leq j \leq 2n-3$, such that $\bar{\boldsymbol{v}}_j^T \boldsymbol{x} \neq 0$. Therefore,

$$\begin{aligned} \boldsymbol{x}^T A \boldsymbol{x} &= \boldsymbol{x}^T \left(\sum_{k=1}^{2n-3} \frac{1}{\lambda_k} \bar{\boldsymbol{v}}_k \bar{\boldsymbol{v}}_k^T \right) \boldsymbol{x} \\ &\geq \frac{1}{\lambda_j} (\bar{\boldsymbol{v}}_j^T \boldsymbol{x})^2 \\ &> 0. \end{aligned}$$

□

Theorem 4 *The matrix M is nonsingular for $m \geq 2$.*

Proof We prove that $M\binom{\bar{\boldsymbol{f}}}{\boldsymbol{g}} \neq \mathbf{0}$ whenever $\bar{\boldsymbol{f}} \neq \mathbf{0}$. There are two cases:

(a) $B^T\boldsymbol{f} \neq \mathbf{0}$. We have

$$\begin{pmatrix} A & B \\ B^T & 0 \end{pmatrix}\binom{\bar{\boldsymbol{f}}}{\boldsymbol{g}} = \binom{A\bar{\boldsymbol{f}} + B\boldsymbol{g}}{B^T\bar{\boldsymbol{f}}} \neq \mathbf{0}.$$

(b) $B^T\bar{\boldsymbol{f}} = \mathbf{0}$. We have

$$\begin{aligned} & (\bar{\boldsymbol{f}}^T, \boldsymbol{g}^T)\begin{pmatrix} A & B \\ B^T & 0 \end{pmatrix}\binom{\bar{\boldsymbol{f}}}{\boldsymbol{g}} \\ = \;& \bar{\boldsymbol{f}}^T A\bar{\boldsymbol{f}} + \boldsymbol{g}^T B^T\bar{\boldsymbol{f}} + \bar{\boldsymbol{f}}^T B\boldsymbol{g} \\ = \;& \bar{\boldsymbol{f}}^T A\bar{\boldsymbol{f}} && \text{(since } B^T\bar{\boldsymbol{f}} = \mathbf{0} \text{ and } \bar{\boldsymbol{f}}^T B = \mathbf{0}\text{)} \\ > \;& 0 && \text{(by Lemma 3).} \end{aligned}$$

This implies $M\binom{\bar{\boldsymbol{f}}}{\boldsymbol{g}} \neq \mathbf{0}$.

□

Since M is nonsingular, its inverse M^{-1} exists and is symmetric because M is:

$$M^{-1} = \begin{pmatrix} C & E \\ E^T & H \end{pmatrix}, \tag{24}$$

where C, E, and H have dimensions $2m \times 2m$, $2m \times 3$, and 3×3, respectively.

From (22) we obtain

$$\binom{\bar{\boldsymbol{f}}}{\boldsymbol{g}} = \binom{C}{E^T}\bar{\boldsymbol{\delta}}. \tag{25}$$

We refer to C as the *reduced stiffness matrix* as it relates the specified nodal displacements to the forces exerted at the corresponding nodes. The displacement field from (17) can be rewritten as follows:

$$\begin{aligned} \boldsymbol{\delta} &= (\boldsymbol{v}_1, \ldots \boldsymbol{v}_{2n})\begin{pmatrix} \bar{\boldsymbol{v}}_1^T\bar{\boldsymbol{f}}/\lambda_1 \\ \vdots \\ \bar{\boldsymbol{v}}_1^T\bar{\boldsymbol{f}}/\lambda_{2n-3} \\ \boldsymbol{g} \end{pmatrix} \\ &= V\begin{pmatrix} \bar{\boldsymbol{v}}_1^T C/\lambda_1 \\ \vdots \\ \bar{\boldsymbol{v}}_{2n-3}^T C/\lambda_{2n-3} \\ E^T \end{pmatrix}\bar{\boldsymbol{\delta}}. \qquad \text{(by (25))} \end{aligned} \tag{26}$$

The potential energy form (6) is simplified to

$$\begin{aligned} U &= \frac{1}{2}\boldsymbol{\delta}^T\boldsymbol{f} \\ &= \frac{1}{2}\bar{\boldsymbol{\delta}}^T\bar{\boldsymbol{f}} \qquad \text{(since } \boldsymbol{f}_j = 0 \text{ for } j \neq i_1, \ldots, i_m\text{)} \\ &= \frac{1}{2}\bar{\boldsymbol{\delta}}^T C\bar{\boldsymbol{\delta}}. \qquad \text{(by (25))} \end{aligned} \tag{27}$$

Next, let us take a closer look at the submatrices of M^{-1} in (24). Multiply M and M^{-1}:

$$MM^{-1} = \begin{pmatrix} AC + BE^T & AE + BH \\ B^T C & B^T E \end{pmatrix} = I_{2m+3}. \tag{28}$$

Using the above identity we can determine H as follows:

$$\begin{aligned} AE + BH = 0 \quad &\Rightarrow \quad E^T AE + E^T BH = 0 \\ &\Rightarrow \quad E^T AE + (B^T E)^T H = 0 \\ &\Rightarrow \quad E^T AE + H = 0 \qquad\qquad (\text{since } B^T E = I_3) \\ &\Rightarrow \quad H = -E^T AE. \end{aligned}$$

Theorem 5 *Suppose $m \geq 2$. Consider the submatrices of M in (23) and M^{-1} in (24).*

(i) The $2m \times 3$ submatrix B has rank 3.

(ii) The $2m \times 2m$ submatrix C is symmetric and positive semidefinite such that

$$\text{null}(C) = \text{col}(B). \tag{29}$$

This implies that the $2m$-dimensional space is a direct sum of the column spaces of C and B:

$$\mathbb{R}^{2m} = \text{col}(C) \oplus \text{col}(B). \tag{30}$$

(iii) The $2m \times 3$ submatrix E has rank 3.

(iv) The product AC has rank $2m - 3$ and only one eigenvalue 1 (of multiplicity $2m - 3$).

(v) The column spaces of AC and E are orthogonal such that

$$\mathbb{R}^{2m} = \text{col}(AC) \oplus \text{col}(E). \tag{31}$$

We refer the reader to Appendix A for the proof of Theorem 5.

Corollary 6 *Suppose $\bar{\boldsymbol{\delta}}$ is part of some rigid body displacement $\boldsymbol{\delta}$. Then $\bar{\boldsymbol{f}} = \mathbf{0}$. If $m \geq 2$, then $\boldsymbol{\delta}$ is given as (26).*

Proof In the case $m = 1$, we know that the 2×3 matrix B has rank 2 and contains the identity matrix formed by $\bar{\boldsymbol{v}}_{2n-2}$ and $\bar{\boldsymbol{v}}_{2n-1}$. The vector $B^T \bar{\boldsymbol{f}}$ contains $\bar{\boldsymbol{f}}$. Equation (21) immediately implies that $\bar{\boldsymbol{f}} = \mathbf{0}$.

Suppose $m \geq 2$. Let $\boldsymbol{\delta}$ be a rigid body displacement that contains $\bar{\boldsymbol{\delta}}$. By Theorem 4, M^{-1} (and thus C) uniquely exists. Therefore, $\boldsymbol{\delta}$ is uniquely determined from (26). This one-to-one correspondence between $\bar{\boldsymbol{\delta}}$ and $\boldsymbol{\delta}$ implies that the vector $\bar{\boldsymbol{f}} = C\bar{\boldsymbol{\delta}}$ must be contained in $\boldsymbol{f} = K\boldsymbol{\delta} = 0$. Hence $\bar{\boldsymbol{f}} = \mathbf{0}$. □

The spectral decomposition (9) of the stiffness matrix can be computed via singular value decomposition (SVD) in $O(n^3)$ time. The matrix A requires $O(nm^2)$ time to set up, so does the system (22). The inverse A^{-1} can be computed in $O(m^{2.807})$ time using Strassen's algorithm (Strassen, 1969), or in $O(m^{2.376})$ time using the Coppersmith-Winograd algorithm[5] (Coppersmith and Winograd, 1990), which is also the time to solve for $\bar{\boldsymbol{f}}$ and $\boldsymbol{g}$. The displacement of a non-contact boundary node is computed according to (26) as

[5]This algorithm is mainly useful for proving theoretical time bounds.

follows. First, compute the product $(\bar{\boldsymbol{v}}_1, \ldots, \bar{\boldsymbol{v}}_{2n-3})^T C$ in $O(m^2 n)$ time. This determines the second matrix in (26) after divisions of the first $2n-3$ entries in the product by $\lambda_1, \ldots, \lambda_{2n-3}$. Multiply the matrix with $\bar{\boldsymbol{\delta}}$ in $O(mn)$ time. Then left multiply the resulting vector with the two rows in V whose indices correspond to that of the node, spending extra $O(n)$ time to obtain its displacement. After SVD, the total computation time is $O(m^2 n)$.

To determine the deformed shape, the displacement of every boundary node needs to be computed. For a uniform mesh, there are $O(\sqrt{n})$ nodes on the boundary. Therefore, $O(\sqrt{n})$ rows from V need to be multiplied in the last stage described in the above paragraph, taking $O(n^{3/2})$ time. The overall computation after SVD therefore takes $O(n(m^2 + \sqrt{n}))$ time after SVD. Since m is often very small and can be treated as a constant, the computation time reduces to $O(n^{3/2})$.

4 Foundation of Squeezing

A human being often easily grasps a deformable object by squeezing it with two fingers. This section examines the reason behind under the point contact model, paving the way for a two-finger grasp strategy to be introduced in Section 5.

4.1 Stable Deformation

Consider all displacements $\bar{\boldsymbol{\delta}} = (\boldsymbol{\delta}_{i_1}, \ldots, \boldsymbol{\delta}_{i_m})^T$ of the contact nodes $\boldsymbol{p}_{i_1}, \ldots, \boldsymbol{p}_{i_m}$ such that $\|\bar{\boldsymbol{\delta}}\| = 1$. We want to find the one that minimizes the potential energy Π given in (13). This is equivalent to maximizing the strain energy U over the unit hypersphere in $\mathbb{R}^{2m}$, more specifically,

$$\max_{\|\bar{\boldsymbol{\delta}}\|=1} \frac{1}{2} \bar{\boldsymbol{\delta}}^T C \bar{\boldsymbol{\delta}}.$$

The component of $\bar{\boldsymbol{\delta}}$ that is in the $\mathrm{null}(C)$ has no effect on the strain energy. Under Corollary 6, such component would induce a component of the displacement field $\boldsymbol{\delta}$ that represents a rigid body motion (in other words, a component that is a combination of the translation and rotation vectors $\boldsymbol{w}_x$, $\boldsymbol{w}_y$, and $\boldsymbol{w}_r$). For strain energy maximization over unit displacement vectors, we can exclude any unit displacement $\bar{\boldsymbol{\delta}}$ that has a non-zero component $\boldsymbol{\xi} \in \mathrm{null}(C)$. This is because the unit displacement $(\bar{\boldsymbol{\delta}} - \boldsymbol{\xi})/\|\bar{\boldsymbol{\delta}} - \boldsymbol{\xi}\|$, which is orthogonal to $\mathrm{null}(C)$, would increase the strain energy by a factor of $1/\|\bar{\boldsymbol{\delta}} - \boldsymbol{\xi}\|^2 - 1$.

Hence we need only consider a unit $\bar{\boldsymbol{\delta}}$ such that $\bar{\boldsymbol{\delta}} \perp \mathrm{null}(C)$. Given the symmetry of C, $\bar{\boldsymbol{\delta}} \perp \mathrm{null}(C)$ is equivalent to $\bar{\boldsymbol{\delta}} \in \mathrm{row}(C) = \mathrm{col}(C)$.

For optimization we use the method by Horn (1987). Let $\lambda_1, \lambda_2, \ldots, \lambda_{2m-3}$ be the eigenvalues of C such that $\lambda_1 \geq \lambda_2 \geq \cdots \geq \lambda_{2m-3} > 0$. Let $\hat{\boldsymbol{u}}_1, \hat{\boldsymbol{u}}_2, \ldots, \hat{\boldsymbol{u}}_{2m-3}$ be the corresponding orthogonal unit eigenvectors. Decompose $\bar{\boldsymbol{\delta}}$ in terms of the eigenvectors

$$\bar{\boldsymbol{\delta}} = \alpha_1 \hat{\boldsymbol{u}}_1 + \cdots + \alpha_{2m-3} \hat{\boldsymbol{u}}_{2m-3}. \tag{32}$$

It follows from (27) that

$$U = \frac{1}{2}(\lambda_1 \alpha_1^2 + \cdots + \lambda_{2m-3} \alpha_{2m-3}^2). \tag{33}$$

The potential energy has the maximum value $\frac{1}{2}\lambda_1$ when $\bar{\boldsymbol{\delta}} = \pm \hat{\boldsymbol{u}}_1$.

Each eigenvector $\hat{\boldsymbol{u}}_i$, $1 \leq i \leq 2m-3$, results in a force vector $\bar{\boldsymbol{f}} = \lambda_i \hat{\boldsymbol{u}}_i$ that is collinear with $\hat{\boldsymbol{u}}_i$. Alternatively, let us maximize the strain energy U under the constraint $\frac{1}{2}(1 - \bar{\boldsymbol{\delta}}^T \bar{\boldsymbol{\delta}}) = 0$ using a Lagrange

multiplier λ. This reduces to an unconstrained problem of maximizing the Lagrangian

$$L = U + \lambda \cdot \frac{1}{2}(1 - \bar{\boldsymbol{\delta}}^T \bar{\boldsymbol{\delta}}). \tag{34}$$

The first order necessary condition yields

$$\boldsymbol{f} = C\bar{\boldsymbol{\delta}} = \lambda \bar{\boldsymbol{\delta}}, \tag{35}$$

which states that λ is an eigenvalue and $\bar{\boldsymbol{\delta}}$ the corresponding eigenvector, i.e., one of $\hat{\boldsymbol{u}}_i$, $1 \leq i \leq 2m-3$.

Theorem 7 *The strain energy U due to unit displacement $\bar{\boldsymbol{\delta}}$ has no local maximum other than the absolute maximum.*

Proof By contradiction. Suppose a local minimum is achieved at some unit eigenvector $\hat{\boldsymbol{u}}_k$ such that $\lambda_k < \lambda_1$. Show that U can be increased locally on the unit hypersphere $\|\bar{\boldsymbol{\delta}}\| = 1$. Details omitted. □

To be "stable", a unit displacement $\bar{\boldsymbol{\delta}}$ needs to yield a local maximum value of U. Under the above theorem, the only stable displacements are in the subspace spanned by $\hat{\boldsymbol{u}}_1, \ldots, \hat{\boldsymbol{u}}_l$, where $l \geq 1$ and $\lambda_1 = \cdots = \lambda_l > \lambda_{l+1}$.

In the context of grasping, the contact force at a node must be compressive.[6] The corresponding nodal displacement cannot have a component along the outward contact normal. This excludes an extremizing eigenvector $\hat{\boldsymbol{u}}_i$ that contains both inward and outward nodal displacements.[7] If $\hat{\boldsymbol{u}}_i$ consists of outward nodal displacements only, then $-\hat{\boldsymbol{u}}_i$ should be considered.

4.2 Pure Deformation

We look at a $\bar{\boldsymbol{\delta}}$ that will induce a displacement field $\boldsymbol{\delta}$ according to (26) that contains no rigid body motion. This requires $\bar{\boldsymbol{\delta}} \perp \mathrm{null}(K)$. Two reasons interest us here. First, a rigid body displacement (even just a translation) is unnecessary from the perspective of grasping. Second, since a large rotation cannot be modeled by the linear elasticity theory, it is desirable if any rotation is prevented.

The null space of the stiffness matrix K is spanned by $\boldsymbol{v}_{2n-2}, \boldsymbol{v}_{2n-1}, \boldsymbol{v}_{2n}$. Perform left multiplications of these vectors with (26):

$$\begin{aligned}
(\boldsymbol{v}_{2n-2}, \boldsymbol{v}_{2n-1}, \boldsymbol{v}_{2n})^T \boldsymbol{\delta} &= (\boldsymbol{v}_{2n-2}, \boldsymbol{v}_{2n-1}, \boldsymbol{v}_{2n})^T V \begin{pmatrix} \bar{\boldsymbol{v}}_1^T C/\lambda_1 \\ \vdots \\ \bar{\boldsymbol{v}}_{2n-3}^T C/\lambda_{2n-3} \\ E^T \end{pmatrix} \bar{\boldsymbol{\delta}} \\
&= (\boldsymbol{0}, I_3) \begin{pmatrix} \bar{\boldsymbol{v}}_1^T C/\lambda_1 \\ \vdots \\ \bar{\boldsymbol{v}}_{2n-3}^T C/\lambda_{2n-3} \\ E^T \end{pmatrix} \bar{\boldsymbol{\delta}} \\
&= E^T \bar{\boldsymbol{\delta}}.
\end{aligned}$$

[6] Sticky fingers are not considered in this paper, as in the robot grasping literature.

[7] In such a case, the eigenvector corresponding to the second largest eigenvalue will be considered (and checked), and so on.

Equivalently, we have

$$\begin{aligned}\{\bar{\boldsymbol{\delta}} \mid \boldsymbol{\delta} \perp \mathrm{null}(K)\} &= \{\bar{\boldsymbol{\delta}} \mid \bar{\boldsymbol{\delta}} \in \mathrm{null}(E^T)\} \\ &= \{\bar{\boldsymbol{\delta}} \mid \bar{\boldsymbol{\delta}} \perp \mathrm{col}(E)\}. \\ &= \mathrm{col}(AC). \qquad \text{(by (v) of Theorem 5)} \end{aligned} \tag{36}$$

4.3 Stable and Pure Squeezes

To prepare for an introduction to two-finger grasps, from now on we will focus on the special case of two contact nodes $\boldsymbol{p}_i$ and $\boldsymbol{p}_j$. Define the unit vector

$$\hat{\boldsymbol{u}} = \begin{pmatrix} \boldsymbol{\delta}_i \\ \boldsymbol{\delta}_j \end{pmatrix} = \frac{1}{\sqrt{2}\|\boldsymbol{p}_i - \boldsymbol{p}_j\|} \begin{pmatrix} \boldsymbol{p}_j - \boldsymbol{p}_i \\ \boldsymbol{p}_i - \boldsymbol{p}_j \end{pmatrix}. \tag{37}$$

It specifies the two nodes moving toward each other.

Theorem 8 *In the case of only two contact nodes $\boldsymbol{p}_i$ and $\boldsymbol{p}_j$, the vector $\hat{\boldsymbol{u}}$ is orthogonal to* $\mathrm{null}(C)$. *Moreover,*

$$C = \frac{1}{\hat{\boldsymbol{u}}^T A \hat{\boldsymbol{u}}} \hat{\boldsymbol{u}}\hat{\boldsymbol{u}}^T. \tag{38}$$

Proof By (29), $\mathrm{null}(C)$ is spanned by $\bar{\boldsymbol{w}}_x = (1,0,1,0)^T$, $\bar{\boldsymbol{w}}_y = (0,1,0,1)^T$, and $\bar{\boldsymbol{w}}_r = (-y_i, x_i, -y_j, x_j)^T$. The vector

$$\boldsymbol{\xi} = \begin{pmatrix} \boldsymbol{p}_j - \boldsymbol{p}_i \\ \boldsymbol{p}_i - \boldsymbol{p}_j \end{pmatrix}$$

is orthogonal to this space, for

$$\begin{aligned} \boldsymbol{\xi}^T(\bar{\boldsymbol{w}}_x, \bar{\boldsymbol{w}}_y) &= (0,0); \\ \boldsymbol{\xi}^T \bar{\boldsymbol{w}}_r &= \boldsymbol{p}_i \times (\boldsymbol{p}_j - \boldsymbol{p}_i) + \boldsymbol{p}_j \times (\boldsymbol{p}_i - \boldsymbol{p}_j) \\ &= \boldsymbol{p}_i \times \boldsymbol{p}_j + \boldsymbol{p}_j \times \boldsymbol{p}_i \\ &= 0. \end{aligned}$$

Thus, $\hat{\boldsymbol{u}} = \boldsymbol{\xi}/\|\boldsymbol{\xi}\| \perp \mathrm{null}(C)$.

Because $\mathrm{null}(C)$ has rank 3. The 4×4 matrix C must have a one-dimensional row space (and thus a one-dimensional column space due to symmetry). Therefore, the four columns of C must be collinear with $\hat{\boldsymbol{u}}$. We write

$$C = \hat{\boldsymbol{u}}\boldsymbol{c}^T,$$

and perform the following steps of reasoning:

$$\begin{aligned} C = C^T &\Rightarrow \hat{\boldsymbol{u}}\boldsymbol{c}^T = \boldsymbol{c}\hat{\boldsymbol{u}}^T \\ &\Rightarrow \hat{\boldsymbol{u}}(\boldsymbol{c}^T\hat{\boldsymbol{u}}) = \boldsymbol{c}(\hat{\boldsymbol{u}}^T\hat{\boldsymbol{u}}) = \boldsymbol{c} \qquad \text{(right multiplication with } \hat{\boldsymbol{u}}) \\ &\Rightarrow \boldsymbol{c} = \lambda\hat{\boldsymbol{u}}, \end{aligned}$$

where $\lambda = \boldsymbol{c}^T\hat{\boldsymbol{u}}$. This establishes

$$C = \lambda\hat{\boldsymbol{u}}\hat{\boldsymbol{u}}^T. \tag{39}$$

Meanwhile, from (28) we have

$$\begin{array}{rcll} AC + BE^T = I_4 & \Rightarrow & A(\lambda \hat{\boldsymbol{u}}\hat{\boldsymbol{u}}^T) + BE^T = I_4 & \\ & \Rightarrow & \lambda A\hat{\boldsymbol{u}} + B(E^T\hat{\boldsymbol{u}}) = \hat{\boldsymbol{u}} & \text{(right multiplications with } \hat{\boldsymbol{u}}\text{)} \\ & \Rightarrow & \lambda \hat{\boldsymbol{u}}^T A\hat{\boldsymbol{u}} + (\hat{\boldsymbol{u}}^T B)(E^T\hat{\boldsymbol{u}}) = \hat{\boldsymbol{u}}^T\hat{\boldsymbol{u}} & \text{(left multiplications with } \hat{\boldsymbol{u}}^T\text{)} \\ & \Rightarrow & \lambda \hat{\boldsymbol{u}}^T A\hat{\boldsymbol{u}} = 1. & \text{(since } \hat{\boldsymbol{u}} \perp \mathrm{null}(C) = \mathrm{col}(B)\text{)} \end{array}$$

The last equation implies $\hat{\boldsymbol{u}}^T A\hat{\boldsymbol{u}} \neq 0$ and $\lambda = 1/(\hat{\boldsymbol{u}}^T A\hat{\boldsymbol{u}})$. Equation (38) then follows from a substitution for λ into (39).

□

We refer to the squeeze specified by $\boldsymbol{\delta} = \rho\hat{\boldsymbol{u}}$, $\rho > 0$, as a *stable squeeze*. Via a substitution of (38) into (27), we rewrite the strain energy as

$$\begin{aligned} U_s &= \frac{1}{2}\rho^2 \hat{\boldsymbol{u}}^T C\hat{\boldsymbol{u}} \\ &= \frac{1}{2}\rho^2 \hat{\boldsymbol{u}}^T \left(\frac{1}{\hat{\boldsymbol{u}}^T A\hat{\boldsymbol{u}}}\hat{\boldsymbol{u}}\hat{\boldsymbol{u}}^T\right)\hat{\boldsymbol{u}} \\ &= \frac{\rho^2}{2\hat{\boldsymbol{u}}^T A\hat{\boldsymbol{u}}}. \end{aligned} \tag{40}$$

Similarly, with a substitution of (38) into (25), in particular, $\bar{\boldsymbol{f}} = C\bar{\boldsymbol{\delta}}$, with $\bar{\boldsymbol{\delta}} = \rho\hat{\boldsymbol{u}}$, the nodal contact forces are

$$\bar{\boldsymbol{f}} = \frac{\rho\hat{\boldsymbol{u}}}{\hat{\boldsymbol{u}}^T A\hat{\boldsymbol{u}}}. \tag{41}$$

A stable squeeze does not guarantee that the resulting displacement field $\boldsymbol{\delta}$ has no rigid body motion component. From Section 4.2, a squeeze from the set $\mathrm{col}(AC)$ causes pure deformation on the object with no rigid body motion. We refer to it as a *pure squeeze*. Since $AC = A\hat{\boldsymbol{u}}\hat{\boldsymbol{u}}^T/(\hat{\boldsymbol{u}}^T A\hat{\boldsymbol{u}})$ following Theorem 8, we infer that $\mathrm{col}(AC)$ is spanned by $A\hat{\boldsymbol{u}}$. Let

$$\hat{\boldsymbol{v}} = A\hat{\boldsymbol{u}}/\|A\hat{\boldsymbol{u}}\| = A\begin{pmatrix}\boldsymbol{p}_j - \boldsymbol{p}_i \\ \boldsymbol{p}_i - \boldsymbol{p}_j\end{pmatrix} \Bigg/ \left\| A\begin{pmatrix}\boldsymbol{p}_j - \boldsymbol{p}_i \\ \boldsymbol{p}_i - \boldsymbol{p}_j\end{pmatrix} \right\|. \tag{42}$$

We derive the resulting strain energy and contact forces for a pure squeeze specified by $\rho\hat{\boldsymbol{v}}$, $\rho > 0$, as follows:

$$\begin{aligned} U_p &= \frac{1}{2}\rho^2 \hat{\boldsymbol{v}}^T C\hat{\boldsymbol{v}} \\ &= \frac{1}{2}\rho^2 \frac{(A\hat{\boldsymbol{u}})^T}{\|A\hat{\boldsymbol{u}}\|} \cdot \frac{1}{\hat{\boldsymbol{u}}^T A\hat{\boldsymbol{u}}}\hat{\boldsymbol{u}}\hat{\boldsymbol{u}}^T \cdot \frac{A\hat{\boldsymbol{u}}}{\|A\hat{\boldsymbol{u}}\|} \\ &= \frac{\rho^2 \hat{\boldsymbol{u}}^T A\hat{\boldsymbol{u}}}{2\hat{\boldsymbol{u}}^T AA\hat{\boldsymbol{u}}}, \end{aligned} \tag{43}$$

$$\begin{aligned} \bar{\boldsymbol{f}} &= \frac{1}{\hat{\boldsymbol{u}}^T A\hat{\boldsymbol{u}}}\hat{\boldsymbol{u}}\hat{\boldsymbol{u}}^T \cdot \frac{\rho A\hat{\boldsymbol{u}}}{\|A\hat{\boldsymbol{u}}\|} \\ &= \frac{\rho\hat{\boldsymbol{u}}}{\|A\hat{\boldsymbol{u}}\|}. \end{aligned} \tag{44}$$

Figure 3 compares the effects of the unit stable squeeze $\hat{\boldsymbol{u}}$ and the unit pure squeeze $\hat{\boldsymbol{v}}$ on the object in Figure 2 with the same contact nodes $\boldsymbol{p}_i$ and $\boldsymbol{p}_j$. For clarity, all solid objects from now on will be drawn

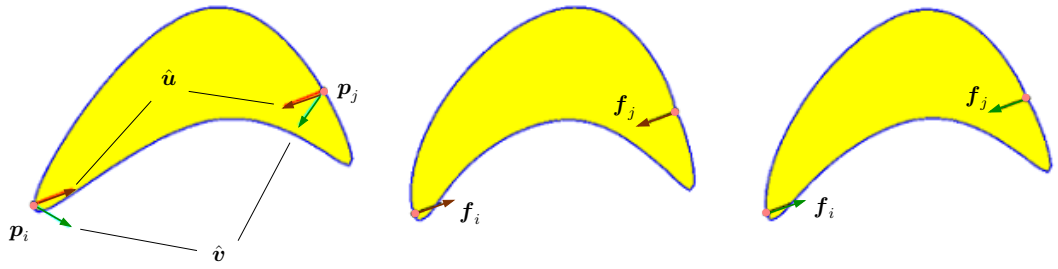

Figure 3: Comparison between unit stable and pure squeezes: (a) original shape from Figure 2 shown with a stable squeeze $\hat{\boldsymbol{u}} = (0.65923,\ 0.25577, -0.65923, -0.25577)^T$ in brown and a pure squeeze $\hat{\boldsymbol{v}} = (0.79644, -0.49167, -0.20702, -0.28477)^T$ in green; (b) deformed shape under $\hat{\boldsymbol{u}}$ with resulting contact forces $\boldsymbol{f}_i = (0.90772, 0.35218)^T$ and $\boldsymbol{f}_j = (-0.90772, -0.35218)^T$; (c) deformed shape under $\hat{\boldsymbol{v}}$ with $\boldsymbol{f}_i = (0.55243, 0.21433)^T$ and $\boldsymbol{f}_j = (-0.55243, -0.21433)^T$.

non-meshed but filled with the yellow color. Imagine that the squeezes in the figure are performed by two point fingers placed at these two nodes. While under $\hat{\boldsymbol{u}}$ the fingers drive the two contact points toward each other, under $\hat{\boldsymbol{v}}$ they bend the object to prevent any Euclidean motion, in a "smart" way by exerting smaller contact forces.

We refer to ρ in a squeeze $\rho\hat{\boldsymbol{u}}$ or $\rho\hat{\boldsymbol{v}}$ as the *squeeze depth*. This is different from the relative distance by which one finger moves toward the other during the squeeze. Such relative distance is $\sqrt{2}\rho$ for a stable squeeze, and $\rho\sqrt{\|\boldsymbol{v}_i - \boldsymbol{v}_j\|^2}$, where $\hat{\boldsymbol{v}} = (\boldsymbol{v}_i^T, \boldsymbol{v}_j^T)^T$, for a pure squeeze.

A squeeze specified by $(\boldsymbol{\delta}_i^T, \boldsymbol{\delta}_j^T)^T$ is equivalent to that of fixing one contact, say, $\boldsymbol{p}_i$, while moving the other contact $\boldsymbol{p}_j$ by $\boldsymbol{\delta}_j - \boldsymbol{\delta}_i$. To see this, observe that

$$\begin{pmatrix} \boldsymbol{\delta}_i \\ \boldsymbol{\delta}_j \end{pmatrix} = \begin{pmatrix} \boldsymbol{\delta}_i \\ \boldsymbol{\delta}_i \end{pmatrix} + \begin{pmatrix} \boldsymbol{0} \\ \boldsymbol{\delta}_j - \boldsymbol{\delta}_i \end{pmatrix}.$$

The displacement is carried out in two steps. First, translate both nodes by $\boldsymbol{\delta}_i$. Under Corollary 6, this is a rigid body motion that yields no deformation. After the translation, move the node $\boldsymbol{p}_j$ by $\boldsymbol{\delta}_j - \boldsymbol{\delta}_i$.

5 Squeeze Grasping with Rounded Fingers and Contact Mode Analysis

A *squeeze grasp* of a deformable object using two fingers is achieved by translating the fingers to squeeze the object. In this section, we investigate squeeze grasps with frictional contacts. A solid object caves in under a squeeze. With point fingers, this would create tangential discontinuities (and piercing effects), and in theory, infinite displacements at the contact points.[8] They are assumed in grasping hollow elastic objects where contact areas are small. This will be deferred to Section 7.

Curved fingertips are assumed in grasping solid objects for both practicality and analysis purposes. They make area contacts with an object being grasped. Here we consider two grasping fingers $\mathcal{F}_1$ and $\mathcal{F}_2$ that have identical semicircular tips with radius r. They are initially placed on an object at its boundary nodal points, say, $\boldsymbol{p}_i$ and $\boldsymbol{p}_j$, respectively, as shown in Figure 4(a). Denote the placement by $\mathcal{G}(\boldsymbol{p}_i, \boldsymbol{p}_j)$. We assume that during the grasp the object will not make contact with a finger outside its semicircular tip.

[8] In Flamant's problem (Lurie 2005, pp. 570–575), in the two-dimensional space a concentrated normal force acting on a half-plane can create infinite displacements at both a location at infinity and one that approaches the point of force application.

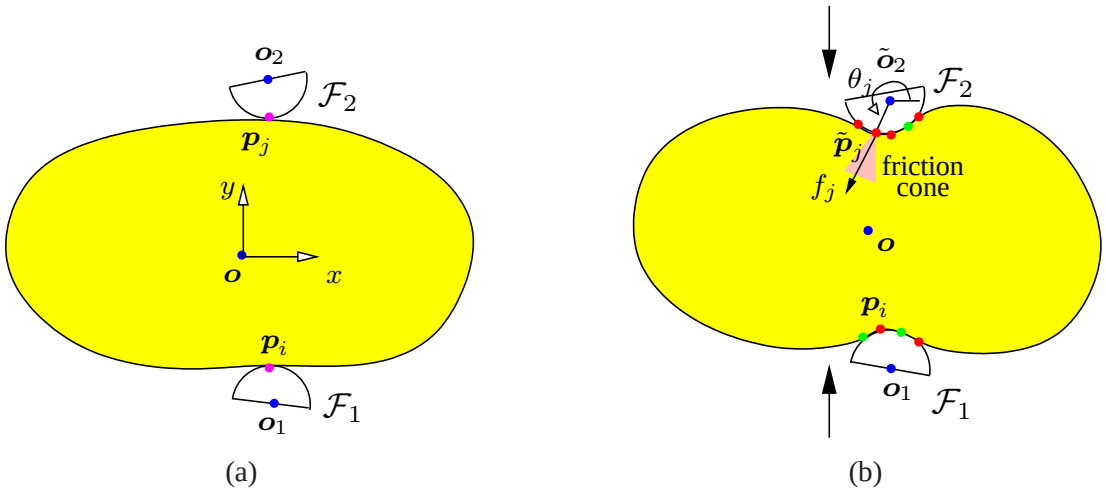

Figure 4: Object (a) before and (b) after a squeeze grasp.

A frame is placed at the centroid $\boldsymbol{o}$ of all nodes in the mesh representing the object. The finger's orientation is irrelevant due to rotational symmetry of its tip. The two fingertip centers $\boldsymbol{o}_1$ and $\boldsymbol{o}_2$ are located on the outward normals at $\boldsymbol{p}_i$ and $\boldsymbol{p}_j$, respectively.

For squeezing to be possible, the object must be initially restrained by $\mathcal{F}_1$ and $\mathcal{F}_2$ under contact friction from any rigid body displacement. This requires the finger placement $\mathcal{G}(\boldsymbol{p}_i, \boldsymbol{p}_j)$ to be in a "force-closure" configuration. By the result of Nguyen (1988), the line segment $\overline{\boldsymbol{p}_i\boldsymbol{p}_j}$ must lie within the contact friction cones at $\boldsymbol{p}_i$ and $\boldsymbol{p}_j$. We can immediately reject a finger placement $\mathcal{G}(\boldsymbol{p}_i, \boldsymbol{p}_j)$ that violates this constraint.

After some squeeze, the configuration is shown in Figure 4(b), where red dots represent the contact nodes that are (hypothetically) sticking on the fingertips and green dots represent those nodes that are sliding.

5.1 Termination Criteria

A squeeze continues until one of the following three situations arises:

(i) One of the grasping fingers starts to slip at its contact. This happens when all contact nodes with the finger are slipping (in one direction).

(ii) The strain at some node exceeds the value ϵ^* corresponding to the material's proportional limit.

(iii) The object can be picked up against its weight vertically from the plane (if this is the objective).

The maximum squeeze depth ρ^* should be the smallest value at which one of the above situations occurs. The grasp is a success if the first two situations do not occur before a specified squeeze depth is reached or before the third situation occurs. If a pickup is not the objective and no squeeze depth is specified, the squeeze may stop before slip happens or the strain exceeds ϵ^* at some node.

Finally, to pick up the object from the horizontal plane, the vertical frictional forces generated by the two fingers at their contacts must balance the object's weight w. Let $\mathbb{I}$ be the set of indices of the nodes in contact with the finger $\mathcal{F}_1$, and $\mathbb{J}$ the set of indices of those in contact with the finger $\mathcal{F}_2$. Denote by $\boldsymbol{n}_k$ and $\boldsymbol{t}_k$ the unit normal and tangent at a contact node $\boldsymbol{p}_k$, $k \in \mathbb{I} \cup \mathbb{J}$, on the deformed shape. Under Coulomb's friction

law, the vertical frictional force at $\boldsymbol{p}_k$ is of magnitude at most $c_k = \sqrt{\mu^2(\boldsymbol{f}_k \cdot \boldsymbol{n}_k)^2 - (\boldsymbol{f}_k \cdot \boldsymbol{t}_k)^2}$, where μ is the coefficient of friction. Then the object can be picked up if both $\sum_{k\in\mathbb{I}} c_k$ and $\sum_{l\in\mathbb{J}} c_l$ exceed $\frac{w}{2\mu}$.[9]

5.2 Contact Configuration

As the squeeze in Figure 4(a) begins, some boundary nodal points may come into contact with the fingertips, as illustrated in Figure 4(b), while others may break contact with them. A node in contact may be sticking to a fingertip or it may be sliding on it. The *contact configuration* at a squeeze depth ρ describes which nodal points are in contact, and among them, which are sticking and which are sliding.

Knowing a contact configuration is critical because it yields some position and force constraints that will be needed by FEM to compute the deformed shape for the current squeeze depth. This will allow us to track the change in the contact configuration as the squeeze continues.

A squeeze is represented by some displacement $\rho\hat{\boldsymbol{u}}$ or $\rho\hat{\boldsymbol{v}}$, where $\hat{\boldsymbol{u}}$ or $\hat{\boldsymbol{v}}$ is calculated from the initial contact points according to (37) or (42). The magnitude ρ will be sequenced into $\rho_0 = 0 < \rho_1 < \cdots$ such that at $\rho = \rho_l$ some event happens to trigger a change in the contact configuration. Under the contact configuration at ρ_l, we evaluate the changes in the contact forces $\bar{\boldsymbol{f}}$ and the displacements $\boldsymbol{\delta}$ of all nodes using the FEM for $\rho > \rho_l$, and predict the squeeze depth ρ_{l+1} at which the next event will happen.

At ρ_l, the following two index sets are maintained for the nodes that are in contact with the fingers:

$$\begin{aligned} \mathbb{T} &= \{k \mid \text{the node } \boldsymbol{p}_k \text{ sticks on a finger}\}, \\ \mathbb{P} &= \{k \mid \text{the node } \boldsymbol{p}_k \text{ slides on a finger}\}. \end{aligned}$$

They are referred to as the *contact sets*. Now, increase ρ by $\xi\hat{\boldsymbol{u}}$ (or $\xi\hat{\boldsymbol{v}}$), for small $\xi > 0$. Suppose that $\mathbb{T}$ and $\mathbb{P}$ do not change as ρ varies within $[\rho_l, \rho_l + \xi)$.

For $k \in \mathbb{T} \cup \mathbb{P}$, denote by θ_k the polar angle of the node $\boldsymbol{p}_k$ with respect to the center of the fingertip that it is in contact with. See Figure 4(b) for an illustration on $\boldsymbol{p}_j$. Denote by $\boldsymbol{\delta}_k^{(l)}$, $\boldsymbol{f}_k^{(l)}$ and $\theta_k^{(l)}$ the values of $\boldsymbol{\delta}_k$, $\boldsymbol{f}_k$, and θ_k, respectively, when $\rho = \rho_l$. We can determine the change $\Delta\boldsymbol{\delta}_k$ in $\boldsymbol{\delta}_k$ at $\rho = \rho_l + \xi$ as follows:

$$\Delta\boldsymbol{\delta}_k = \xi\hat{\boldsymbol{t}} + r \begin{pmatrix} \cos\theta_k - \cos\theta_k^{(l)} \\ \sin\theta_k - \sin\theta_k^{(l)} \end{pmatrix}, \tag{45}$$

where $\hat{\boldsymbol{t}}$ is the first or the last two entries from $\hat{\boldsymbol{u}}$ (or $\hat{\boldsymbol{v}}$) depending on $\boldsymbol{p}_k$ is in contact with $\mathcal{F}_1$ or $\mathcal{F}_2$.

A node $\boldsymbol{p}_k$ in sticking contact imposes a position constraint on deformation such that $\theta_k = \theta_k^{(l)}$. If $\boldsymbol{p}_k$ slips, then the contact force $\boldsymbol{f}_k = \boldsymbol{f}_k^{(l)} + \Delta\boldsymbol{f}_k$ must stay on one edge of the friction cone at $\boldsymbol{p}_k$ as the node moves. Let $\phi = \tan^{-1}\mu$, where μ is the coefficient of contact friction. This imposes a force constraint:

$$\left(\boldsymbol{f}_k^{(l)} + \Delta\boldsymbol{f}_k\right) \times \begin{pmatrix} \cos(\theta_k \pm \phi) \\ \sin(\theta_k \pm \phi) \end{pmatrix} = 0, \tag{46}$$

where the sign '$+$' or '$-$' can be determined either from the previous step or using hypothesis-and-test.

Denote by $C^{(l)}$ the value of the reduced stiffness matrix C that is computed based on the current contact set $\mathbb{T} \cup \mathbb{P}$. We gather all $\Delta\boldsymbol{\delta}_k$, $k \in \mathbb{T} \cup \mathbb{P}$, into a vector $\Delta\bar{\boldsymbol{\delta}}$. Due to its linearity, the equation $\bar{\boldsymbol{f}} = C\bar{\boldsymbol{\delta}}$ as part of (25) implies the change in $\bar{\boldsymbol{f}}$ to be $\Delta\bar{\boldsymbol{f}} = C^{(l)}\Delta\bar{\boldsymbol{\delta}}$. Substitute the expression for $\Delta\boldsymbol{f}_k$, $k \in \mathbb{P}$, into (46). This yields an equation linear in ξ and quadratic in $\cos\theta_t$ and $\sin\theta_t$, for every node $\boldsymbol{p}_t$, $t \in \mathbb{P}$. There are a

[9] Assume that the torques generated by the fingers are small and negligible due to the small contact areas relative to the object's size.

total of $|\mathbb{P}|$ such equations that form a system S in the same number of variables θ_t. Given a value of ξ, we can solve for these θ_ts. Since ξ is small, Newton's method has fast convergence with the initial values $\theta_t^{(l)}$. Hence $\boldsymbol{\delta}$ and $\bar{\boldsymbol{f}}$ are updated.

With θ_k known for every node $\boldsymbol{p}_k$ in sliding contact, we can also determine the derivative $\frac{d\theta_k}{d\xi}$, which will be used in checking whether the node switches from slip to stick. Differentiate both sides of every equation in the system S with respect to ξ. This yields a new linear system of $|\mathbb{P}|$ equations in $|\mathbb{P}|$ derivatives $\frac{d\theta_t}{d\xi}$, $t \in \mathbb{P}$. Simply solve the system.

5.3 Contact Event Detection

We track the movements of all sliding nodes as ξ increases until an event occurs to trigger a change in one or both of the contact sets $\mathbb{T}$ and $\mathbb{P}$. There are four types of events: a node comes into contact with a finger (event A); contact breaks at a node (event B); contact at a node switches from stick to slip (event C); and contact at a node switches from slip to stick (event D).

We check for the values of ξ at which all possible events could happen, and select the minimum. The next event occurs at $\rho^{(l+1)} = \rho^{(l)} + \xi$.

a) Event A — New Contact A boundary node $\boldsymbol{p}_k$ in its deformed position $\tilde{\boldsymbol{p}}_k$ comes into contact with one of the two fingers. This happens when its distance to the center of the contacting fingertip reduces to r, or equivalently, when the following condition holds:

$$\left(\tilde{\boldsymbol{p}}_k - \boldsymbol{o}_i^{(l)} + \xi\hat{\boldsymbol{t}}\right) \cdot \left(\tilde{\boldsymbol{p}}_k - \boldsymbol{o}_i^{(l)} + \xi\hat{\boldsymbol{t}}\right) = r^2, \tag{47}$$

where $\boldsymbol{o}_i^{(l)}$ is the position of the fingertip's center at $\rho = \rho_l$.

To determine the mode of contact for $\boldsymbol{p}_k$, we first hypothesize that it sticks, apply a small extra squeeze, and check if the resulting contact force $\boldsymbol{f}_k$ will stay inside the friction cone. If not, the node slips. Add k to $\mathbb{T}$ or $\mathbb{P}$ accordingly.

b) Event B — Contact Break As ξ increases, the force $\boldsymbol{f}_k$ at a node $\boldsymbol{p}_k$ varies inside or on one edge of the contact friction cone. When its magnitude reduces to zero, it is about to point into the finger. The contact breaks when

$$\|\boldsymbol{f}_k\| = 0. \tag{48}$$

Remove k from either $\mathbb{P}$ or $\mathbb{T}$ that contains it.

c) Event C — Stick to Slip When the contact force $\boldsymbol{f}_k$ applied on a sticking node $\boldsymbol{p}_k$ is rotating out of the inward friction cone (see Figure 4(b)) as ρ increases, the contact mode switches to slip. The rotation of the force $\boldsymbol{f}_k$ at the moment is indicated by its derivative with respect to ξ. We need to check the conditions:

$$\boldsymbol{f}_k \times \begin{pmatrix}\cos(\theta_k \mp \phi)\\ \sin(\theta_k \mp \phi)\end{pmatrix} = 0 \ \text{ and } \ \mp \frac{d\boldsymbol{f}_k}{d\xi} \times \begin{pmatrix}\cos(\theta_k \mp \phi)\\ \sin(\theta_k \mp \phi)\end{pmatrix} > 0 \tag{49}$$

for reaching the left (sign '$-$') or right ('$+$') edge, respectively. Remove k from $\mathbb{T}$ and add it to $\mathbb{P}$.

d) Event D — Slip to Stick As ξ increases, the contact node $\boldsymbol{p}_k$ slides, and its polar angle θ_k with respect to the corresponding fingertip's center varies. Slip changes to stick when

$$\frac{d\theta_k}{d\xi} = 0. \tag{50}$$

In this case, remove k from $\mathbb{P}$ and add it to $\mathbb{T}$.

Algorithm 1 Two-Finger Squeeze

Input: initial contacts $\boldsymbol{p}_i$ and $\boldsymbol{p}_j$, squeeze type and depth ρ^*

1: $\rho \leftarrow 0$
2: initialize $\mathbb{T}$ and $\mathbb{P}$ by determining if $\boldsymbol{p}_i$ and $\boldsymbol{p}_j$ stick or slip
3: **while** $\rho < \rho^*$ and no finger slips and the proportional limit ϵ^* is not exceeded at any node **do**
4: $\quad \xi \leftarrow 0$
5: $\quad$ compute the matrix C based on $\mathbb{T} \cup \mathbb{P}$
6: $\quad$ **repeat**
7: $\quad\quad \xi \leftarrow \xi + h$
8: $\quad\quad$ solve for all θ_k, $k \in \mathbb{P}$, together from $|P|$ equations (46) using Newton's method with their current values as the initial estimates
9: $\quad\quad$ set $\Delta\boldsymbol{\delta}_k$, $\forall\, k \in \mathbb{T} \cup \mathbb{P}$, according to (45)
10: $\quad\quad \Delta\bar{\boldsymbol{f}} \leftarrow C\Delta\bar{\boldsymbol{\delta}}$
11: $\quad$ **until** one of (47)–(50) is true
12: $\quad$ **if** event A occurs **then**
13: $\quad\quad$ determine the mode of the new contact
14: $\quad$ **end if**
15: $\quad$ update $\mathbb{P}$ or $\mathbb{T}$ according to the event type
16: $\quad \rho \leftarrow \rho + \xi$
17: **end while**
18: **if** either finger slips **then**
19: $\quad$ **return** squeeze failure
20: **end if**

Equations (47)–(50) each requires $O(n)$ time to set up, and $O(1)$ time to solve for ξ. All events except Event A need only be checked over the contact nodes. The size of $\mathbb{P} \cup \mathbb{T}$ is bounded by $2\pi r$ divided by the average arc length between two adjacent boundary nodes. It is typically very small. Because the squeeze is also small, it often suffices to check Event A on a few nodes in the neighborhoods of the outermost contact nodes. In summary, $O(1)$ nodes are checked for the events at $\rho^{(l)}$ at the time cost of $O(n)$.

5.4 The Squeeze Algorithm

The algorithm performs a squeeze grasp operation given some squeeze depth ρ^*. It starts at $\rho = 0$. At step l, it hypothesizes each of the four events for each of the current contact nodes (and their adjacent nodes), and computes the extra squeeze distance ξ for the hypothesized event to happen. Then it selects the minimum such distance $\xi_{\min}$, and let $\rho_{l+1} = \rho_l + \xi_{\min}$.

Each of the event conditions (47)–(50) involves solving for ξ and the polar angles θ_t of all nodes $\boldsymbol{p}_t$ in sliding contact from the event condition and the corresponding $|\mathbb{P}|$ equations. Solution of this system of $|\mathbb{P}| + 1$ nonlinear equations is not easy, and repeatedly doing so would be too time consuming. For these reasons, we resort to a numerical routine described in Algorithm 1. It increments the squeeze depth ρ by setting ξ to a small step size h (which allows Newton's method to converge fast in computing θ_t for $t \in \mathbb{P}$).

On line 11 checking whether an event happens becomes testing either an inequality or whether an expression changes sign. For instance, we check the inequality

$$\left(\tilde{\boldsymbol{p}}_k - \boldsymbol{o}_2^{(l)} + \begin{pmatrix} 0 \\ \xi \end{pmatrix}\right) \cdot \left(\tilde{\boldsymbol{p}}_k - \boldsymbol{o}_2^{(l)} + \begin{pmatrix} 0 \\ \xi \end{pmatrix}\right) \leq r^2.$$

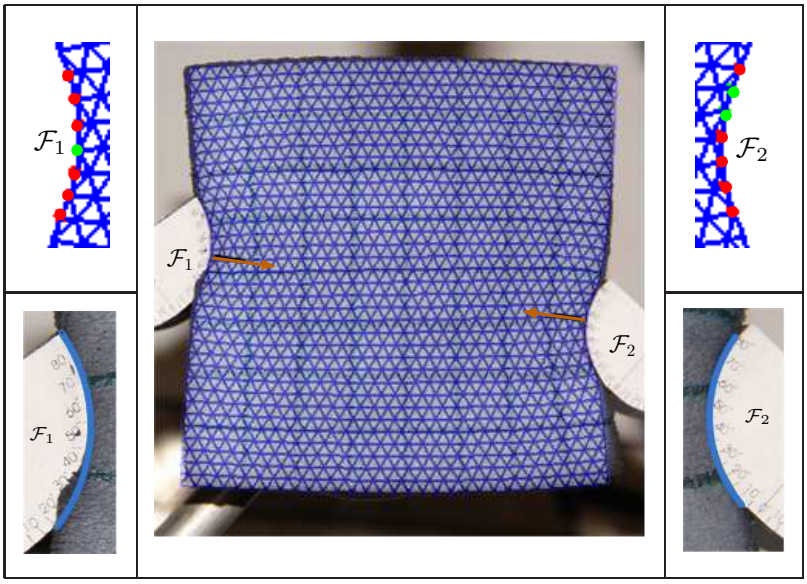

Table 1: Grasped foam rubber square superposed by its deformed mesh (center): the contact segments from simulation (row 1) composed of sticking nodes (red) and sliding nodes (green); the contact segments in the experiment (row 3) enlarged from the center image.

for an occurrence of event A with the node $\boldsymbol{p}_k$. When the condition holds, we use bisection to find the value $\xi \in (0, h]$ that satisfies (47).

The change in the displacement (45) of a contact node at each step is not proportional to the squeeze distance ξ, neither is the overall displacement of a node during the squeeze grasp. The strain at a node is still a linear expression of ξ but with a constant term. The maximum strain will not be achieved at the same nodes. This implies that we need to update the node with the maximum strain as ρ changes from ρ_l to ρ_{l+1} in case ρ^* might cause the proportional limit to be exceeded.

Most objects have proportional limits that are beyond what the squeeze forces need to generate in order to pick up the objects. For this reason, we will only pay attention to the possibly of finger sliding from now on.

5.5 Experiment with Foam Rubber Objects

A $0.1 \times 0.1 \times 0.0254$ square made of foam rubber was grasped by a three-fingered Barrett Hand. The two grasping fingers were mounted with semicircular plastic tips of radius 0.02. We measured Young's modulus $E \approx 5 \times 10^4$Pa and Poisson's ratio $\nu \approx 0.3$. The coefficient of contact friction μ between a fingertip and the foam rubber was measured to be 0.4. The measurement methods are described in Appendix B.

Table 1 compares an actual grasp configuration with its guiding simulation by Algorithm 1 from Section 5.4. Here, a stable squeeze was carried out such that the two fingers translated toward each other along the line connecting their initial contact points (aligned with the two arrows in the central image). Under the squeeze, the distance between the two initial contact points was reduced by 12%. The deformed mesh from simulation is superposed onto the real shape almost perfectly by a matching algorithm described in Appendix C. The algorithm minimized in the least-squares sense the average error per node (1.3mm for the displayed object) while filtering out the effects due to different coordinate systems used in the simulation

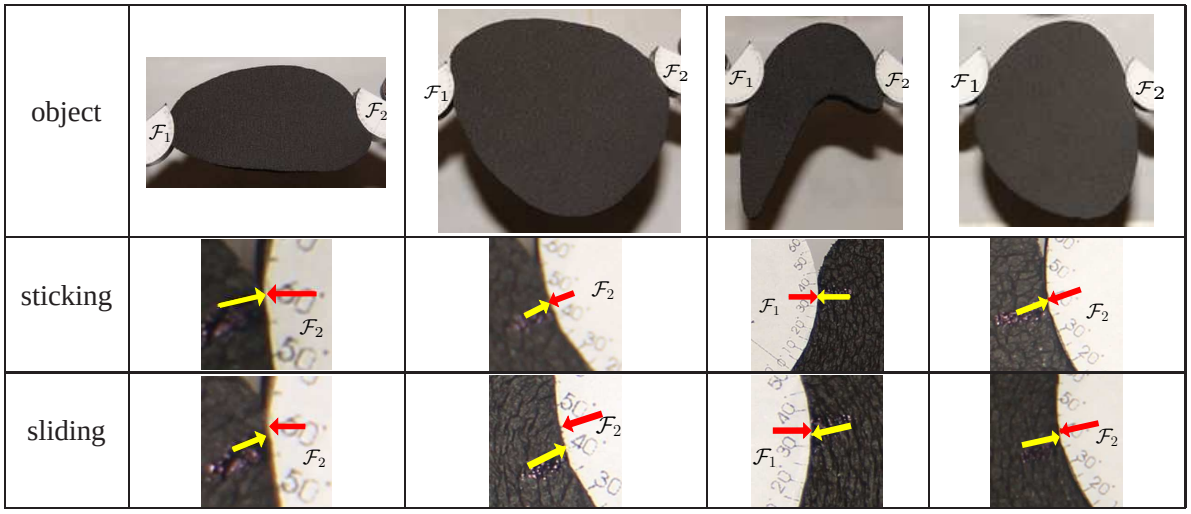

Table 2: Occurrences of Event C (stick-to-slip transition) during squeeze grasps of four objects.

and the experiment. Columns 1 and 3 in the table compare the contact regions generated by the simulation and observed in the experiment, on the left finger and the right finger, respectively.

At the end of the squeeze shown in the center, a total of 14 nodes are in contact with the fingertips. These contact nodes are shown in the first row of Figure 1. Among them, the 11 red nodes represent sticking contacts, while the 3 green nodes represent sliding contacts. In reaching the final configuration, events A had occurred 12 times, event B only 2 times (marked by the two green dots on the right fingertip $\mathcal{F}_2$). The green dot on the left fingertip $\mathcal{F}_1$ was established as a sliding contact and did not change its mode later on.

Among the four types of events introduced in Section 5, Event A of contact establishment is destined to occur (unless the squeeze depth is very small). Event B of contact breaking is so rare that it was not observed in the experiment. We suspect it to happen often with large rotations which are nonetheless beyond the scope of linear elasticity.

Event C of stick-to-slip transition was widely observed in both simulation and experiment wherever friction was insufficient. Table 2 shows some grasps during which events of this type happened. Each of columns 2–5 displays one object, using yellow and red arrows to respectively indicate movements of two points, one on the object and the other on the fingertip. These two points were shown initially in sticking contact (in row 2) and later separated from each other due to sliding (in row 3), as the squeezes continued.

Event D happened a lot less often than Event C according to our observations. This is in part because most contacts are established as sticking ones. In such a case, Event D may happen only after Event C does. In Figure 5, parts (a) and (b) show simulation results that correspond to the experiment images in the entries (2, 3) and (3, 3) in Table 2. The blue arrows mark the same node on the object that started out sticking in (a), transitioned into sliding in (b), and switched back to sticking in (c). Shown in (d) is an experiment image that displays the distance of sliding (about five degrees) on the fingertip by the same node identified with arrows in (a)–(c) from the fingertip contact location in (b), pointed at by the red arrow in (d), to the location of the new fingertip contact in (c), pointed at by the yellow arrow in (d).

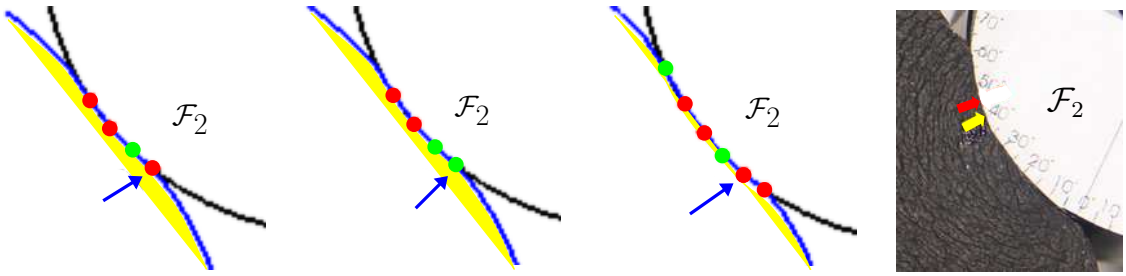

(a) (b) (c) (d)

Figure 5: Transitions of a contact from stick (a) to slip (b) to slick (c). Here (a) and (b) are the simulation results over the second object in Table 2 that correspond to its entries (2, 3) and (3, 3), respectively. In (c), the contact has stopped sliding, as also indicated by the experiment in (d).

6 Resisting an Adversary Finger

Consider a finger placement $\mathcal{G}(\boldsymbol{p}_i, \boldsymbol{p}_j)$ on the deformable object. Suppose an adversary finger $\mathcal{A}$ makes contact with the object at $\boldsymbol{p}_k$, and tries to break the grasp via a translation by $\boldsymbol{a}$. To resist $\mathcal{A}$, the two grasping fingers $\mathcal{F}_1$ and $\mathcal{F}_2$, making initial contacts at $\boldsymbol{p}_i$ and $\boldsymbol{p}_j$, translate by $\boldsymbol{d}_1$ and $\boldsymbol{d}_2$, respectively.[10] We would like to find $\boldsymbol{d}_1$ and $\boldsymbol{d}_2$ that result in the minimum total effort by $\mathcal{F}_1$ and $\mathcal{F}_2$ in such resistance. The effort of resistance is best characterized as the total work performed by these two fingers.

The general scenario is depicted in Figure 6, in which the finger contacts have evolved from the nodes $\boldsymbol{p}_i, \boldsymbol{p}_j, \boldsymbol{p}_k$ into segments as $\mathcal{F}_1, \mathcal{F}_2, \mathcal{A}$ translate. Every contact segment is uniquely represented by a sequence of nodes on it[11]. At an instant during the resistance, $\mathcal{F}_1$ makes contact with the set of nodes $\{\boldsymbol{p}_t \mid t \in \mathbb{I}\}$, $\mathcal{F}_2$ with $\{\boldsymbol{p}_t \mid t \in \mathbb{J}\}$, and $\mathcal{A}$ with $\{\boldsymbol{p}_t \mid t \in \mathbb{K}\}$. Some nodes (colored red in the figure) are sticking on the fingertips, while others (green) are sliding. We can partition the scenario into small periods, within each of which the contact sets $\mathbb{I}, \mathbb{J}, \mathbb{K}$ do not change.

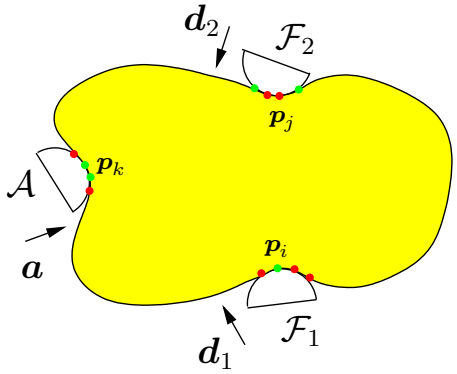

Figure 6: Resisting a translating adversary finger.

This optimization problem will be approached in three steps. In Section 6.1, we will look at fixed point contacts (i.e., $|\mathbb{I}| = |\mathbb{J}| = |\mathbb{K}| = 1$ and the three sets never change) during the resistance. In Section 6.2, we will generalize the result to fixed segment contacts. Finally, in Section 6.3, we will tackle the general situation with varying $\mathbb{I}$, $\mathbb{J}$, $\mathbb{K}$ and changes of modes at individual nodal contacts under Coulomb friction.

We do not want to minimize the potential energy of the object here because its negation — the object's strain energy — can be made as large as we like with large $\boldsymbol{d}_1$ and $\boldsymbol{d}_2$, as long as the stress everywhere does not exceed the material's proportional limit.

[10] The grasping fingers under the placement $\mathcal{G}(\boldsymbol{p}_i, \boldsymbol{p}_j)$ may have applied some initial squeeze $\boldsymbol{d}_1^{(0)}$ and $\boldsymbol{d}_2^{(0)}$ before $\mathcal{A}$ makes contact with the object. In this case, they need to execute extra translations $\boldsymbol{d}_1 - \boldsymbol{d}_1^{(0)}$ and $\boldsymbol{d}_2 - \boldsymbol{d}_2^{(0)}$ to resist $\mathcal{A}$.

[11] under an implicit assumption (consistent with the use of FEM) that a segment always ends at two nodes.

6.1 The Case of Fixed Point Contacts

The nodes $\boldsymbol{p}_i, \boldsymbol{p}_j$, and $\boldsymbol{p}_k$ stay as the only contact points with the fingers $\mathcal{F}_1$, $\mathcal{F}_2$, and $\mathcal{A}$, respectively (as if the fingers and the object are glued together). Deformation of the object is due to their displacements

$$\bar{\boldsymbol{\delta}} = \begin{pmatrix} \boldsymbol{\delta}_i \\ \boldsymbol{\delta}_j \\ \boldsymbol{\delta}_k \end{pmatrix} = \begin{pmatrix} \boldsymbol{d}_1 \\ \boldsymbol{d}_2 \\ \boldsymbol{a} \end{pmatrix}, \tag{51}$$

which results in the nodal forces $\bar{\boldsymbol{f}}$:

$$\bar{\boldsymbol{f}} = \begin{pmatrix} \boldsymbol{f}_i \\ \boldsymbol{f}_j \\ \boldsymbol{f}_k \end{pmatrix}.$$

Following the steps in Sections 3.1–3.2, we obtain the matrices A in (19), B in (20), and C in (24), with $m = 3$ and $i_1 = i, i_2 = j, i_3 = k$.

The work done by the grasping fingers is derived as follows:

$$\begin{aligned} W_{\mathcal{F}} &= \frac{1}{2}(\boldsymbol{d}_1^T \boldsymbol{f}_i + \boldsymbol{d}_2^T \boldsymbol{f}_j + \boldsymbol{0}^T \boldsymbol{f}_k) \\ &= \frac{1}{2} \begin{pmatrix} \boldsymbol{d}_1 \\ \boldsymbol{d}_2 \\ 0 \end{pmatrix}^T C \begin{pmatrix} \boldsymbol{d}_1 \\ \boldsymbol{d}_2 \\ \boldsymbol{a} \end{pmatrix}. \qquad (\text{since } \bar{\boldsymbol{f}} = C\bar{\boldsymbol{\delta}}\ ) \end{aligned} \tag{52}$$

As in the case of a two-finger squeeze from Section 4.3, we call $\bar{\boldsymbol{\delta}}$ a stable squeeze if $\bar{\boldsymbol{\delta}} \in \mathrm{col}(C)$, and a pure squeeze if $\bar{\boldsymbol{\delta}} \in \mathrm{col}(AC)$. In resisting $\mathcal{A}$, $\mathcal{F}_1$ and $\mathcal{F}_2$ commanding displacements $\boldsymbol{d}_1$ and $\boldsymbol{d}_2$ of a stable squeeze will yield the minimum potential energy of the system among all displacements of $\boldsymbol{p}_i$ and $\boldsymbol{p}_j$ with the same combined magnitude $\|\boldsymbol{d}_1\|^2 + \|\boldsymbol{d}_2\|^2$. Meanwhile, $\mathcal{F}_1$ and $\mathcal{F}_2$ executing $\boldsymbol{d}_1$ and $\boldsymbol{d}_2$ of a pure squeeze will generate no rigid body motion of the object during their resistance to $\mathcal{A}$.

6.1.1 Resistance via a Stable Squeeze

The displacement vector $\bar{\boldsymbol{\delta}}$ is orthogonal to $\mathrm{null}(C)$, i.e., $\mathrm{col}(B)$, which by (20), (8), and (7) is spanned by three vectors: $\bar{\boldsymbol{w}}_x = (1,0,1,0,1,0)^T$, $\bar{\boldsymbol{w}}_y = (0,1,0,1,0,1)^T$, and $\bar{\boldsymbol{w}}_r = (-y_i, x_i, -y_j, x_j, -y_k, x_k)^T$. Such orthogonality is equivalent to the following two conditions:

$$\boldsymbol{d}_1 + \boldsymbol{d}_2 + \boldsymbol{a} = \boldsymbol{0}, \tag{53}$$

$$\boldsymbol{p}_i \times \boldsymbol{d}_1 + \boldsymbol{p}_j \times \boldsymbol{d}_2 + \boldsymbol{p}_k \times \boldsymbol{a} = 0. \tag{54}$$

Immediately, $\boldsymbol{d}_2$ can be eliminated via a substitution of (53) into (54):

$$(\boldsymbol{p}_i - \boldsymbol{p}_j) \times \boldsymbol{d}_1 + (\boldsymbol{p}_k - \boldsymbol{p}_j) \times \boldsymbol{a} = 0. \tag{55}$$

Denote by $\hat{\boldsymbol{t}}$ the unit vector in the direction of $\boldsymbol{p}_i - \boldsymbol{p}_j$, and $\hat{\boldsymbol{n}}$ the unit vector such that $\hat{\boldsymbol{t}} \cdot \hat{\boldsymbol{n}} = 0$ and $\hat{\boldsymbol{t}} \times \hat{\boldsymbol{n}} = 1$. Decompose $\boldsymbol{d}_1$ along $\hat{\boldsymbol{t}}$ and $\hat{\boldsymbol{n}}$:

$$\boldsymbol{d}_1 = \tau \hat{\boldsymbol{t}} + \eta \hat{\boldsymbol{n}}. \tag{56}$$

Equation (55) can be rewritten as $\|\boldsymbol{p}_i - \boldsymbol{p}_j\| \hat{\boldsymbol{n}} \cdot \boldsymbol{d}_1 = (\boldsymbol{p}_j - \boldsymbol{p}_k) \times \boldsymbol{a}$, from which we obtain

$$\eta = \boldsymbol{d}_1 \cdot \hat{\boldsymbol{n}} = \frac{(\boldsymbol{p}_j - \boldsymbol{p}_k) \times \boldsymbol{a}}{\|\boldsymbol{p}_i - \boldsymbol{p}_j\|}. \tag{57}$$

From the above reasoning, we see that $\boldsymbol{d}_1$ in (56), with η given above and arbitrary τ, and $\boldsymbol{d}_2 = -\boldsymbol{a} - \boldsymbol{d}_1$ satisfy (53) and (54).

Proposition 9 *The lines ℓ_i, ℓ_j, ℓ_k of the solution displacements $\boldsymbol{d}_1, \boldsymbol{d}_2, \boldsymbol{a}$ to (53) and (54) through $\boldsymbol{p}_i, \boldsymbol{p}_j, \boldsymbol{p}_k$ must be either parallel or concurrent.*

Proof Suppose that the three lines ℓ_i, ℓ_j, ℓ_k are not parallel. At least two of them, say, ℓ_i and ℓ_j, intersect at some point $\boldsymbol{q}$. Under (53), we subtract $\boldsymbol{q}$ from $\boldsymbol{p}_i$, $\boldsymbol{p}_j$, $\boldsymbol{p}_k$ in (54):

$$(\boldsymbol{p}_i - \boldsymbol{q}) \times \boldsymbol{d}_1 + (\boldsymbol{p}_j - \boldsymbol{q}) \times \boldsymbol{d}_2 + (\boldsymbol{p}_k - \boldsymbol{q}) \times \boldsymbol{a} = 0.$$

The first two summands above vanish, leaving $(\boldsymbol{p}_k - \boldsymbol{q}) \times \boldsymbol{a} = 0$. Namely, $\boldsymbol{q}$ also lies on ℓ_k. □

Let us substitute (53) into (52) for $\boldsymbol{d}_2$, and rewrite $W_{\mathcal{F}}$ as a quadratic form in terms of $\boldsymbol{d}_1$:

$$\begin{aligned} W_{\mathcal{F}} &= \frac{1}{2} \begin{pmatrix} \boldsymbol{d}_1 \\ -\boldsymbol{d}_1 - \boldsymbol{a} \\ 0 \end{pmatrix}^T C \begin{pmatrix} \boldsymbol{d}_1 \\ -\boldsymbol{d}_1 - \boldsymbol{a} \\ \boldsymbol{a} \end{pmatrix} && (58) \\ &= \frac{1}{2} \boldsymbol{d}_1^T H \boldsymbol{d}_1 + \boldsymbol{c}^T \boldsymbol{d}_1 + \omega, && (59) \end{aligned}$$

where

$$\begin{aligned} S &= \begin{pmatrix} 1 & 0 & -1 & 0 & 0 & 0 \\ 0 & 1 & 0 & -1 & 0 & 0 \end{pmatrix}^T, \\ H &= S^T C S, && (60) \\ \boldsymbol{c}^T &= \begin{pmatrix} 0 \\ -\boldsymbol{a} \\ \boldsymbol{a}/2 \end{pmatrix}^T C S, && (61) \\ \omega &= \frac{1}{2} \begin{pmatrix} 0 \\ -\boldsymbol{a} \\ 0 \end{pmatrix}^T C \begin{pmatrix} 0 \\ -\boldsymbol{a} \\ \boldsymbol{a} \end{pmatrix}. && (62) \end{aligned}$$

Theorem 10 *The matrix H is positive semi-definite. Furthermore, $\boldsymbol{d}_1 \in \mathrm{null}(H)$ if and only if*

$$\boldsymbol{p}_k = \frac{1}{2}(\boldsymbol{p}_i + \boldsymbol{p}_j) \qquad \textit{and} \qquad \boldsymbol{d}_1 \cdot (\boldsymbol{p}_i - \boldsymbol{p}_j) = 0. \tag{63}$$

The proof is given in Appendix D. The first condition in the lemma is rarely satisfied because the midpoint of $\boldsymbol{p}_i$ and $\boldsymbol{p}_j$ often lies in the interior of the object, and thus cannot be in contact with the adversary finger.

Plug (56) into (59). After a few steps, we derive a new form for the work:

$$W_{\mathcal{F}} = \frac{1}{2} b_2 \tau^2 + b_1 \tau + b_0, \tag{64}$$

where $b_0 = \omega + \eta \left(\frac{1}{2} \eta \hat{\boldsymbol{n}}^T H + \boldsymbol{c}^T \right) \hat{\boldsymbol{n}}$, $b_1 = (\eta \hat{\boldsymbol{n}}^T H + \boldsymbol{c}^T) \hat{\boldsymbol{t}}$, and $b_2 = \hat{\boldsymbol{t}}^T H \hat{\boldsymbol{t}}$.

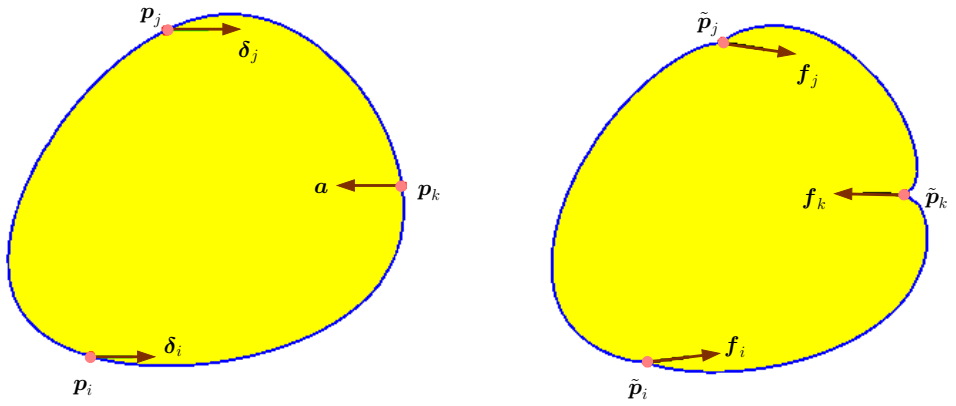

(a) (b)

Figure 7: Resisting an adversary finger at $\boldsymbol{p}_k = (0.05900, 0.00502)^T$ under translation $\boldsymbol{\delta}_k = \boldsymbol{a} = (-0.01, 0)^T$ by the grasping fingers placed at $\boldsymbol{p}_i = (-0.03537, -0.04685)^T$ and $\boldsymbol{p}_j = (-0.01256, 0.05212)^T$: (a) undeformed shape marked with optimal displacements: $\boldsymbol{d}_1^* = (0.00475, 0.00006)^T$ and $\boldsymbol{d}_2^* = (0.00525, -0.00006)^T$; and (b) deformed shape marked with the corresponding nodal forces: $\boldsymbol{f}_i = (2.5031, 0.3105)^T$, $\boldsymbol{f}_j = (2.8792, -0.4901)^T$, and $\boldsymbol{f}_k = (-5.3823, 0.1796)^T$. Here, Young's modulus $E = 5 \times 10^4$ Pa and Poisson's ratio $\nu = 0.3$, the same as measured in the experiment in Section 5.5.

Since $\hat{\boldsymbol{t}} \cdot (\boldsymbol{p}_i - \boldsymbol{p}_j) = \|\boldsymbol{p}_i - \boldsymbol{p}_j\| > 0$, it follows from Theorem 10 that $\hat{\boldsymbol{t}} \notin \text{null}(H)$. The positive semi-definiteness of H implies that $b_2 > 0$. Therefore, $W_{\mathcal{F}}$ in (64) is a parabola with the minimum value

$$W_{\mathcal{F}}^* = b_0 - \frac{b_1^2}{2b_2} \tag{65}$$

achieved at $\tau = -b_1/b_2$ by the displacement $\boldsymbol{d}_1^*$, which is determined according to (56) and (57).

Write $\boldsymbol{a} = \|\boldsymbol{a}\|\hat{\boldsymbol{a}}$ with $\hat{\boldsymbol{a}}$ being a unit vector. We plug the expression first into (62) of ω, (61) of $\boldsymbol{c}$, and (57) of η, then the resulting expressions into b_0 and b_1, finally into the expressions of $\boldsymbol{d}_1^*$ and $\boldsymbol{d}_2^*$. This finally leads to

$$\begin{pmatrix} \boldsymbol{d}_1^* \\ \boldsymbol{d}_2^* \end{pmatrix} = \|\boldsymbol{a}\| \begin{pmatrix} \boldsymbol{\psi} \\ -\hat{\boldsymbol{a}} - \boldsymbol{\psi} \end{pmatrix}, \tag{66}$$

where

$$\boldsymbol{\psi} = -\left(\left(\frac{(\boldsymbol{p}_j - \boldsymbol{p}_k) \times \hat{\boldsymbol{a}}}{\|\boldsymbol{p}_i - \boldsymbol{p}_j\|} \hat{\boldsymbol{n}}^T H + \begin{pmatrix} 0 \\ -\hat{\boldsymbol{a}} \\ \hat{\boldsymbol{a}}/2 \end{pmatrix}^T CS \right) \hat{\boldsymbol{t}} \Big/ (\hat{\boldsymbol{t}}^T H \hat{\boldsymbol{t}}) \right) \hat{\boldsymbol{t}} + \frac{(\boldsymbol{p}_j - \boldsymbol{p}_k) \times \hat{\boldsymbol{a}}}{\|\boldsymbol{p}_i - \boldsymbol{p}_j\|} \hat{\boldsymbol{n}}. \tag{67}$$

Under (66), the optimal directions of translations by the grasping fingers $\mathcal{F}_1$ and $\mathcal{F}_2$ are invariant to the amount $\|\boldsymbol{a}\|$ of the adversary finger translation. If $\mathcal{A}$ squeezes harder, $\mathcal{F}_1$ and $\mathcal{F}_2$ just need to translate more proportionally along these directions.

Note that b_0 scales with $\|\boldsymbol{a}\|^2$ and b_1 scales with $\|\boldsymbol{a}\|$, while b_2 is constant. The minimum work $W_{\mathcal{F}}^*$ scales quadratically with $\|\boldsymbol{a}\|$.

Figure 7 shows a grasp $\mathcal{G}(\boldsymbol{p}_i, \boldsymbol{p}_j)$ optimally resisting an adversary finger placed at $\boldsymbol{p}_k$ and translating leftward. The minimum work is $W_{\mathcal{F}}^* = 0.01031$. The average rotation per node is $\boldsymbol{\delta} \cdot \boldsymbol{v}_{2n} = 0.0035418$.

In the degenerate case, $\boldsymbol{p}_k = \frac{1}{2}(\boldsymbol{p}_i + \boldsymbol{p}_j)$. Since $\hat{\boldsymbol{n}} \cdot (\boldsymbol{p}_i - \boldsymbol{p}_j) = 0$, by Theorem 10 the vector $\hat{\boldsymbol{n}} \in \text{null}(H)$. Suppose we let $\boldsymbol{d}_1 = \hat{\boldsymbol{n}}$. By Lemma 12 in Appendix D, $\boldsymbol{0} = C\boldsymbol{\delta}' = CS\boldsymbol{d}_1$, which implies $\boldsymbol{c}^T \hat{\boldsymbol{n}} = 0$ by (61).

Two of the coefficients can be reduced: $b_1 = \boldsymbol{c}^T\hat{\boldsymbol{t}}$ and $b_0 = \omega$. Since b_0, b_1, b_2 are now independent of $\eta = \boldsymbol{d}_1 \cdot \hat{\boldsymbol{n}}$, $W_{\mathcal{F}}$ has the same value over $\tau\hat{\boldsymbol{t}} + \lambda\hat{\boldsymbol{n}}$, for all $\lambda \in \mathbb{R}$ and a given τ. We simply let $\eta = 0$, and $\boldsymbol{d}_1^* = -b_1/b_2$.

6.1.2 Resistance via a Pure Squeeze

Here we consider minimization of $W_{\mathcal{F}}$ over

$$\left\{ \begin{pmatrix} \boldsymbol{d}_1 \\ \boldsymbol{d}_2 \end{pmatrix} \middle| \begin{pmatrix} \boldsymbol{d}_1 \\ \boldsymbol{d}_2 \\ \boldsymbol{a} \end{pmatrix} \in \mathrm{col}(AC) \right\}.$$

There is one complication. Whereas $\boldsymbol{d}_1$ and $\boldsymbol{d}_2$ always exist for a given $\boldsymbol{a}$ such that $\bar{\boldsymbol{\delta}} \in \mathrm{col}(C)$, this is not the case for $\bar{\boldsymbol{\delta}} \in \mathrm{col}(AC)$.

Under Theorem 5(iv), the matrix AC has rank $2m - 3 = 3$. Denote by $\hat{\boldsymbol{u}}_1, \hat{\boldsymbol{u}}_2, \hat{\boldsymbol{u}}_3$ the orthogonal unit vectors that span $\mathrm{col}(AC)$.[12] Then we decompose $\bar{\boldsymbol{\delta}}$ along them:

$$\bar{\boldsymbol{\delta}} = \begin{pmatrix} \boldsymbol{d}_1 \\ \boldsymbol{d}_2 \\ \boldsymbol{a} \end{pmatrix} = \tau_1\hat{\boldsymbol{u}}_1 + \tau_2\hat{\boldsymbol{u}}_2 + \tau_3\hat{\boldsymbol{u}}_3. \tag{68}$$

The following needs to hold:

$$\boldsymbol{a} = Q \begin{pmatrix} \tau_1 \\ \tau_2 \\ \tau_3 \end{pmatrix}, \tag{69}$$

where

$$Q = (\boldsymbol{0}, I_2)(\hat{\boldsymbol{u}}_1, \hat{\boldsymbol{u}}_2, \hat{\boldsymbol{u}}_3). \tag{70}$$

If the 2×3 matrix Q is not of full rank and $\boldsymbol{a}$ is not in its column space $\mathrm{col}(Q) = \mathrm{col}((\boldsymbol{0}, I_2)AC)$, then we infer that $\bar{\boldsymbol{\delta}} \notin \mathrm{col}(AC)$ and the adversary finger cannot be resisted. If $\mathrm{rank}(Q) = 1$ and $\boldsymbol{a} \in \mathrm{col}(Q)$, we permute the subscripts of $\hat{\boldsymbol{u}}_1, \hat{\boldsymbol{u}}_2, \hat{\boldsymbol{u}}_3$ such that the last two entries in $\hat{\boldsymbol{u}}_1$ are $\tau_1\boldsymbol{a}$ for some τ_1. Simply let $\tau_2 = \tau_3 = 0$.

Let us focus on the general case that $\mathrm{rank}(Q) = 2$. We can always permute the subscripts of $\hat{\boldsymbol{u}}_1, \hat{\boldsymbol{u}}_2, \hat{\boldsymbol{u}}_3$ to make the matrix

$$N = (\boldsymbol{0}, I_2)(\hat{\boldsymbol{u}}_2, \hat{\boldsymbol{u}}_3)$$

has full rank. Then, from (69) we obtain $\binom{\tau_2}{\tau_3} = N^{-1}(\boldsymbol{a} - \tau_1\boldsymbol{b})$, where $\boldsymbol{b} = (\boldsymbol{0}, I_2)\hat{\boldsymbol{u}}_1$. Subsequently,

$$\bar{\boldsymbol{\delta}} = (\hat{\boldsymbol{u}}_1, \hat{\boldsymbol{u}}_2, \hat{\boldsymbol{u}}_3) \begin{pmatrix} \tau_1 \\ N^{-1}(\boldsymbol{a} - \tau_1\boldsymbol{b}) \end{pmatrix}. \tag{71}$$

Substitute the above into (52):

$$W_{\mathcal{F}} = \frac{1}{2} \left((\hat{\boldsymbol{u}}_1, \hat{\boldsymbol{u}}_2, \hat{\boldsymbol{u}}_3) \begin{pmatrix} \tau_1 \\ N^{-1}(\boldsymbol{a} - \tau_1\boldsymbol{b}) \end{pmatrix} - \begin{pmatrix} \boldsymbol{0} \\ \boldsymbol{0} \\ \boldsymbol{a} \end{pmatrix} \right)^T C \left((\hat{\boldsymbol{u}}_1, \hat{\boldsymbol{u}}_2, \hat{\boldsymbol{u}}_3) \begin{pmatrix} \tau_1 \\ N^{-1}(\boldsymbol{a} - \tau_1\boldsymbol{b}) \end{pmatrix} \right).$$

[12] They can be easily computed from the columns of AC using the Gram-Schmidt procedure.

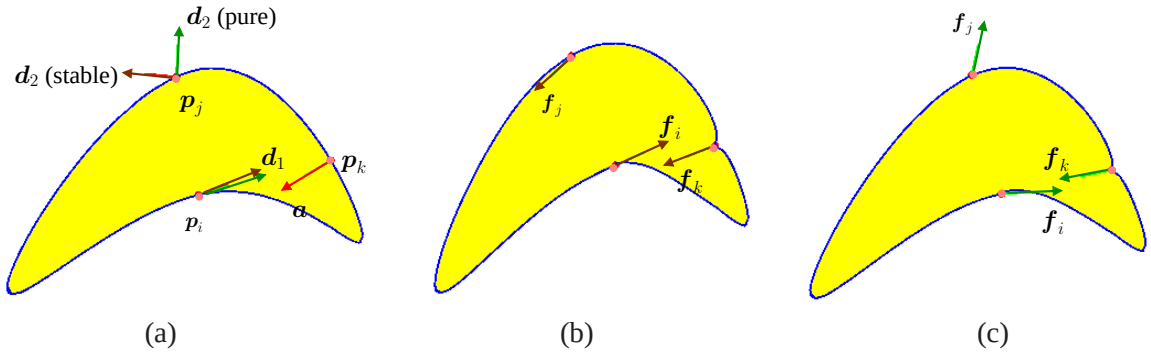

(a) (b) (c)

Figure 8: Resisting an adversary finger at $\boldsymbol{p}_k = (0.05908, 0.00432)^T$ under translation $\boldsymbol{a} = (-0.00514, -0.00309)^T$ by the grasping fingers placed at $\boldsymbol{p}_i = (0.00580, -0.00964)^T$ and $\boldsymbol{p}_j = (-0.00323, 0.03804)^T$: (a) undeformed shape marked with optimal displacements for the optimal stable squeeze (brown) and the optimal pure squeeze (green); (b) deformed shape under stable squeeze marked with the corresponding nodal forces; and (c) deformed shape under pure squeeze.

The leading coefficient of τ_1,

$$\begin{pmatrix} 1 \\ -N^{-1}\boldsymbol{b} \end{pmatrix}^T L \begin{pmatrix} 1 \\ -N^{-1}\boldsymbol{b} \end{pmatrix},$$

where $L = (\hat{\boldsymbol{u}}_1, \hat{\boldsymbol{u}}_2, \hat{\boldsymbol{u}}_3)^T C (\hat{\boldsymbol{u}}_1, \hat{\boldsymbol{u}}_2, \hat{\boldsymbol{u}}_3)$, is non-negative and often non-zero due to positive semidefiniteness of C. This means that $W_{\mathcal{F}}$ is a parabola in τ_1.

At the minimum, the derivative of $W_{\mathcal{F}}$ with respect to τ_1 vanishes, yielding

$$\begin{pmatrix} 1 \\ -N^{-1}\boldsymbol{b} \end{pmatrix}^T L \begin{pmatrix} \tau_1 \\ N^{-1}(\boldsymbol{a} - \tau_1 \boldsymbol{b}) \end{pmatrix} - \frac{1}{2} \begin{pmatrix} \mathbf{0} \\ \mathbf{0} \\ \boldsymbol{a} \end{pmatrix}^T C(\hat{\boldsymbol{u}}_1, \hat{\boldsymbol{u}}_2, \hat{\boldsymbol{u}}_3) \begin{pmatrix} 1 \\ -N^{-1}\boldsymbol{b} \end{pmatrix} = 0.$$

Solving the above equation, we obtain

$$\tau_1 = \begin{pmatrix} 1 \\ N^{-1}\boldsymbol{b} \end{pmatrix}^T \left(L \begin{pmatrix} \mathbf{0} \\ N^{-1}\boldsymbol{a} \end{pmatrix} - \frac{1}{2} (\hat{\boldsymbol{u}}_1, \hat{\boldsymbol{u}}_2, \hat{\boldsymbol{u}}_3)^T C \begin{pmatrix} \mathbf{0} \\ \mathbf{0} \\ \boldsymbol{a} \end{pmatrix} \right) \Big/ \left(\begin{pmatrix} 1 \\ -N^{-1}\boldsymbol{b} \end{pmatrix}^T L \begin{pmatrix} 1 \\ -N^{-1}\boldsymbol{b} \end{pmatrix} \right). \quad (72)$$

Equation (72) can be rewritten as $\tau_1 = \|\boldsymbol{a}\| \tau_1^*$, where τ_1^* is evaluated according to (72) after a simple replacement of $\boldsymbol{a}$ with $\hat{\boldsymbol{a}}$. Truncating off the last two entries of $\bar{\boldsymbol{\delta}}$ in (71), we obtain the optimal grasping finger displacements:

$$\begin{pmatrix} \boldsymbol{d}_1^* \\ \boldsymbol{d}_2^* \end{pmatrix} = \|\boldsymbol{a}\| \begin{pmatrix} \boldsymbol{\psi}_1 \\ \boldsymbol{\psi}_2 \end{pmatrix}, \quad (73)$$

where

$$\begin{pmatrix} \boldsymbol{\psi}_1 \\ \boldsymbol{\psi}_2 \end{pmatrix} = (I_4, \mathbf{0})(\hat{\boldsymbol{u}}_1, \hat{\boldsymbol{u}}_2, \hat{\boldsymbol{u}}_3) \begin{pmatrix} \tau_1^* \\ N^{-1}(\hat{\boldsymbol{a}} - \tau_1^* \boldsymbol{b}) \end{pmatrix}.$$

Figure 8 compares the resistances to the same adversary finger translation by a stable squeeze in (a) and a pure squeeze in (b). In the both instances, the finger $\mathcal{F}_2$ placed at $\boldsymbol{p}_j$ moves away from the object under displacements $(-0.00199, 0.00019)^T$ and $(0.00009, 0.00184)^T$, respectively. Also, in (c) the contact force $\boldsymbol{f}_j$ is pulling outward for the pure squeeze. Such unrealistic results are generated under the assumption of

non-breaking contact as if the fingers and the object were "glued" together. They will be easily avoided when frictional segment contacts are considered, as will be demonstrated over the same shape and the same finger placement in Section 6.3.

6.2 The Case of Fixed Segment Contacts

The contact sets $\mathbb{I}, \mathbb{J}, \mathbb{K}$ may have sizes greater than one. However, they do not change. In other words, no existing contact will break and no new contacts will be established. To resist the adversary finger $\mathcal{A}$, the grasping finger $\mathcal{F}_i$, $i = 1, 2$, translates by $\boldsymbol{d}_i$. All the nodes in contact with the same finger undergo the same displacement. More specifically, a contact node $\boldsymbol{p}_t$ is displaced by

$$\boldsymbol{\delta}_t = \begin{cases} \boldsymbol{d}_1, & \text{if } t \in \mathbb{I}; \\ \boldsymbol{d}_2, & \text{if } t \in \mathbb{J}; \\ \boldsymbol{a}, & \text{if } t \in \mathbb{K}. \end{cases} \tag{74}$$

Let $\bar{\boldsymbol{\delta}}$ be the column vector that gathers $\boldsymbol{\delta}_t$, for all $t \in \mathbb{I}$, followed by $\boldsymbol{\delta}_t$, for all $t \in \mathbb{J}$, and then by $\boldsymbol{\delta}_t$, for all $t \in \mathbb{K}$. In other words,

$$\bar{\boldsymbol{\delta}} = (\boldsymbol{d}_1^T, \ldots, \boldsymbol{d}_1^T, \boldsymbol{d}_2^T, \ldots, \boldsymbol{d}_2^T, \boldsymbol{a}^T, \ldots, \boldsymbol{a}^T)^T. \tag{75}$$

Rearrange the rows and columns of the matrix C introduced in (24) in the same index order as in $\bar{\boldsymbol{\delta}}$. The displacements of all contact nodes induced by $\bar{\boldsymbol{\delta}}$ can be computed according to (17) in Section 3.1. As in Section 6.1, we consider the optimal stable squeeze followed by the optimal pure squeeze.

6.2.1 Resistance via a Stable Squeeze

The condition $\bar{\boldsymbol{\delta}} \perp \mathrm{null}(C)$, or equivalently, $\bar{\boldsymbol{\delta}} \perp \mathrm{col}(B)$, splits into the following conditions that generalize (53) and (54):

$$\begin{aligned} \sum_{t \in \mathbb{I} \cup \mathbb{J} \cup \mathbb{K}} \boldsymbol{\delta}_t &= \mathbf{0}, \\ \sum_{t \in \mathbb{I}} \boldsymbol{p}_t \times \boldsymbol{d}_1 + \sum_{t \in \mathbb{J}} \boldsymbol{p}_t \times \boldsymbol{d}_2 + \sum_{t \in \mathbb{K}} \boldsymbol{p}_t \times \boldsymbol{a} &= 0. \end{aligned}$$

After plugging in (74), the first condition above yields

$$\boldsymbol{d}_2 = -\frac{1}{|\mathbb{J}|}(|\mathbb{I}|\boldsymbol{d}_1 + |\mathbb{K}|\boldsymbol{a}), \tag{76}$$

which is then substituted into the second condition to yield

$$|\mathbb{I}|(\breve{\boldsymbol{p}} - \breve{\boldsymbol{q}}) \times \boldsymbol{d}_1 + |\mathbb{K}|(\breve{\boldsymbol{r}} - \breve{\boldsymbol{q}}) \times \boldsymbol{a} = 0, \tag{77}$$

where

$$\breve{\boldsymbol{p}} = \frac{1}{|\mathbb{I}|} \sum_{t \in \mathbb{I}} \boldsymbol{p}_t, \qquad \breve{\boldsymbol{q}} = \frac{1}{|\mathbb{J}|} \sum_{t \in \mathbb{J}} \boldsymbol{p}_t, \qquad \text{and} \qquad \breve{\boldsymbol{r}} = \frac{1}{|\mathbb{K}|} \sum_{t \in \mathbb{K}} \boldsymbol{p}_t. \tag{78}$$

We refer to $\breve{\boldsymbol{p}}, \breve{\boldsymbol{q}}, \breve{\boldsymbol{r}}$ as the *contact centroids* of the fingers $\mathcal{F}_1, \mathcal{F}_2, \mathcal{A}$, respectively. Proposition 9 easily generalizes to state that the displacements $\boldsymbol{d}_1$, $\boldsymbol{d}_2$, and $\boldsymbol{a}$, if transplanted to these centroids, must be either parallel or on concurrent lines.

As in the case of fixed point contacts treated in Section 6.1.1, we write the work done by $\mathcal{F}_1$ and $\mathcal{F}_2$ into the following form:

$$\begin{aligned} W_{\mathcal{F}} &= \frac{1}{2}\sum_{t\in\mathbb{I}\cup\mathbb{J}} \boldsymbol{\delta}_t^T \boldsymbol{f}_t \\ &= \frac{1}{2}\boldsymbol{d}_1^T H \boldsymbol{d}_1 + \boldsymbol{c}^T \boldsymbol{d}_1 + \omega, \end{aligned} \tag{79}$$

where $H = S^T C S$ with

$$S = \left(I_2, \ldots, I_2, -\frac{|\mathbb{I}|}{|\mathbb{J}|}I_2, \ldots, -\frac{|\mathbb{I}|}{|\mathbb{J}|}I_2, \mathbf{0}, \ldots, \mathbf{0}\right)^T, \tag{80}$$

$$\boldsymbol{c}^T = \begin{pmatrix} 0 \\ \vdots \\ 0 \\ -\frac{|\mathbb{K}|}{|\mathbb{J}|}\boldsymbol{a} \\ \vdots \\ -\frac{|\mathbb{K}|}{|\mathbb{J}|}\boldsymbol{a} \\ \boldsymbol{a}/2 \\ \vdots \\ \boldsymbol{a}/2 \end{pmatrix}^T CS, \qquad \text{and} \qquad \omega = \frac{1}{2}\begin{pmatrix} 0 \\ \vdots \\ 0 \\ -\frac{|\mathbb{K}|}{|\mathbb{J}|}\boldsymbol{a} \\ \vdots \\ -\frac{|\mathbb{K}|}{|\mathbb{J}|}\boldsymbol{a} \\ 0 \\ \vdots \\ 0 \end{pmatrix}^T C \begin{pmatrix} 0 \\ \vdots \\ 0 \\ -\frac{|\mathbb{K}|}{|\mathbb{J}|}\boldsymbol{a} \\ \vdots \\ -\frac{|\mathbb{K}|}{|\mathbb{J}|}\boldsymbol{a} \\ \boldsymbol{a} \\ \vdots \\ \boldsymbol{a} \end{pmatrix}.$$

Proposition 11 *The matrix H is positive semidefinite. That $\boldsymbol{d}_1 \in \mathrm{null(H)}$ if and only if the following three conditions are all satisfied: i) $|\mathbb{I}| = |\mathbb{J}| = |\mathbb{K}| = 1$; ii) $\boldsymbol{p}_k = \frac{1}{2}(\boldsymbol{p}_i + \boldsymbol{p}_j)$; and iii) $\boldsymbol{d}_1 \cdot (\boldsymbol{p}_i - \boldsymbol{p}_j) = 0$. In ii) and iii), i, j, k must be the unique indices in $\mathbb{I}, \mathbb{J}, \mathbb{K}$, respectively, following i).*

See Appendix E for the proof of the proposition. Minimization of the work (79) parallels that of (59) in Section 6.1.1. Briefly, we decompose $\boldsymbol{d}_1$ along the direction $\hat{\boldsymbol{t}}$ of $\breve{\boldsymbol{p}} - \breve{\boldsymbol{q}}$, and its orthogonal direction $\hat{\boldsymbol{n}}$. The component $\eta = \boldsymbol{d}_1 \cdot \hat{\boldsymbol{n}}$ can be determined from (77). The work (79) becomes a parabola in the form of (64) in terms of $\tau = \boldsymbol{d}_1 \cdot \hat{\boldsymbol{t}}$. It is straightforward to obtain the minimizing displacements $\boldsymbol{d}_1^*$ of $\mathcal{F}_1$ and $\boldsymbol{d}_2^*$ of $\mathcal{F}_2$. They assume the forms in (66), except that $\boldsymbol{p}_i, \boldsymbol{p}_j, \boldsymbol{p}_k$ are now replaced with $\breve{\boldsymbol{p}}, \breve{\boldsymbol{q}}, \breve{\boldsymbol{r}}$, respectively, and S is now redefined in (80).

6.2.2 Resistance via a Pure Squeeze

We consider $\boldsymbol{d}_1$ and $\boldsymbol{d}_2$ such that $\bar{\boldsymbol{\delta}}$ by (75) is in $\mathrm{col}(AC)$. Equivalently, $\bar{\boldsymbol{\delta}} \perp \mathrm{col}(E)$ following Theorem 5(v). The $2m \times 3$ matrix $E = (\boldsymbol{e}_1, \boldsymbol{e}_2, \boldsymbol{e}_3)$ has full rank 3 by Theorem 5(iii). For $1 \le t \le 3$ denote $\boldsymbol{e}_t = (e_{1t}, \ldots, e_{2m,t})^T$. The conditions $\boldsymbol{e}_t^T \bar{\boldsymbol{\delta}} = 0$, $1 \le t \le 3$, can be rewritten as

$$\begin{pmatrix} \breve{\boldsymbol{e}}_{11} & \breve{\boldsymbol{e}}_{12} & \breve{\boldsymbol{e}}_{13} \\ \breve{\boldsymbol{e}}_{21} & \breve{\boldsymbol{e}}_{22} & \breve{\boldsymbol{e}}_{23} \\ \breve{\boldsymbol{e}}_{31} & \breve{\boldsymbol{e}}_{32} & \breve{\boldsymbol{e}}_{33} \end{pmatrix}^T \begin{pmatrix} \boldsymbol{d}_1 \\ \boldsymbol{d}_2 \\ \boldsymbol{a} \end{pmatrix} = \mathbf{0},$$

where the 6×3 matrix has entries:

$$\breve{\boldsymbol{e}}_{st} = \begin{cases} \sum_{u \in \mathbb{I}} \binom{e_{2u-1,t}}{e_{2u,t}}, & \text{if } s = 1, \\ \sum_{u \in \mathbb{J}} \binom{e_{2u-1,t}}{e_{2u,t}}, & \text{if } s = 2, \\ \sum_{u \in \mathbb{K}} \binom{e_{2u-1,t}}{e_{2u,t}}, & \text{if } s = 3. \end{cases}$$

Generally, this matrix has rank 3, so does its null space. We use SVD to find three unit orthogonal vectors $\hat{\boldsymbol{u}}'_1, \hat{\boldsymbol{u}}'_2, \hat{\boldsymbol{u}}'_3$ that span its null space. Perform the following projection like in (68):

$$\begin{pmatrix} \boldsymbol{d}_1 \\ \boldsymbol{d}_2 \\ \boldsymbol{a} \end{pmatrix} = \tau'_1 \hat{\boldsymbol{u}}'_1 + \tau'_2 \hat{\boldsymbol{u}}'_2 + \tau'_3 \hat{\boldsymbol{u}}'_3.$$

Also similarly as in Section 6.2.1, we introduce a $2m \times 6$ "expansion" matrix P with

$$P^T = \begin{pmatrix} I_2 & \cdots & I_2 & \mathbf{0} & \cdots & \mathbf{0} & \mathbf{0} & \cdots & \mathbf{0} \\ \mathbf{0} & \cdots & \mathbf{0} & I_2 & \cdots & I_2 & \mathbf{0} & \cdots & \mathbf{0} \\ \mathbf{0} & \cdots & \mathbf{0} & \mathbf{0} & \cdots & \mathbf{0} & I_2 & \cdots & I_2 \end{pmatrix}$$

such that

$$P \begin{pmatrix} \boldsymbol{d}_1 \\ \boldsymbol{d}_2 \\ \boldsymbol{a} \end{pmatrix} = \bar{\boldsymbol{\delta}},$$

The work done by the grasping fingers can be rewritten into the following form:

$$W_{\mathcal{F}} = \frac{1}{2} \begin{pmatrix} \boldsymbol{d}_1 \\ \boldsymbol{d}_2 \\ \mathbf{0} \end{pmatrix}^T P^T C P \begin{pmatrix} \boldsymbol{d}_1 \\ \boldsymbol{d}_2 \\ \boldsymbol{a} \end{pmatrix}. \tag{81}$$

Thus, we have arrived at an optimization problem very similar to the one for point contacts treated in Section 6.1.2. Aside from the different form of $W_{\mathcal{F}}$ and different variables $\tau'_1, \tau'_2, \tau'_3$, the constraint over these variables has the format of (69) except that τ'_i replaces τ_i and $\hat{\boldsymbol{u}}'_i$ replaces $\hat{\boldsymbol{u}}_i$, $i = 1, 2, 3$.

6.3 Adversary Finger Resistance with Frictional Segment Contacts

We are finally ready to consider optimal resistance with segment contacts under friction. The two grasping fingers and the adversary finger have semicircular fingertips with possibly different radii. With the object they make point contacts that later on grow into segments as the finger translations continue. A contact node may stick or slide on a fingertip. Here we modify the squeeze algorithm from Section 5.4 which works for two grasping fingers but with no adversary finger. Instead of the squeeze depth, the translation distance by the adversary finger $\mathcal{A}$ will be sequenced into $a_0 = 0 < a_1 < \cdots < \|\boldsymbol{a}\|$ such that at every a_l, one of the four contact events A, B, C, and D described in Section 5.3 takes place.

Denote by $\mathbb{I}, \mathbb{J}, \mathbb{K}$ the sets of indices of the nodes that are in contact with $\mathcal{F}_1$, $\mathcal{F}_2$, and $\mathcal{A}$, respectively. Every finger must be in sticking contact with at least one node on the object. Otherwise, the resistance either fails or succeeds, before $\mathcal{A}$ finishes its translation. This will be described in details later.

Consider the moment when $\mathcal{A}$ has translated by the distance a_l. As before, for a contact node $\boldsymbol{p}_t$ we use $\boldsymbol{\delta}_t^{(l)}$, $\boldsymbol{f}_t^{(l)}$, and $\theta_t^{(l)}$ to refer to its displacement, contact force, and polar angle (with respect to the center of its contacting fingertip).

Consider an additional translation of $\mathcal{A}$ in the direction $\hat{\boldsymbol{a}} = \boldsymbol{a}/\|\boldsymbol{a}\|$ by the distance ξ. Suppose that ξ is small enough such that all contacts and their modes will not change. We determine the extra translations $\Delta\boldsymbol{d}_1$ of $\mathcal{F}_1$ and $\Delta\boldsymbol{d}_2$ of $\mathcal{F}_2$ to resist this extra movement by $\mathcal{A}$, via minimizing the extra work done by these two fingers:

$$\Delta W_{\mathcal{F}} = \sum_{t\in\mathbb{I}\cup\mathbb{J}} \Delta\boldsymbol{\delta}_t^T \boldsymbol{f}_t^{(l)} + \frac{1}{2}\sum_{t\in\mathbb{I}\cup\mathbb{J}} \Delta\boldsymbol{\delta}_t^T \Delta\boldsymbol{f}_t. \tag{82}$$

In the above, for $t \in \mathbb{I}\cup\mathbb{J}$, $\Delta\boldsymbol{\delta}_t$ is the change in the displacement of the contact node $\boldsymbol{p}_t$ from $\boldsymbol{\delta}_t^{(l)}$, and $\Delta\boldsymbol{f}_t$ the change in its contact force from $\boldsymbol{f}_t^{(l)}$.

During this extra translation by $\mathcal{A}$ and its resistance via extra movements by $\mathcal{F}_1$ and $\mathcal{F}_2$, if a node $\boldsymbol{p}_t$, $t \in \mathbb{I}\cup\mathbb{J}$, sticks, then $\Delta\boldsymbol{\delta}_t = \Delta\boldsymbol{d}_1$ or $\Delta\boldsymbol{d}_2$. If it slides, then $\Delta\boldsymbol{\delta}_t$ will be the sum of $\Delta\boldsymbol{d}_1$ or $\Delta\boldsymbol{d}_2$ and the node's movement $r\binom{\cos\theta_t - \cos\theta_t^{(l)}}{\sin\theta_t - \sin\theta_t^{(l)}}$ on the tip of $\mathcal{F}_1$ or $\mathcal{F}_2$ that it is in contact with. Given a value of ξ, we would be able to determine θ_t via numerical root finding based on the contact force constraint (46), where every $\Delta\boldsymbol{f}_t$ is now linear in all $\Delta\boldsymbol{\delta}_s$, $s \in \mathbb{I}\cup\mathbb{J}\cup\mathbb{K}$, similarly as described in Section 5.2. However, minimization of $\Delta W_{\mathcal{F}}$ would become significantly more complicated since, in addition to $\Delta\boldsymbol{\delta}_1$ and $\Delta\boldsymbol{\delta}_2$, every sliding contact $\boldsymbol{p}_t$ would introduce an extra variable θ_t.

We stipulate that the work done by the contacting finger $\mathcal{F}_1$ or $\mathcal{F}_2$ on $\boldsymbol{p}_t$, $t \in \mathbb{I}\cup\mathbb{J}$, due to its sliding will be significantly less than that due to its translation with the fingertip. Instead of minimizing $\Delta W_{\mathcal{F}}$, we minimize its approximation $\Delta\tilde{W}_{\mathcal{F}}$ by treating every sliding node in contact with $\mathcal{F}_1$ or $\mathcal{F}_2$ as if it were sticking during the extra resistance period. Whether a contact node $\boldsymbol{p}_t$ sticks or slips, its extra displacement will be set as follows:

$$\Delta\boldsymbol{\delta}_t = \begin{cases} \Delta\boldsymbol{d}_1, & \text{if } t \in \mathbb{I}; \\ \Delta\boldsymbol{d}_2, & \text{if } t \in \mathbb{J}; \\ \xi\frac{\boldsymbol{a}}{\|\boldsymbol{a}\|}, & \text{if } t \in \mathbb{K}. \end{cases} \tag{83}$$

Then $\Delta\boldsymbol{d}_1$ and $\Delta\boldsymbol{d}_2$ can be determined via minimization of $\Delta\tilde{W}_{\mathcal{F}}$ just like described in Section 6.2. For extra translation $\xi\hat{\boldsymbol{a}}$ of $\mathcal{A}$, suppose that the grasping fingers $\mathcal{F}_1$ and $\mathcal{F}_2$ perform extra translations with the "effect" of a stable squeeze. Then the translations are given by $\Delta\boldsymbol{d}_1 = \xi\boldsymbol{\psi}$ and $\Delta\boldsymbol{d}_2 = \xi(-\hat{\boldsymbol{a}} - \boldsymbol{\psi})$, where $\boldsymbol{\psi}$ is according to (67) except with replacements of $\boldsymbol{p}_i, \boldsymbol{p}_j, \boldsymbol{p}_k$ respectively by $\breve{\boldsymbol{p}}, \breve{\boldsymbol{q}}, \breve{\boldsymbol{r}}$, S according to (80), and C determined by the combined index set $\mathbb{I}\cup\mathbb{J}\cup\mathbb{K}$. For the "effect" of a pure squeeze, we can obtain $\Delta\boldsymbol{d}_1$ and $\Delta\boldsymbol{d}_2$ via a generalization of (73) to segment contacts.

Now we determine the extra distance ξ by which $\mathcal{A}$ translates until the next contact event happens, by extending Algorithm 1 to the present case with three fingers. The extension is straightforward because all three fingers are under translations that depend on ξ only. Event conditions (47)–(50) are tested, with every increment h of ξ. Here, we must take into account contact node sliding. Once an event occurs, the overall translation distance for $\mathcal{A}$ is updated as $a_{l+1} = a_l + \xi$. In addition to the index sets $\mathbb{I}, \mathbb{J}, \mathbb{K}$, update the set $\mathbb{P}$ of sliding contacts and the set $\mathbb{T}$ of sticking contacts (with any of $\mathcal{F}_1, \mathcal{F}_2$, and $\mathcal{A}$).

If the adversary finger $\mathcal{A}$ has all contacts sliding in the same direction after an event, it will slip. In this case, it has been successfully resisted. If either $\mathcal{F}_1$ or $\mathcal{F}_2$ is sliding, the grasping fingers fail to resist $\mathcal{A}$. If none of the above two cases happens, $\mathcal{A}$ will complete its translation $\boldsymbol{a}$ while being resisted.

Algorithm 2 summarizes the steps for resisting the translating adversary finger.

Figure 9 displays the same object from Figure 8 in initial contact with two rounded fingers $\mathcal{F}_1$ and $\mathcal{F}_2$ at the same nodes $\boldsymbol{p}_i$ and $\boldsymbol{p}_j$. The fingers first grasped the object via a pure squeeze with depth 0.006156 (see (a)), performing work 0.010048. In (b), the adversary finger $\mathcal{A}$ then establishes contact at the same node $\boldsymbol{p}_k$ in Figure 8 and translates by $\boldsymbol{a} = (-0.00849, -0.00489)^T$. The trajectory of $\mathcal{A}$ is shown as the black

Algorithm 2 Resisting a Translating Adversary Finger under Frictional Segment Contact

Input: contact index sets $\mathbb{I}, \mathbb{J}, \mathbb{K}$ for $\mathcal{F}_1, \mathcal{F}_2, \mathcal{A}$, translation $\boldsymbol{a}$ of $\mathcal{A}$

1: $a \leftarrow 0$
2: let $\mathbb{I}, \mathbb{J}, \mathbb{K}$ contain the indices of the initial point contacts with $\mathcal{F}_1, \mathcal{F}_2, \mathcal{A}$, respectively
3: initialize $\mathbb{T}$ and $\mathbb{P}$
4: **while** $a < \|\boldsymbol{a}\|$ and no finger slips **do**
5: construct the form of $\Delta\tilde{W}_{\mathcal{F}}$ based on (82), (83), and $\mathbb{I}, \mathbb{J}, \mathbb{K}$
6: minimize $\Delta\tilde{W}_{\mathcal{F}}$ to obtain $\boldsymbol{\psi}_1$ and $\boldsymbol{\psi}_2$ as the translations of $\mathcal{F}_1$ and $\mathcal{F}_2$ in response to a (hypothesized) unit translation $\boldsymbol{a}/\|\boldsymbol{a}\|$ by $\mathcal{A}$
7: execute lines 4–10 of Algorithm 1 until the next contact event occurs (inside the **repeat-until** statement, increment $\Delta\boldsymbol{\delta}_t$ by $h\boldsymbol{\psi}_1$ if $t \in \mathbb{I}$, by $h\boldsymbol{\psi}_2$ if $t \in \mathbb{J}$, or by $h\hat{\boldsymbol{a}}$ if $t \in \mathbb{K}$)
8: compute the actual work $\Delta W_{\mathcal{F}}$
9: $W_{\mathcal{F}} \leftarrow W_{\mathcal{F}} + \Delta W_{\mathcal{F}}$
10: update $\mathbb{I}, \mathbb{J}, \mathbb{K}, \mathbb{T}, \mathbb{P}$ according to the contact event
11: update the contact force $\boldsymbol{f}_t, \forall\, t \in \mathbb{I} \cup \mathbb{J} \cup \mathbb{K}$
12: **end while**
13: **if** $a < \|\boldsymbol{a}\|$ and ($\mathcal{F}_1$ or $\mathcal{F}_2$ slips) **then**
14: **return** failure
15: **else**
16: **return** $W_{\mathcal{F}}$
17: **end if**

directed line in (c). Simultaneously, $\mathcal{F}_1$ and $\mathcal{F}_2$ translate along two trajectories generated by Algorithm 2 which are shown as the directed polylines in (c). They have performed additional work of 0.02586 to resist $\mathcal{A}$, which has performed work 0.034036. The object in the final configuration (b) has strain energy 0.06991, after small energy loss due to sliding of some nodes. Contact events A, B, C, D have occurred 13, 0, 7, and 4 times, respectively, during the resistance phase.

6.4 Experiment on Grasp Resistance

Shown in Figure 10 is an experiment conducted with semi-circular fingertips of radius 0.02. Because the three fingers of our BarrettHand could not be controlled to perform independent translations in the same plane, human hands were employed to hold the semicircular fingertips and translate them.

The fingers $\mathcal{F}_1$ and $\mathcal{F}_2$ first made contact with a foam object of the same material as those involved in the grasping experiment in Section 5.5. While $\mathcal{F}_2$ stayed still, $\mathcal{F}_1$ squeezed the object via a translation $(-0.00068, 0.002)^T$ along the line through their initial contact points with the object. Afterward, the adversary finger $\mathcal{A}$ started pushing the object via a translation $\boldsymbol{a} = (0.0024, 0.0044)^T$. Algorithm 2 from Section 6.3 generated two trajectories respectively for $\mathcal{F}_1$ and $\mathcal{F}_2$ based on stable squeezes. For ease of hand control, each trajectory was straightened by connecting its starting location to its final location, yielding overall translations $\boldsymbol{d}_1 = (-0.0008, -0.0019)^T$ and $\boldsymbol{d}_2 = (-0.0007, -0.0005)^T$. We refer to the resistance specified by $\boldsymbol{d}_1$ and $\boldsymbol{d}_2$ as the "optimal" resistance. During the resistance, $\mathcal{F}_2$ retreated slightly (i.e., moved away from the object).

We attached a force meter shown in Figure 10(c) to a fingertip such that the meter's axis was aligned with the fingertip translation. The work done by the fingertip was estimated as half the product of the translation distance with the sum of the initial and final force readings. The squeeze-and-resistance process

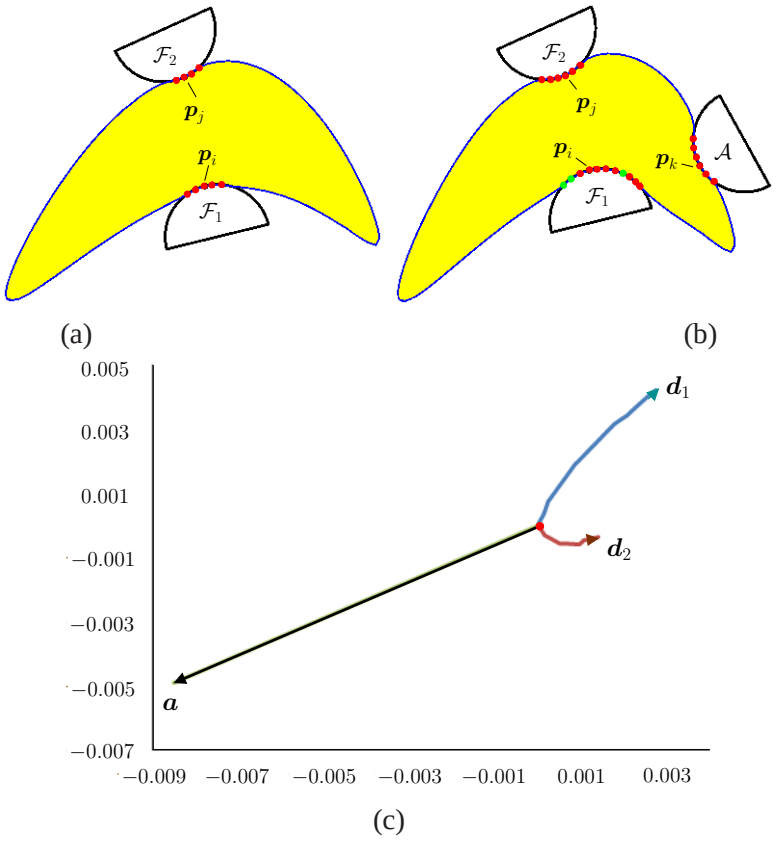

Figure 9: Adversary finger resistance with frictional segment contacts: (a) the shape from Figure 8 grasped via a pure squeeze at the same initial contact nodes; (b) successful resistance to the same adversary finger disturbance as in Figure 8; and (c) trajectories of the three fingers during the resistance. Sticking contacts are in red, and sliding contacts are in green.

was repeated three times, each time with the force meter attached to a different fingertip, for measuring its exerted force. Guided by the generated trajectories (plotted on the platform), the three repeats yielded outcomes with slight differences that were within the acceptable range.

For comparison, we also tested an "arbitrary" resistance strategy against the same adversary finger disturbance. We arbitrarily chose a translation direction $\boldsymbol{d}_2/\|\boldsymbol{d}_2\| = (0.447, -0.894)^T$ for $\mathcal{F}_2$. Then $\boldsymbol{d}_1 = (-0.004, -0.0012)^T$ and $\boldsymbol{d}_2 = (0.0016, -0.0032)^T$ were determined from the condition $(\boldsymbol{d}_1^T, \boldsymbol{d}_2^T, \boldsymbol{a}^T)^T \perp \mathrm{col}(B)$ for a stable squeeze.

Table 3 displayed the force readings on each finger at the start and the end of each resistance strategy, and the work performed by the finger. It can be seen that much less work was carried out by $\mathcal{F}_1$ and $\mathcal{F}_2$ under the "optimal" resistance strategy.

7 Squeezing Ring-like Objects

A variety of objects, from plastic and metal cookie cutters to cross sections of medicine and food bottles, are hollow. More likely to bend than solid objects, they tend to make very small contact areas with the grasping fingers such that these contacts are well approximated by points.

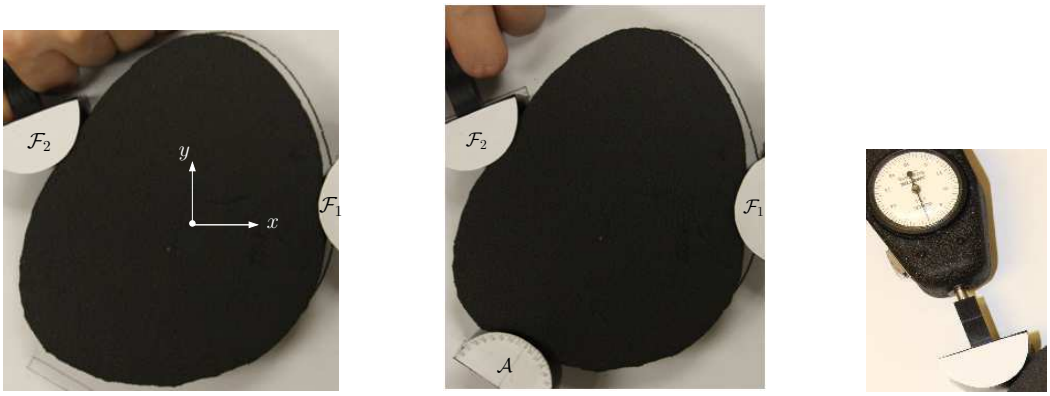

(a) (b) (c)

Figure 10: Experiment on adversary finger resistance: (a) grasp of a foam rubber object; (b) its resistance to a translating finger $\mathcal{A}$; (c) force meter (from Ametek Hunter Spring) attached to a finger for force measurement.

	"optimal" resistance			"arbitrary" resistance		
finger	$\mathcal{F}_1$	$\mathcal{F}_2$	$\mathcal{A}$	$\mathcal{F}_1$	$\mathcal{F}_2$	$\mathcal{A}$
force (start)	2.2	-3.1	0	6.9	4.17	0
force (end)	8.3	-1.7	7.2	14.45	13.61	10
work	**0.011**	$\mathbf{-0.002}$	0.018	**0.045**	**0.032**	0.025

Table 3: Forces exerted and work performed by the three fingers in Figure 10 under $\boldsymbol{d}_1$ and $\boldsymbol{d}_2$ computed by the resistance algorithm (columns 2–4) or arbitrarily chosen (columns 5–7).

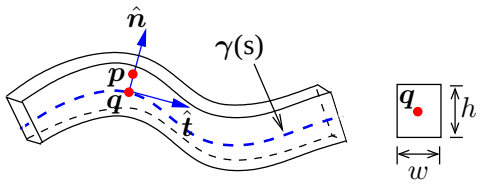

Figure 11: Segment of a curve-like shape with rectangular cross section.

Such a ring-like object may be viewed as being swept out by a rectangular cross section with width w and height h along a closed plane curve $\boldsymbol{\gamma}(s)$ parametrized by arc length s. The curve's perimeter l is significantly greater than w and h. Figure 11 illustrates a section of the object. Denote by $\hat{\boldsymbol{t}}$ and $\hat{\boldsymbol{n}}$ the unit tangent and normal at a point on the curve $\boldsymbol{\gamma}$. Because of its small dimensions, the cross section is assumed to have no deformation. So Poisson's ratio is treated as zero. The object is essentially a degenerated shell that is very small in two out of three dimensions.

7.1 Strain Energy

We follow Kirchhoff's assumptions (Reddy, 2007, p. 96) that fibers initially normal to $\boldsymbol{\gamma}$ remain straight after deformation, do not change their lengths, and remain normal to the middle curve of the deformed geometry. The stress and strain at any point $\boldsymbol{p}$ (cf. Figure 11) inside the object can be represented in terms of those at the intersection point $\boldsymbol{q}$ of $\boldsymbol{\gamma}(s)$ with the normal section through $\boldsymbol{p}$. The displacement of $\boldsymbol{q}$ is described as $\boldsymbol{\delta}(s) = \alpha(s)\hat{\boldsymbol{t}} + \beta(s)\hat{\boldsymbol{n}}$.

For a small deformation, we obtain the extensional strain ϵ and the change in curvature ζ at $\boldsymbol{q}$ with a reduction of one dimension from those for shells (Tian and Jia, 2010):

$$\epsilon \;=\; \nabla_{\hat{t}}\alpha + (\nabla_{\hat{t}}\hat{\boldsymbol{n}} \cdot \hat{\boldsymbol{t}})\beta$$

$$= \frac{d\alpha}{ds} - \kappa\beta, \tag{84}$$

$$\begin{aligned}\zeta &= \nabla_{\hat{t}}\left(-\nabla_{\hat{t}}\beta + (\nabla_{\hat{t}}\hat{\boldsymbol{n}}\cdot\hat{\boldsymbol{t}})\alpha\right)\\ &= -\frac{d^2\beta}{ds^2} - \frac{d\kappa}{ds}\alpha - \kappa\frac{d\alpha}{ds}.\end{aligned} \tag{85}$$

In the above, $\nabla_{\hat{t}}\alpha$ is the *directional derivative* of α with respect to $\hat{\boldsymbol{t}}$, and $\nabla_{\hat{t}}\hat{\boldsymbol{n}}$ is the *covariant derivative* which measures the rate of change of the normal $\hat{\boldsymbol{n}}$ along the curve $\boldsymbol{\gamma}$ at $\boldsymbol{q}$.[13]

Let $y = \|\boldsymbol{p} - \boldsymbol{q}\|$. The strain and stress at $\boldsymbol{p}$ are respectively $\epsilon + y\zeta$ and $E(\epsilon + y\zeta)$. The object's strain energy is obtained via integration:

$$\begin{aligned}U &= \int_V dU = \int_V \frac{1}{2}\sigma\epsilon\, dV\\ &= \frac{1}{2}\int_V E(\epsilon + y\zeta)^2 w\, dyds\\ &= \frac{1}{2}Ew\int_0^l\int_{-\frac{h}{2}}^{\frac{h}{2}}(\epsilon + y\zeta)^2\, dyds\\ &= \frac{1}{2}Ew\int_0^l\left(h\epsilon^2 + \frac{h^3}{12}\zeta^2\right)ds.\end{aligned} \tag{86}$$

In (86), the component linear in the height h represents the extensional energy, while the cubic component represents the bending energy.

Under FEM, we discretize the middle curve into linear elements and rewrite the strain energy into the standard form $U = \frac{1}{2}\boldsymbol{\delta}^T K\boldsymbol{\delta}$, where $\boldsymbol{\delta}$ gathers the displacements of all nodes on the middle curve. The stiffness matrix thus obtained again has a three-dimensional null space that comprises of all translations and rotations in the plane. Results from Section 4 on the uniqueness of deformation carry over given specified displacements of two contact nodes.

7.2 Contact Friction and Maximum Squeeze Depth

Unlike on a solid object, no tangent discontinuity occurs at a point contact on a ring-like object under deformation caused by point loads. For $t = i, j$, denote by $\boldsymbol{l}_t(\rho)$ and $\boldsymbol{r}_t(\rho)$ the directed left and right edges of the friction cone at $\boldsymbol{p}_t$ of the deformed shape under a stable squeeze $\rho\hat{\boldsymbol{u}}$ or a pure squeeze $\rho\hat{\boldsymbol{v}}$. Appendix F estimates the friction cone using the displaced locations of $\boldsymbol{p}_i$ and its two adjacent nodes $\boldsymbol{p}_{i-1}$ and $\boldsymbol{p}_{i+1}$. It returns $\boldsymbol{l}_i$ in (106) and $\boldsymbol{r}_i$ in (107). Similarly, the friction cone at the other point contact $\boldsymbol{p}_j$ is estimated.

As the squeeze depth ρ increases, the friction cone rotates at the displaced location $\tilde{\boldsymbol{p}}_t = \boldsymbol{p}_t + \boldsymbol{\delta}_t$ of $\boldsymbol{p}_t$ since the contact normal also depends on the displacements of the boundary nodes neighboring the node $\boldsymbol{p}_t$. The value of ρ needs to stop increasing as soon as $\boldsymbol{f}_t$ is aligned with one edge of the friction cone, that is,

$$(\tilde{\boldsymbol{p}}_i - \tilde{\boldsymbol{p}}_j)\times\boldsymbol{l}_t(\rho) = 0, \tag{87}$$

or

$$(\tilde{\boldsymbol{p}}_i - \tilde{\boldsymbol{p}}_j)\times\boldsymbol{r}_t(\rho) = 0. \tag{88}$$

[13] If the curve parametrization is arbitrary-speed, say, in the form of $\boldsymbol{\gamma}(t)$, we can easily evaluate ϵ and ζ according to (84) and (85) based on $ds/dt = \|d\boldsymbol{\gamma}/dt\|$.

This is when the node starts sliding.[14]

The displaced locations $\tilde{\boldsymbol{p}}_t$, $t = i-1, i, i+1$, are all linear functions of ρ. The estimated normal $\boldsymbol{n}_i$ in (105) has a fractional term with numerator and denominator being cubic and quadratic polynomials in ρ, respectively. It is easy to see that conditions (87) and (88) reduce to quartic polynomial equations in ρ. Closed-form roots thus exist. We keep the smallest positive one among all the roots of these two equations.[15] Similarly, we obtain the the smallest positive root of all the roots of (87) or (88) with $t = j$. Let ρ_1 be the smaller one of the two retained roots. It corresponds to the maximum squeeze depth before a finger slips.

Computation of ρ_1 is analyzed as follows. Assume that the spectral decomposition (9) has already been obtained. Since there are two contacts ($m = 2$), the matrices A in (19), B in (20), and M in (23) are constructed in time $O(n)$, $O(1)$, and $O(n)$, respectively. Because M is 7×7, the inverse M^{-1} and C are obtained in $O(1)$ time. The expressions for the displacements of $\boldsymbol{p}_i$ and $\boldsymbol{p}_j$ and their neighboring nodes are computed according to (26) in $O(n)$ time. Finding the roots of (87) and (88) takes time $O(1)$. Overall, ρ_1 is computable in time $O(n)$ for a given finger placement $\mathcal{G}(\boldsymbol{p}_i, \boldsymbol{p}_j)$.

We need to check if the material's proportional limit is exceeded anywhere. From $\bar{\boldsymbol{\delta}} = \rho\hat{\boldsymbol{u}}$ and (26), every nodal displacement is a constant vector scaled by ρ. The object is represented as a linear mesh consisting a sequence of segments. This means that the strain within a line segment is everywhere the same, and proportional to ρ. The element with the highest strain will stay the same as ρ increases. It is located by an $O(n)$ time search. This allows us to efficiently determine the depth $\rho_{\max}$ at which the proportional limit will be reached. Given a squeeze depth ρ, we can answer if the squeeze will be successful by simply checking the truth of $\rho \leq \rho_{\max}$. Such a *grasp test* can be done in $O(n)$ time.

7.3 Experiment with Ring-like Objects

The shape of an object in the experiment was either obtained using a scanner or reconstructed over sampled points from a closed form. Two fingers of the Barrett Hand were used directly in grasping without mounting any external tips. Their tips were much more pointed than the semicircular ones used in the experiments described in Sections 5.5 and 6.4. We chose the two fingers that had one coupled control to ensure that their tips were always at the same height during the grasping operation as if the object stayed in one horizontal plane. Since the fingers could move toward each other but not in different directions independently, only stable squeezes were tested. The grasp testing routine from Section 7.2 was employed to predict all finger placements that could result in grasps under specified squeeze depths. The Barrett Hand then performed grasping operations under some placements randomly selected from the predictions.

Table 4 shows successful grasps of five objects. The boundary of each object is marked with two pink dots to indicate the finger placement to be executed. The second row displays these objects under the resulting squeeze grasps by the Barrett Hand. The third row shows the simulation results, with contact friction cones drawn as gray triangles and forces indicated by short purple lines. At every contact, the friction was enough to keep the contact force pointing at the opposite contact, which ensures equilibrium. The last row lists the estimated values of the physical parameters for these grasps: Young's Modulus E (GPa), coefficient of friction μ, thickness h, and the change (in positive percentage) ϱ in the distance between the two contacts.

Figure 12 shows an example in which the finger placement from entry (1, 3) in Table 4 failed when $\varrho = 15.0884\%$, but succeeded on a "rigid" object. The "rigid" object, shown in part (d), was made from stuffing the deformable one with plastic foam. The two objects had identical boundaries and boundary

[14] Strictly, we will also need to check the derivative $\boldsymbol{f}'_t \times \boldsymbol{l}'_t$ or $\boldsymbol{f}'_t \times \boldsymbol{r}'_t$ with respect to ρ to confirm that $\boldsymbol{f}_t$ is rotating out of the friction cone.

[15] In case of no positive root, use ∞ if an arbitrary positive value satisfies the friction cone constraint, or 0 otherwise.

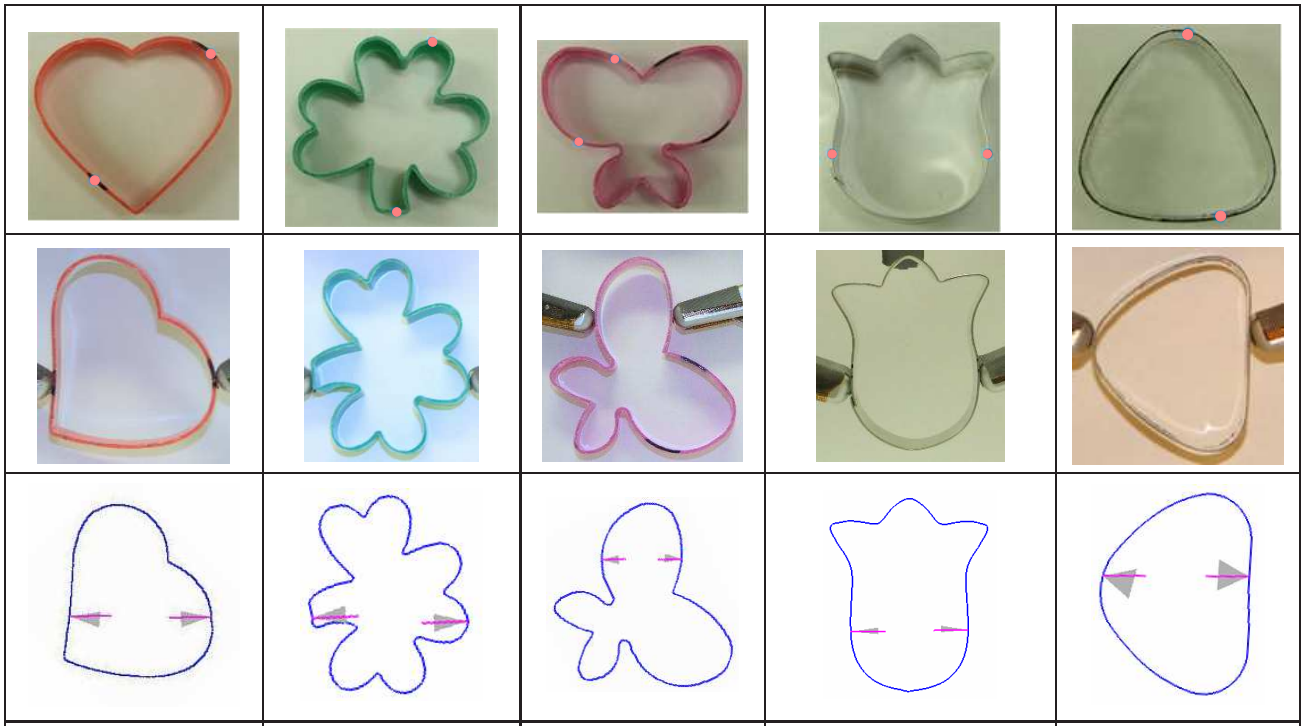

$(2, 0.26, 0.005, 10\%)$	$(2, 0.26, 0.005, 11\%)$	$(2, 0.26, 0.005, 9\%)$	$(200, 0.12, 0.003, 15\%)$	$(3, 0.5, 0.003, 15\%)$

Table 4: Successful grasps of five deformable objects (row 1) both in an experiment (row 2) and by simulation (row 3) under specified values of the physical parameters (E, μ, h, ϱ) (row 4).

material. In part (b), both friction cones have rotated (in the directions marked by the arrows) during the deformation caused by the squeeze. The computed force $\boldsymbol{f}_j$ at the upper contact $\boldsymbol{p}_j$ is out of its friction cone, while the $\boldsymbol{f}_i$ at the lower contact $\boldsymbol{p}_i$ is aligned with the right edge of its friction cone. The object escaped completely from the grasp, releasing its strain energy in (c).

Rotations of contact friction cones caused by deformation do not always lead to a grasp failure. On some occasions, they rotate toward each other, so that the grasping forces become more aligned with the cone axes to strengthen the grasp. See an example in Figure 13.

8 Discussion and Future Work

This paper studies how to grasp a planar deformable object by squeezing it with two fingers. One key idea is to specify the displacements of the grasping fingers rather than the forces they need to exert, and to use these displacements as constraints under which the deformed shape of the object can be computed using the FEM. In the general case of frictional segment contacts, at a squeeze depth the contact configuration is needed for computing the deformed shape. The second idea is to track this contact configuration, which includes contact nodes and their modes of contact, as the squeeze depth increases in an event-driven manner.

Algorithm 1 is similar in its iterative contact updates to previous FEM-based solutions to elastic contact problems (Okamoto and Nakazawa, 1979; Sachdeva and Ramakrishnan, 1981; Chandrasekaran et al., 1987). Contact constraints (45) for sticking and force constraints (46) for sliding were also used in the

(a) (b) (c) (d)

Figure 12: Grasp failure due to deformation: (a) attempt with a 15% relative squeeze; (b) contact forces out of the friction cones; (c) escape of the object; (d) success at grasping a "rigid" identical shape with the same placement.

(a) (b)

Figure 13: Rotations of two contact friction cones make the grasping forces more aligned in (a) experiment and (b) corresponding simulation, where the arrows indicate the rotation directions. The contact forces are collinear and opposed.

deformation computation by Sachdeva and Ramakrishnan (1981). However, these methods had to assume extra constraints to compute deformation under input loads. Unlike them, our algorithm takes as input specified displacements that can serve as constraints directly. In addition to providing analyses, we also describe contact events and their conditions (47)–(50) in the new context of grasping, with nonlinear root finding involved in the numerical solution.

We have introduced two types of squeezes to grasp a deformable planar object. A stable squeeze minimizes the potential energy for the same amount of squeeze by moving the two fingers toward each other. A pure squeeze ensures that the grasped object undergoes no rigid body motion as it deforms, addressing the inapplicability of linear elasticity to modeling of large rotations.

We have also looked at the best strategy to resist an adversary finger pushing against a grasped object via translation. The measure is the amount of work performed by the two grasping fingers. Optimal resistance strategies are first analyzed for fixed point and segment contacts. Built upon them, Algorithm 2 for grasp resistance is offered for rounded fingers under Coulomb friction, by incorporating the contact event detection subroutine from Algorithm 1.

Further investigation and experimental validation need to be conducted for the introduced grasp quality measures. We will consider extending the squeeze grasp strategy to three-dimensional deformable objects. We would also like to explore, at more depth, the stability of grasping in the presence of a disturbance, especially the grasped object's ability to absorb the disturbance into its strain energy.

A deformable object is often easier to grasp than a rigid object. We will investigate this via a comparison between rigid body grasping and deformable body grasping. To resist an adversary finger on a rigid body, frictional forces exerted by the grasping fingers often play the main role. Since the coefficient of friction is typically less than one, this often requires the grasping fingers to exert large normal forces. Resistance on a deformable body, however, is easier because not only does deformation enlarge the contact regions but also the concavities of these regions allow some normal contact forces to be directly engaged in the resistance.

Acknowledgment

Support for this research was provided in part by Iowa State University (ISU), and in part by the National Science Foundation through the grant IIS-0915876. Any opinions, findings, and conclusions or recommendations expressed in this material are those of the author(s) and do not necessarily reflect the views of the National Science Foundation. Part of the results (Guo et al., 2013), including Sections 3, 5, and 7, will be presented at the 2012 IEEE International Conference on Robotics and Automation, Karlsruhe, Germany. Thanks to former ISU undergraduate Trenton Anagnostopoulos for writing the mesh generation code.

References

[1] Besl PJ and McKay ND (1992) A method for registration of 3-D shapes. *IEEE Transactions on Pattern Analysis and Machine Intelligence*, 14(2):239–256.

[2] Bicchi A and Kumar V (2000) Robotic grasping and contact: a review. In *Proceedings of the IEEE International Conference on Robotics and Automation*, pp. 348–353.

[3] Bower AF (2009) *Applied Mechanics of Solids*. CRC Press.

[4] Boyd SP and Wegbreit B (2007) Fast computation of optimal contact forces. *IEEE Transactions on Robotics*, 23(6):1117–1132.

[5] Brost RC and Goldberg KY (1994) A complete algorithm for synthesizing modular fixtures for polygonal parts. In *Proceedings of the IEEE International Conference on Robotics and Automation*, pp. 535–542.

[6] Buss M, Faybusovich L, and Moore J (1998) Dikin-type algorithms for dexterous grasping force optimization. *International Journal of Robotics Research*, 17(8):831–839.

[7] ChandraseKaran N, Haisler WE, and Goforth RE (1987) A finite element solution method for contact problems with friction. *International Journal for Numerical Methods in Engineering*, 24:477–495.

[8] Coppersmith D and Winograd S (1990) Matrix multiplication via arithmetic progressions. *Journal of Symbolic Computation*, 9(3):251–280.

[9] Crandall SH, Dahl NC, and Lardner TJ (1978) *An Introduction to the Mechanics of Solids*. McGraw-Hill, Inc., 2nd edition.

[10] Faugeras OD and Hebert M (1986) The representation, recognition, and locating of 3-d objects. *International Journal of Robotics Research*, 5(3):27–52.

[11] Francavilla A and Zienkiewicz OC (1975) A note on numerical computation of elastic contact problems. *International Journal for Numerical Methods in Engineering*, 9:913–924.

[12] Fung YC and Tong P (2001) *Classical and Computational Solid Mechanics*. World Scientific.

[13] Gallagher RH (1975) *Finite Element Analysis*. Prentice-Hall, Inc.

[14] Gopalakrishnan K and Goldberg K (2005) D-space and deform closure grasps of deformable parts. *International Journal of Robotics Research*, 24(11):899–910.

[15] Guo F, Lin H, and Jia YB (2013) Squeeze grasping of deformable planar objects with segment contact and stick/slip transitions. To appear in *Proceedings of the IEEE International Conference on Robotics and Automation*.

[16] Hirai S, Tsuboi T, and Wada T (2001) Robust grasping manipulation of deformable objects. In *Proceedings of the IEEE International Symposium on Assembly and Task Planning*, pp. 411–416.

[17] Horn BKP (1987) Closed-form solution of absolute orientation using unit quaternions. *Journal of Optical Society of America A*, 4(4):629–642.

[18] Jia YB (1995) On computing optimal planar grasps. In *Proceedings of the IEEE/RSJ International Conference on Intelligent Robots and Systems*, pp. 3:427–434.

[19] Jia YB, Guo F, and Tian J (2011) On two-finger grasping of deformable planar objects. In *Proceedings of the IEEE International Conference on Robotics and Automation*, pp. 5261–5266.

[20] Kerr J and Roth B (1986) Analysis of multifingered hands. *International Journal of Robotics Research*, 4(4):3–17.

[21] Ladd AM and Kavraki LE (2004) Using motion planning for knot untangling. *International Journal of Robotics Research*, 23(7):797–808.

[22] Li Z and Sastry SS (1988) Task-oriented optimal grasping by multifingered robot hands. *IEEE Journal of Robotics and Automation*, 4(1):32–44.

[23] Luenberger DG (1973) *Introduction to Linear and Nonlinear Programming*. Addison-Wesley, 2nd edition.

[24] Luo Q and Xiao J (2006) Geometric properties of contacts involving a deformable object. In *Proceedings of the IEEE Symposium on Haptic Interfaces for Virtual Environment and Teleoperator Systems*, pp. 533–538.

[25] Lurie AI (2005) *Theory of Elasticity*. Springer-Verlag Berlin Heidelberg.

[26] Markenscoff X, Ni L, and Papadimitriou CH (1990) The geometry of grasping. *International Journal of Robotics Research*, 9(1):61–74.

[27] Markenscoff X and Papadimitriou CH (1989) Optimum grip of a polygon. *International Journal of Robotics Research*, 8(2):17–29.

[28] Matsuno T and Fukuda T (2006) Manipulation of flexible rope using topological model based on sensor information. In *Proceedings of the IEEE/RSJ International Conference on Intelligent Robots and Systems*, pp. 2638–2643.

[29] Mirtich B and Canny J (1994) Easily computable optimum grasps in 2-D and 3-D. In *Proceedings of the IEEE International Conference on Robotics and Automation*, pp. 739–741.

[30] Mishra B, Schwartz JT, and Sharir M (1987) On the existence and synthesis of multifinger positive grips. *Algorithmica*, 2(4):541–558.

[31] Mishra B (1995) Grasp metrics: optimality and complexity. In Goldberg K et al., editor, *Algorithmic Foundations of Robotics*, pp. 137–165. A. K. Peters, Boston, MA.

[32] Moll M and Kavraki LE (2006) Path planning for deformable linear objects. *IEEE Transactions on Robotics and Automation*, 22(4):625–636.

[33] Negi LS (2008) *Strength of Materials*. Tata McGraw-Hill Education.

[34] Nguyen V-D (1998) Constructing force-closure grasps. *International Journal of Robotics Research*, 7(3):3–16.

[35] Okamoto N and Nakazawa M (1979) Finite element incremental contact analysis with various frictional conditions. *International Journal for Numerical Methods in Engineering*, 14:337–357.

[36] Ponce J, Sullivan S, Sudsang A, Boissonnat J, and Merlet JP (1997) On computing four-finger equilibrium and force-closure grasps of polyhedral objects. *International Journal of Robotics Research*, 16(1):11–35.

[37] Ponce J, Stam D, and Faverjon B (1993) On computing two-finger force-closure grasps of curved 2D objects. *International Journal of Robotics Research*, 12(3):263–273.

[38] Pressley A (2001) *Elementary Differential Geometry*. Springer-Verlag.

[39] Reddy JN (2007) *Theory and Analysis of Elastic Plates and Shells*. CRC Press, second edition.

[40] Remde A, Henrich D, and Worn H (1999) Picking-up deformable linear objects with industrial robots. In *Proceedings of the International Symposium on Robotics*,

[41] Reuleaux F (1875) *Kinematics of Machinery*. Dover, New York, 1963. Original title *Theoretische Kinematic*.

[42] Rimon E and Blake A (1999) Caging planar bodies by one-parameter two-fingered gripping systems. *International Journal of Robotics Research*, 18:299–318.

[43] Rimon E and Burdick J (1996) On force and form closure for multiple finger grasps. In *Proceedings of the IEEE International Conference on Robotics and Automation*, pp. 1795–1800.

[44] Rodriguez A, Mason MT, and Ferry S (2012) From caging to grasping. *International Journal of Robotics Research*, 31(7):886–900.

[45] Saada AS (1993) *Elasticity: Theory and Applications*. Krieger Publishing Company.

[46] Sachdeva TD and Ramakrishnan CV (1981) A finite element solution for the two-dimensional elastic contact problems with friction. *International Journal for Numerical Methods in Engineering*, 17:1257–1271.

[47] Saha M and Isto P (2006) Motion planning for robotic manipulation of deformable linear objects. In *Proceedings of the IEEE International Conference on Robotics and Automation*, pp. 2478–2484.

[48] Salisbury JK and Roth B (1983) Kinematic and force analysis of articulated mechanical hands. *Journal of Mechanisms, Transmissions, and Automation in Design*, 105:35–41.

[49] Schwartz JG and Sharir M (1987) Identification of partially obscured objects in two and three dimensions by matching noisy characteristic curves. *International Journal of Robotics Research*, 6(2):29–44.

[50] Sinha PR and Abel JM (1992) A contact stress model for multifingered grasps of rough objects. *IEEE Transactions on Robotics and Automation*, 8(1):7–22.

[51] Strang G (1993) *Introduction to Linear Algebra*. Wellesley-Cambridge Press, 2nd edition.

[52] Strassen V (1969) Gaussian elimination is not optimal. *Numerische Mathematik*, 13(4):354–356.

[53] Tian J and Jia YB (2010) Modeling deformations of general parametric shells grasped by a robot hand. *IEEE Transactions on Robotics*, 26(5):837–852.

[54] Trinkle JC (1992) On the stability and instantaneous velocity of grasped frictionless objects. *IEEE Transactions on Robotics and Automation*, 8(5):560–572.

[55] van der Stappen AF, Wentink C, and Overmars MH (2000) Computing immobilizing grasps of polygonal parts. *International Journal of Robotics Research*, 19(5):467–479.

[56] van der Waerden BL (1991) *Algebra, Volume I*. Springer-Verlag.

[57] Wakamatsu H, Arai E, and Hirai S (2006) Knotting/unknotting manipulation of deformable linear objects. *International Journal of Robotics Research*, 25(4):371–395.

[58] Wakamatsu H and Hirai S (2004) Static modeling of linear object deformation based on differential geometry. *International Journal of Robotics Research*, 23(3):293–311.

[59] Wakamatsu H, Hirai S, and Iwata K (1996) Static analysis of deformable object grasping based on bounded force closure. In *Proceedings of the IEEE/RSJ International Conference on Intelligent Robots and Systems*, pp. 3324–3329.

A Proof of Theorem 5

Proof (i) It suffices to establish the claim for $m = 2$. Equivalently, we show that the following three vectors are linearly independent:

$$\bar{\boldsymbol{w}}_x = \begin{pmatrix} 1 \\ 0 \\ 1 \\ 0 \end{pmatrix}, \qquad \bar{\boldsymbol{w}}_y = \begin{pmatrix} 0 \\ 1 \\ 0 \\ 1 \end{pmatrix}, \qquad \text{and} \qquad \bar{\boldsymbol{w}}_r = \begin{pmatrix} -y_{i_1} \\ x_{i_1} \\ -y_{i_2} \\ x_{i_2} \end{pmatrix}.$$

Clearly, $\bar{\boldsymbol{w}}_x$ and $\bar{\boldsymbol{w}}_y$ are orthogonal to each other. Subtract from $\bar{\boldsymbol{w}}_r$ its components that are along $\bar{\boldsymbol{w}}_x$ and $\bar{\boldsymbol{w}}_y$, yielding

$$\begin{aligned}\bar{\boldsymbol{w}}_\perp &= \bar{\boldsymbol{w}}_r - \frac{\bar{\boldsymbol{w}}_r^T\bar{\boldsymbol{w}}_x}{\bar{\boldsymbol{w}}_x^T\bar{\boldsymbol{w}}_x}\bar{\boldsymbol{w}}_x - \frac{\bar{\boldsymbol{w}}_r^T\bar{\boldsymbol{w}}_y}{\bar{\boldsymbol{w}}_y^T\bar{\boldsymbol{w}}_y}\bar{\boldsymbol{w}}_y \\ &= \frac{1}{2}\begin{pmatrix} y_{i_2} - y_{i_1} \\ x_{i_1} - x_{i_2} \\ y_{i_1} - y_{i_2} \\ x_{i_2} - x_{i_1} \end{pmatrix}.\end{aligned}$$

The vector $\bar{\boldsymbol{w}}_\perp$ does not vanish because $\boldsymbol{p}_{i_1} \neq \boldsymbol{p}_{i_2}$. It is trivial to verify that $\bar{\boldsymbol{w}}_\perp$ is orthogonal to $\bar{\boldsymbol{w}}_x$ and $\bar{\boldsymbol{w}}_y$.

(ii) The symmetry of C follows that of M^{-1}, which exists by Theorem 4 since $m \geq 2$. Any $\bar{\boldsymbol{\delta}}$ uniquely induces a $2n$-vector $\boldsymbol{\delta}$ in the form of (26). Because K is positive semidefinite, by (27) we have $\bar{\boldsymbol{\delta}}^T C\bar{\boldsymbol{\delta}} = \boldsymbol{\delta}^T K\boldsymbol{\delta} \geq 0$, This establishes that C is also positive semidefinite.

In (28) we observe that $B^TC = \mathbf{0}$, which implies $C^TB = CB = \mathbf{0}$ given the symmetry of C. Therefore, $\mathrm{col}(B) \subseteq \mathrm{null}(C)$. Meanwhile, $\mathrm{null}(C)$ has no other independent vector. Suppose there is one, say, $\bar{\boldsymbol{\xi}}$. Then it would induce a rigid body displacement $\boldsymbol{\xi}$ given by (26). This is because by (27) we have

$$\frac{1}{2}\boldsymbol{\xi}^T K\boldsymbol{\xi} = \frac{1}{2}\bar{\boldsymbol{\xi}}^T C\bar{\boldsymbol{\xi}} = 0,$$

which implies $\boldsymbol{\xi} \in \mathrm{null}(K)$. However, since $\bar{\boldsymbol{\xi}}$ is independent of $\bar{\boldsymbol{v}}_{2n-2}$, $\bar{\boldsymbol{v}}_{2n-1}$, and $\bar{\boldsymbol{v}}_{2n}$, $\boldsymbol{\xi}$ must be independent of $\boldsymbol{v}_{2n-2}$, $\boldsymbol{v}_{2n-1}$, and $\boldsymbol{v}_{2n}$, or equivalently, independent of $\boldsymbol{w}_x$, $\boldsymbol{w}_y$, and $\boldsymbol{w}_r$. This contradicts that $\mathrm{null}(K)$ has rank 3. Therefore, $\mathrm{col}(B) = \mathrm{null}(C)$. Due to the symmetry of C, $\mathrm{row}(C) = \mathrm{col}(C)$. This leads to

$$\begin{aligned}\mathbb{R}^{2m} &= \mathrm{null}(C) \oplus \mathrm{row}(C) \\ &= \mathrm{col}(B) \oplus \mathrm{col}(C).\end{aligned}$$

(iii) Clearly, $\mathrm{rank}(E) \leq 3$. It is well known (and also easy to show) that the rank of the product of two matrices is at most the rank of either matrix. So $\mathrm{rank}(E) \geq \mathrm{rank}(B^TE) = \mathrm{rank}(I_3) = 3$. Hence $\mathrm{rank}(E) = 3$.

(iv) Property (iii) implies that $\mathrm{null}(E^T)$ has rank $2m-3$. For any $\bar{\boldsymbol{\delta}} \in \mathrm{null}(E^T)$,

$$\begin{aligned}E^T\bar{\boldsymbol{\delta}} = 0 &\Rightarrow BE^T\bar{\boldsymbol{\delta}} = 0 \\ &\Rightarrow (I_{2m} - AC)\bar{\boldsymbol{\delta}} = 0 \quad (\text{since } AC + BE^T = I_{2m} \text{ in (28)}) \\ &\Rightarrow (AC)\bar{\boldsymbol{\delta}} = \bar{\boldsymbol{\delta}}.\end{aligned}$$

Thus, $\bar{\boldsymbol{\delta}}$ is an eigenvector of AC corresponding to the eigenvalue 1. Because $\bar{\boldsymbol{\delta}}$ is arbitrary from $\mathrm{null}(E^T)$, AC has rank at least $2m-3$ and a unit eigenvalue of multiplicity at least $2m-3$. Meanwhile, for any $\bar{\boldsymbol{\delta}} \in \mathrm{null}(C)$, we have

$$\begin{aligned}C\bar{\boldsymbol{\delta}} = 0 &\Rightarrow (AC)\bar{\boldsymbol{\delta}} = 0 \\ &\Rightarrow \mathrm{rank}(AC) \leq 2m - \mathrm{rank}(\mathrm{null}(C)).\end{aligned}$$

But $\mathrm{null}(C) = \mathrm{col}(B)$ has rank 3 following part (i) of the theorem. Therefore, AC has rank $2m-3$ and only one eigenvalue 1.

(v) The property will follow from (iii) and (iv) if we show that $\mathrm{col}(AC) \perp \mathrm{col}(E)$. Let us start with vanishing of the upper right block of MM^{-1} in (28):

$$\begin{array}{rcll} AE + BH = 0 & \Rightarrow & CAE + CBH = 0 & \\ & \Rightarrow & CAE = 0 & \text{(since } CB = 0\text{)} \\ & \Rightarrow & (A^T C^T)^T E = 0 & \\ & \Rightarrow & (AC)^T E = 0 & \text{(by the symmetries of } A \text{ and } C\text{)} \\ & \Rightarrow & \mathrm{col}(AC) \perp \mathrm{col}(E). & \end{array}$$

□

B Measurement of Young's Modulus, Poisson's Ratio, and the Coefficient of Contact Friction

Young's Modulus E and Poisson's ratio ν of foam rubber were estimated by deforming multiple cuboids cut from a foam board, and measuring the applied forces and the resulting changes in the geometry of the cuboids.

The longest side l of a cuboid ranged between 0.05 and 0.1. Denote by w and h its two other sides. The cuboid was placed against the surface of the phalanx of a finger of the Barrett Hand such that the side l was perpendicular to the surface. A human finger pushed the cuboid against the phalanx by exerting a vertical force on the facet of the cuboid opposite to the one in contact with the phalanx. Assumed to be equally distributed, the force had its magnitude f measured by a strain gauge sensor mounted at the joint of the fingertip. The changes in the three dimensions of the cuboid were measured as Δl, Δw, and Δh, respectively.

Because Δw and Δh were small compared with w and h, Young's Modulus was estimated as

$$E \approx \frac{fl}{wh\Delta l}.$$

Poisson' ratio was approximated as

$$\nu \approx -\frac{\Delta w/w}{\Delta l/l}.$$

All solid objects in the experiments were made of foam rubber. Our measurements were $E \approx 5 \times 10^4$Pa and $\nu = 0.3$.

To measure the coefficient of friction between an object and a finger, we placed a small piece of the same material of the object on a slope, which was made of the same material of the fingertip. Denote by α the angle between the slope and the horizontal plane. Using bisection, we searched the range $[0, \pi/2]$ for α_0, the critical value below which the piece stayed still on the slope and above which the piece slid. Neglecting the difference between static friction and dynamic friction, the coefficient of friction was taken as $\mu = \tan \alpha_0$. The value 0.4 was used in the experiments in Sections 5.5 and 6.4.

C Matching Deformed Shapes from Simulation and Experiment

A boundary contour was first drawn on the computer screen. Based on its printout (with some enlargement), an object was cut from a foam board. When we compared two deformed shapes, generated by simulation and acquired in the experiment[16], respectively, the two sets of data points differed by scale, orientation, and

[16]The shape data in the experiment was generated by a scanner.

translation. A homogeneous transformation needed to be applied in the matching.

More formally, given two sets of points $P = \{\boldsymbol{p}_1, \ldots, \boldsymbol{p}_n\}$ and $Q = \{\boldsymbol{q}_1, \ldots, \boldsymbol{q}_n\}$ in the plane, where $\boldsymbol{p}_i = (x_i, y_i)^T$ corresponds to $\boldsymbol{q}_i = (u_i, v_i)^T$, for $i = 1, 2, \ldots, n$. We determine the scale s, rotation θ, and translation $(t_x, t_y)^T$ applied to Q to minimize the least-squares difference between these two point sets,

$$\mathcal{E} = \sum_i^n (\boldsymbol{p}_i - M\boldsymbol{q}_i)^T (\boldsymbol{p}_i - M\boldsymbol{q}_i), \tag{89}$$

where M is the transformation matrix given by

$$M = \begin{pmatrix} s\cos\theta & -s\sin\theta & t_x \\ s\sin\theta & s\cos\theta & t_y \\ 0 & 0 & 1 \end{pmatrix}. \tag{90}$$

Least-squares matching of two point sets in two or three dimensions with known correspondences under rigid motions was solved by Faugeras and Hebert (1986), Horn (1987), and Schwartz and Sharir (1987). Matching a set of points against a 3D model up to rotation and translation (with unknown point correspondences) could be effectively carried out by the iterative closest point algorithm (Besl and Mckay, 1992).

Obtain the four partial derivatives of $\mathcal{E}$:

$$\begin{aligned}
\frac{\partial \mathcal{E}}{\partial \theta} &= 2s \sum_i^n (\boldsymbol{p}_i - M\boldsymbol{q}_i)^T \begin{pmatrix} \sin\theta & -\cos\theta & 0 \\ \cos\theta & -\sin\theta & 0 \\ 0 & 0 & 0 \end{pmatrix} \boldsymbol{q}_i, \\
\frac{\partial \mathcal{E}}{\partial s} &= -2 \sum_i^n (\boldsymbol{p}_i - M\boldsymbol{q}_i)^T \begin{pmatrix} \cos\theta & -\sin\theta & 0 \\ \sin\theta & \cos\theta & 0 \\ 0 & 0 & 0 \end{pmatrix} \boldsymbol{q}_i, \\
\frac{\partial \mathcal{E}}{\partial t_x} &= -2 \sum_i^n (x_i - su_i\cos\theta + sv_i\sin\theta - t_x), \\
\frac{\partial \mathcal{E}}{\partial t_y} &= -2 \sum_i^n (y_i - su_i\sin\theta - sv_i\cos\theta - t_y).
\end{aligned}$$

Write

$$(c_1, c_2, c_3, c_4, c_5, c_6, c_7, c_8, c_9, c_{10})^T = \frac{1}{n} \sum_i^n (x_i, y_i, u_i, v_i, x_iu_i, x_iv_i, y_iu_i, y_iv_i, u_i^2, v_i^2)^T.$$

Vanishing of the above four partial derivatives of $\mathcal{E}$ yields the following equations:

$$c_3 s\cos\theta - c_4 s\sin\theta + t_x - c_1 = 0, \tag{91}$$

$$c_3 s\sin\theta + c_4 s\cos\theta + t_y - c_2 = 0, \tag{92}$$

$$(c_3\sin\theta + c_4\cos\theta)t_x + (c_4\sin\theta - c_3\cos\theta)t_y - (c_5 + c_8)\sin\theta + (c_7 - c_6)\cos\theta = 0, \tag{93}$$

$$(c_4\sin\theta - c_3\cos\theta)t_x - (c_3\sin\theta + c_4\cos\theta)t_y + (c_5 + c_8)\cos\theta + (c_7 - c_6)\sin\theta - (c_9 + c_{10})s = 0. \tag{94}$$

For the moment, we assume $c_3^2 + c_4^2 \neq 0$. Multiply (91) with c_3 and (92) with c_4, and then sum them up, yielding

$$s\cos\theta = \frac{c_1c_3 + c_2c_4 - c_3t_x - c_4t_y}{c_3^2 + c_4^2}. \tag{95}$$

We also have, from $c_3 \times (92) - c_4 \times (91)$,

$$s \sin\theta = \frac{c_2c_3 - c_1c_4 + c_4t_x - c_3t_y}{c_3^2 + c_4^2}; \tag{96}$$

from $\cos\theta \times (93) + \sin\theta \times (94)$,

$$s \sin\theta = \frac{c_4t_x - c_3t_y + c_7 - c_6}{c_9 + c_{10}}; \tag{97}$$

and from $\sin\theta \times (93) - \cos\theta \times (94)$,

$$s \cos\theta = -\frac{c_3t_x + c_4t_y - c_5 - c_8}{c_9 + c_{10}}. \tag{98}$$

Eliminate $s\cos\theta$ from (95) and (98), and $s\sin\theta$ from (96) and (97). Then solve the two resultant equations for t_x and t_y. To obtain s, square both sides of (95) and both sides of (96), and add up the two resulting equations to eliminate θ. Finally, from (95) and (96) we obtain θ after plugging the expressions for t_x and t_y. The solution is given below:

$$\begin{aligned}
t_x &= \frac{c_4(c_7 - c_6) - c_3(c_5 + c_8) + c_1(c_9 + c_{10})}{c_9 + c_{10} - (c_3^2 + c_4^2)}, && (99)\\
t_y &= \frac{c_2(c_9 + c_{10}) - c_4(c_5 + c_8) - c_3(c_7 - c_6)}{c_9 + c_{10} - (c_3^2 + c_4^2)}, && (100)\\
s &= \frac{\sqrt{(c_1c_3 + c_2c_4 - (c_5 + c_8))^2 + (c_1c_4 - c_2c_3 + (c_7 - c_6))^2}}{c_9 + c_{10} - (c_3^2 + c_4^2)}, && (101)\\
\theta &= \text{atan2}(c_7 - c_6 + c_1c_4 - c_2c_3, c_5 + c_8 - (c_1c_3 + c_2c_4)). && (102)
\end{aligned}$$

Note that $c_9 + c_{10} > c_3^2 + c_4^2$ for $n \geq 2$.

In the special case $c_3 = c_4 = 0$, by solving the simplified (91)–(94) directly we can verify that the solution (99)–(102) carries over. It is simplified to

$$\begin{aligned}
t_x &= c_1\\
t_y &= c_2\\
s &= \frac{\sqrt{(c_7 - c_6)^2 + (c_5 + c_8)^2}}{c_9 + c_{10}}\\
\theta &= \text{atan2}(c_7 - c_6, c_5 + c_8).
\end{aligned}$$

D Proof of Theorem 10

Before (59) we first write $W_{\mathcal{F}}$ from (58) as a quadratic form

$$W_{\mathcal{F}} = \frac{1}{2}\bar{\boldsymbol{\delta}}'^T C\bar{\boldsymbol{\delta}}' + \begin{pmatrix} 0 \\ -\boldsymbol{a} \\ \boldsymbol{a}/2 \end{pmatrix}^T C\bar{\boldsymbol{\delta}}' + \omega, \tag{103}$$

where $\bar{\boldsymbol{\delta}}' = (\boldsymbol{\delta}_i^T, -\boldsymbol{\delta}_i^T, \mathbf{0}^T)^T$. The proof of Theorem 10 needs the following lemma.

Lemma 12 *The 6-tuple $\bar{\boldsymbol{\delta}}' \in \mathrm{null}(C)$ if and only if conditions (63) hold.*

Proof Note that $\bar{\boldsymbol{\delta}}'$ is already orthogonal to $\bar{\boldsymbol{w}}_x = (1,0,1,0,1,0)^T$ and $\bar{\boldsymbol{w}}_y = (0,1,0,1,0,1)^T$. The vector that represents rotation is $\bar{\boldsymbol{w}}_r = (-y_i, x_i, -y_j, x_j, -y_k, x_k)^T$. Hence $\bar{\boldsymbol{\delta}}'$ is in the null space if and only if it is collinear with the following vector:

$$\begin{aligned} \bar{\boldsymbol{w}}_\perp &= \bar{\boldsymbol{w}}_r - \frac{\bar{\boldsymbol{w}}_r \cdot \bar{\boldsymbol{w}}_x}{\bar{\boldsymbol{w}}_x \cdot \bar{\boldsymbol{w}}_x}\bar{\boldsymbol{w}}_x - \frac{\bar{\boldsymbol{w}}_r \cdot \bar{\boldsymbol{w}}_y}{\bar{\boldsymbol{w}}_y \cdot \bar{\boldsymbol{w}}_y}\bar{\boldsymbol{w}}_y \\ &= \frac{1}{3}\begin{pmatrix} -2y_i + y_j + y_k \\ 2x_i - x_j - x_k \\ y_i - 2y_j + y_k \\ -x_i + 2x_j - x_k \\ y_i + y_j - 2y_k \\ -x_i - x_j + 2x_k \end{pmatrix}. \end{aligned} \tag{104}$$

The collinearity of $\bar{\boldsymbol{\delta}}'$ and $\bar{\boldsymbol{w}}_\perp$ implies the following:

$$\begin{aligned} (-2y_i + y_j + y_k) + (y_i - 2y_j + y_k) &= 0, \\ (2x_i - x_j - x_k) + (-x_i + 2x_j - x_k) &= 0, \\ y_i + y_j - 2y_k &= 0, \\ -x_i - x_j + 2x_k &= 0. \end{aligned}$$

It is easy to verify that the above four equations are equivalent to $\boldsymbol{p}_k = \frac{1}{2}(\boldsymbol{p}_j + \boldsymbol{p}_j)$. Also, for $\bar{\boldsymbol{\delta}}'$ and $\bar{\boldsymbol{w}}_\perp$ to be collinear, $\boldsymbol{\delta}_i$ must be collinear with the first two entries in $\bar{\boldsymbol{w}}_\perp$:

$$\begin{pmatrix} -2y_i + y_j + y_k \\ 2x_i - x_j - x_k \end{pmatrix}, \qquad \text{or equivalently,} \qquad \begin{pmatrix} -y_i + y_j \\ x_i - x_j \end{pmatrix},$$

Under the last two equations above, $\boldsymbol{\delta}_i$ is orthogonal to $\boldsymbol{p}_i - \boldsymbol{p}_j$. □

Proof (Theorem 10) The positive semi-definiteness of H follows from that of C, $\boldsymbol{\delta}'^T C \boldsymbol{\delta}' = \boldsymbol{\delta}_i^T H \boldsymbol{\delta}_i$ by $\bar{\boldsymbol{\delta}}' = S\bar{\boldsymbol{\delta}}_i$ and (60), and the fact that $\boldsymbol{\delta}' = 0$ if and only if $\boldsymbol{\delta}_i = 0$. The second part of the theorem easily follows from Lemma 12. □

E Proof of Proposition 11

Proof Observe that $\boldsymbol{d}_1^T H \boldsymbol{d}_1 = (S\boldsymbol{d}_1)^T C (S\boldsymbol{d}_1)$ given $H = S^T C S$. Here, S is given in (80), and

$$S\boldsymbol{d}_1 = \left(\boldsymbol{d}_1^T, \ldots, \boldsymbol{d}_1^T, -\frac{|\mathbb{I}|}{|\mathbb{J}|}\boldsymbol{d}_1^T, \ldots, -\frac{|\mathbb{I}|}{|\mathbb{J}|}\boldsymbol{d}_1^T, 0, \ldots, 0\right)^T.$$

Clearly, $\boldsymbol{d}_1 = 0$ if and only if $S\boldsymbol{d}_1 = 0$. Thus, the positive semidefiniteness of H follows from that of C.

Sufficiency of conditions i), ii), and iii) for $\boldsymbol{d}_1 \in \mathrm{null}(H)$ trivially follows from Theorem 10. To establish their necessity, suppose $\boldsymbol{d}_1 \in \mathrm{null}(H)$. We just need to establish part i) of the proposition: $|\mathbb{I}| = |\mathbb{J}| = |\mathbb{K}| = 1$, since then parts ii) and iii) will follow from Theorem 10.

As in Appendix D, the $2(|\mathbb{I}| + |\mathbb{J}| + |\mathbb{K}|)$-tuples $\bar{\boldsymbol{w}}_x, \bar{\boldsymbol{w}}_y, \bar{\boldsymbol{w}}_r$ represent unit translations along the x- and y-axes, and a rotation about the origin respectively. In $\bar{\boldsymbol{w}}_r$, the tuples $(-y_t, x_t)^T$ appear in the same index order as their corresponding displacements $\boldsymbol{\delta}_t$ in $\bar{\boldsymbol{\delta}}$.

Since $S\boldsymbol{d}_1$ is orthogonal to $\bar{\boldsymbol{w}}_x$ and $\bar{\boldsymbol{w}}_y$, $S\boldsymbol{d}_1 \in \mathrm{null}(C)$ implies that the vector must be parallel to $\bar{\boldsymbol{w}}_\perp$, defined in (104), which now takes the form of $\frac{1}{q}$, where $q = |\mathbb{I}|+|\mathbb{J}|+|\mathbb{K}|$, times a vector that lists the tuples

$$\begin{pmatrix} \sum_{t\in\mathbb{I}\cup\mathbb{J}\cup\mathbb{K}} y_t - qy_l \\ -\sum_{t\in\mathbb{I}\cup\mathbb{J}\cup\mathbb{K}} x_t + qx_l \end{pmatrix}.$$

In the above, the index l ranges over $\mathbb{I},\mathbb{J},\mathbb{K}$ sequentially. From $S\boldsymbol{d}_1 \parallel \bar{\boldsymbol{w}}_\perp$, we infer that, for any $u, v \in \mathbb{I}$ with $u \neq v$,

$$\begin{aligned} 0 &= \begin{pmatrix} \sum_{t\in\mathbb{I}\cup\mathbb{J}\cup\mathbb{K}} y_t - qy_u \\ -\sum_{t\in\mathbb{I}\cup\mathbb{J}\cup\mathbb{K}} x_t + qx_u \end{pmatrix} - \begin{pmatrix} \sum_{t\in\mathbb{I}\cup\mathbb{J}\cup\mathbb{K}} y_t - qy_v \\ -\sum_{t\in\mathbb{I}\cup\mathbb{J}\cup\mathbb{K}} x_t + qx_v \end{pmatrix} \\ &= q\begin{pmatrix} y_v - y_u \\ x_u - x_v \end{pmatrix}. \end{aligned}$$

Hence $\boldsymbol{p}_u = \boldsymbol{p}_v$ whenever $u, v \in \mathbb{I}$. Similarly, we establish that $\boldsymbol{p}_u = \boldsymbol{p}_v$ whenever $u, v \in \mathbb{J}$. This establishes that $|\mathbb{I}| = |\mathbb{J}| = 1$.

Finally, $S\boldsymbol{d}_1 \parallel \bar{\boldsymbol{w}}_\perp$ implies that the last $2|K|$ entries in $\bar{\boldsymbol{w}}_\perp$ are zero, that is, for $l \in \mathbb{K}$,

$$\begin{aligned} \sum_{t\in\mathbb{I}\cup\mathbb{J}\cup\mathbb{K}} y_t - qy_l &= 0, \\ -\sum_{t\in\mathbb{I}\cup\mathbb{J}\cup\mathbb{K}} x_t + qx_l &= 0. \end{aligned}$$

This yields the same point

$$\boldsymbol{p}_l = \frac{1}{q}\sum_{t\in\mathbb{I}\cup\mathbb{J}\cup\mathbb{K}} \boldsymbol{p}_t,$$

for all $l \in \mathbb{K}$. Therefore, $|\mathbb{K}| = 1$. □

F Friction Cone at Contact with a Point Finger

When a point finger exerts force $\boldsymbol{f}_i$ at the boundary node $\boldsymbol{p}_i$ of a ring-like object, it generates no tangential discontinuity. We obtain the inward normal from estimating the osculating circle[17] of the deformed curve at the displaced location $\tilde{\boldsymbol{p}}_i$ of $\boldsymbol{p}_i$. As illustrated in Figure 14, this circle can be approximated as the one that passes through $\tilde{\boldsymbol{p}}_{i-1}, \tilde{\boldsymbol{p}}_i, \tilde{\boldsymbol{p}}_{i+1}$. The inward normal at $\tilde{\boldsymbol{p}}_i$ points from the center $\boldsymbol{o}$ of the circle to $\tilde{\boldsymbol{p}}_i$.

For $i \leq k \leq i+1$, introduce the following terms:

$$\begin{aligned} \boldsymbol{t}_{k-1} &= \tilde{\boldsymbol{p}}_k - \tilde{\boldsymbol{p}}_{k-1}, \\ \boldsymbol{n}_{k-1} &= R\boldsymbol{t}_{k-1}, \\ \boldsymbol{q}_{k-1} &= \frac{\tilde{\boldsymbol{p}}_{k-1} + \tilde{\boldsymbol{p}}_k}{2}, \end{aligned}$$

[17] The osculating circle (Pressley, 2001, p. 35) of a curve $\boldsymbol{\gamma}$ at a point $\boldsymbol{\gamma}(s)$ has radius equal to the inverse of its curvature $\kappa(s)$. Its center lies along the normal at $\boldsymbol{\rho}(s)$ at distance $1/\|\kappa(s)\|$ away and on the same side of the tangent as the curve does locally. The circle is tangent to $\boldsymbol{\gamma}$.

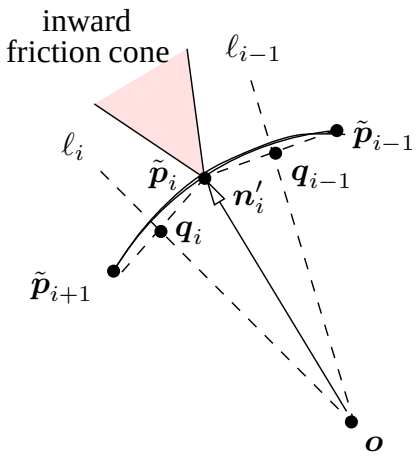

Figure 14: Estimation of the normal at displaced node $\tilde{\boldsymbol{p}}_i$ in contact with a point finger exerting force.

where

$$R = \begin{pmatrix} 0 & -1 \\ 1 & 0 \end{pmatrix}.$$

Note that $\boldsymbol{n}_{i-1} \perp \boldsymbol{t}_{i-1}$ and $\boldsymbol{n}_i \perp \boldsymbol{t}_i$. The perpendicular bisectors of the segments $\overline{\tilde{\boldsymbol{p}}_{i-1}\tilde{\boldsymbol{p}}_i}$ and $\overline{\tilde{\boldsymbol{p}}_i\tilde{\boldsymbol{p}}_{i+1}}$ are respectively along the directions of $\boldsymbol{n}_{i-1}$ and $\boldsymbol{n}_i$, and parametrized below as

$$\begin{aligned} \ell_{i-1}: &\quad \boldsymbol{q}_{i-1} + \xi_{i-1}\boldsymbol{n}_{i-1}, \\ \ell_i: &\quad \boldsymbol{q}_i + \xi_i \boldsymbol{n}_i. \end{aligned}$$

The two lines intersect at the circle's center $\boldsymbol{o}$, where

$$\boldsymbol{q}_{i-1} + \xi_{i-1}\boldsymbol{n}_{i-1} = \boldsymbol{q}_i + \xi_i \boldsymbol{n}_i.$$

Taking the dot products of $\boldsymbol{t}_i$ with both sides of the above equation, we obtain

$$\xi_{i-1} = \frac{\boldsymbol{t}_i \cdot (\boldsymbol{q}_i - \boldsymbol{q}_{i-1})}{\boldsymbol{t}_i \cdot \boldsymbol{n}_{i-1}}.$$

Hence

$$\boldsymbol{o} = \boldsymbol{q}_{i-1} + \frac{\boldsymbol{t}_i \cdot (\boldsymbol{q}_i - \boldsymbol{q}_{i-1})}{\boldsymbol{t}_i \cdot \boldsymbol{n}_{i-1}} \boldsymbol{n}_{i-1}.$$

The inward normal at $\tilde{\boldsymbol{p}}_i$ is in the direction of

$$\begin{aligned} \boldsymbol{n}'_i &= \tilde{\boldsymbol{p}}_i - \boldsymbol{o} \\ &= \tilde{\boldsymbol{p}}_i - \boldsymbol{q}_{i-1} - \frac{\boldsymbol{t}_i \cdot (\boldsymbol{q}_i - \boldsymbol{q}_{i-1})}{\boldsymbol{t}_i \cdot \boldsymbol{n}_{i-1}} \boldsymbol{n}_{i-1} \\ &= \frac{\tilde{\boldsymbol{p}}_i - \tilde{\boldsymbol{p}}_{i-1}}{2} - \frac{(\tilde{\boldsymbol{p}}_{i+1} - \tilde{\boldsymbol{p}}_i)^T (\tilde{\boldsymbol{p}}_{i+1} - \tilde{\boldsymbol{p}}_{i-1})}{2(\tilde{\boldsymbol{p}}_{i+1} - \tilde{\boldsymbol{p}}_i)^T R (\tilde{\boldsymbol{p}}_i - \tilde{\boldsymbol{p}}_{i-1})} R(\tilde{\boldsymbol{p}}_i - \tilde{\boldsymbol{p}}_{i-1}). \end{aligned} \tag{105}$$

Note that $(\tilde{\boldsymbol{p}}_{i+1} - \tilde{\boldsymbol{p}}_i)^T R(\tilde{\boldsymbol{p}}_i - \tilde{\boldsymbol{p}}_{i-1}) \neq 0$ unless $\boldsymbol{p}_{i-1}, \boldsymbol{p}_i$, and $\boldsymbol{p}_{i+1}$ are collinear. Should such collinearity occur, $\boldsymbol{n}'_i$ is easily set to be perpendicular to $\tilde{\boldsymbol{p}}_{i+1} - \tilde{\boldsymbol{p}}_{i-1}$ and point inward.

The left and right edges of the friction cone at $\tilde{\boldsymbol{p}}_i$ are then respectively in the directions of

$$\boldsymbol{l}_i = \begin{pmatrix} \cos\theta & -\sin\theta \\ \sin\theta & \cos\theta \end{pmatrix} \boldsymbol{n}'_i, \tag{106}$$

$$\boldsymbol{r}_i = \begin{pmatrix} \cos\theta & \sin\theta \\ -\sin\theta & \cos\theta \end{pmatrix} \boldsymbol{n}'_i. \tag{107}$$

Here $\theta = \tan^{-1}\mu$ with μ being the coefficient of friction.